



Programa de Doctorado en Medio Ambiente y Sostenibilidad

Tesis doctoral

**CARBONO ORGÁNICO SOLUBLE EN EL MEDITERRÁNEO:
FUENTES E INFLUENCIA EN LAS PROPIEDADES ÓPTICAS**

Alba López Caravaca

Director de la tesis

Dr. D. José Francisco Nicolás Aguilera

Codirector de la tesis

Dr. D. Jaime Javier Crespo Mira

Universidad Miguel Hernández de Elche

- 2024 -

La presente Tesis Doctoral, titulada “Carbono orgánico soluble en el Mediterráneo: fuentes e influencia en las propiedades ópticas”, se presenta bajo la modalidad de **tesis por compendio** de las siguientes **publicaciones**:

- “Sources of water-soluble organic carbon in fine particles at a southern European urban background site.” A. López-Caravaca, J. Crespo, N. Galindo, E. Yubero, N. Juárez, J.F. Nicolás, 2023. Atmospheric Environment, 306, 119844, <https://doi.org/10.1016/j.atmosenv.2023.119844>.
- “Characterization of water-soluble organic carbon absorption at an urban background site in the south-eastern Iberian Peninsula.” A. López-Caravaca, J. Crespo, N. Galindo, E. Yubero, A. Clemente, R. Castañer, J.F. Nicolás, 2024. Atmospheric Environment, 324, 120435, <https://doi.org/10.1016/j.atmosenv.2024.120435>.
- “WSOC in accumulation mode aerosols: Distribution and relationship with BrC light absorption at an urban background site.” A. López-Caravaca, J. Crespo, N. Galindo, E. Yubero, N. Juárez, J.F. Nicolás, 2024. Atmospheric Pollution Research, 15, 102133, <https://doi.org/10.1016/j.apr.2024.102133>.



El Dr. D. José Francisco Nicolás Aguilera, director, y Dr. D. Jaime Javier Crespo Mira, codirector de la tesis doctoral titulada **“Carbono orgánico soluble en el Mediterráneo: fuentes e influencia en las propiedades ópticas”**

INFORMAN:

Que Dña. Alba López Caravaca ha realizado bajo nuestra supervisión el trabajo titulado **“Carbono orgánico soluble en el Mediterráneo: fuentes e influencia en las propiedades ópticas”** conforme a los términos y condiciones definidos en su Plan de Investigación y de acuerdo al Código de Buenas Prácticas de la Universidad Miguel Hernández de Elche, cumpliendo los objetivos previstos de forma satisfactoria para su defensa pública como tesis doctoral.

Lo que firmamos para los efectos oportunos, en Elche

Director de la tesis

Dr. D. José Francisco Nicolás Aguilera

Codirector de la tesis

Dr. D. Jaime Javier Crespo Mira



El Dr. D. José Navarro Pedreño, Coordinador/a del Programa de Doctorado en **Medio Ambiente y Sostenibilidad**

INFORMA:

Que Dña. Alba López Caravaca ha realizado bajo la supervisión de nuestro Programa de Doctorado el trabajo titulado **“Carbono orgánico soluble en el Mediterráneo: fuentes e influencia en las propiedades ópticas”** conforme a los términos y condiciones definidos en su Plan de Investigación y de acuerdo al Código de Buenas Prácticas de la Universidad Miguel Hernández de Elche, cumpliendo los objetivos previstos de forma satisfactoria para su defensa pública como tesis doctoral.

Lo que firmo para los efectos oportunos, en Elche

Prof. Dr. D. José Navarro Pedreño

Coordinador/a del Programa de Doctorado en Medio Ambiente y Sostenibilidad

Agradecimientos

Escribo esto a punto de completar una etapa en mi vida que, años atrás, soñaba con cumplir sin saber si ocurriría. Ponerle fin a esta etapa es comenzar otra con más incertidumbre, si cabe. Ojalá mi yo del futuro lea esto con la estabilidad que deseo alcanzar.

No puedo imaginarme esta aventura sin mis directores de tesis, José y Javier. Gracias por la confianza que depositasteis en mí y por haberme guiado de principio a fin todos estos años.

Eduardo, gracias por esperar de mí cosas que sentía que se me escapaban, puedo decir que gracias a ti he aprendido a querer la Física.

Nuria, eres uno de mis referentes de mujer en la Ciencia. Gracias por toda la paciencia que has tenido conmigo.

Álvaro, encantada de compartir otra etapa más de mi vida contigo. Eres un gran compañero y espero que tengamos la oportunidad de seguir siéndolo.

Nerea, gracias por todo lo que he podido aprender de ti.

Bego, has sido un gran apoyo y te relaciono con todos los momentos graciosos que he vivido en el laboratorio.

Dani y Noelia, gracias por el camino compartido y ánimo que ya (n)os queda poco.

Por supuesto, el gran pilar que me ha apoyado siempre ha sido mi familia. Mari Carmen, eres la mejor madre del mundo. Juli, intento imaginarme un ejército de mini-Albas aplaudiéndome. Javier, seguro que me ayudas a elegir el mejor outfit. Gracias.

Sen, gracias por darme tanta fuerza y por enseñarme a priorizar las cosas buenas de la vida. Sea lo que sea que me espere ahora, estoy tranquila porque sé que vas a estar conmigo.

Charlotte, Fati, Lore, Carla y Eva, gracias por animarme, apoyarme y confiar en mí. Entrenar y comer en la playa siempre será el mejor plan. Paquita y Laupi, gracias por tanto a pesar de no tenernos cerca.

Índice

Acrónimos.....	5
Listado de figuras y tablas.....	7
Resumen.....	9
Abstract.....	11
1. Introducción.....	13
2. Objetivos.....	17
3. Metodología.....	19
3.1 Descripción del punto de muestreo.....	19
3.2 Campaña de muestreo.....	20
3.2.1 Muestreo con LVS 3.1 Derenda.....	21
3.2.2 Muestreo con impactador en cascada MOUDI.....	21
3.3 Análisis de muestras.....	21
3.3.1 Determinación gravimétrica de la concentración ambiental de aerosol.....	21
3.3.2 Análisis elemental.....	22
3.3.3 Análisis termo-óptico de transmisión.....	23
3.3.4 Cromatografía iónica.....	23
3.3.5 Determinación de <i>Water Soluble Organic Carbon</i>	24
3.4 Absorción de la luz.....	24
3.4.1 Absorción de la luz por BrC.....	25
3.4.2 Absorción de la luz por WSOC.....	25
3.5 Datos meteorológicos e identificación de eventos.....	26
3.6 Identificación de fuentes: <i>Positive Matrix Factorization</i>	26
4. Resultados y discusión.....	29
4.1 Concentración y fuentes de WSOC.....	29
4.1.1 WSOC en PM ₁	29
4.1.2 Distribución másica.....	30
4.2 Absorción de la luz por WSOC.....	32
4.2.1 σ_{WSOC} en PM ₁ : caracterización y fuentes.....	32
4.2.2 Eficiencia de la absorción según tamaño.....	35
5. Conclusiones.....	37
5. Conclusions.....	39
6. Referencias.....	41
7. Anexos.....	47
Anexo I: El material particulado.....	47
Anexo II: La absorción de la radiación por aerosoles.....	49

Anexo III: Artículos publicados.....	51
---	-----------

Acrónimos

- AAE → Absorption Angstrom Exponent (Exponente de Absorción de Angstrom)
- AM → Accumulation Mode (Modo Acumulación)
- BB → Biomass Burning (Quema de biomasa)
- BC → Black Carbon (Carbono Negro)
- BrC → Brown Carbon (Carbono Marrón)
- COV → Compuestos Orgánicos Volátiles
- EC → Elemental Carbon (Carbono Elemental)
- EUSAAR → European Supersites for Atmospheric Aerosol Research (Supersitios europeos para la investigación de aerosoles atmosféricos)
- FF → Fossil Fuel (Combustible Fósil)
- FID → Flame Ionization Detector (Detector de Ionización de Llama)
- HPE → High Pollution Episode (Episodio de Alta Contaminación)
- HR → Humedad relativa
- IPCC → Intergovernmental Panel on Climate Change (Grupo Intergubernamental de Expertos sobre el Cambio Climático)
- MAE → Mass Absorption Efficiency (Eficiencia de Absorción Másica)
- MD → Mineral Dust (Polvo Mineral)
- MLR → Multiple Linear Regression (Regresión Multilineal)
- NE → Non-Event (Sin Evento)
- OC → Organic Carbon (Carbono Orgánico)
- OM → Organic Matter (Materia Orgánica)
- OMS → Organización Mundial de la Salud
- PAHs → Polycyclic Aromatic Hydrocarbons (Hidrocarburos Aromáticos Policíclicos)
- PBL → Planetary Boundary Layer (Capa Límite Planetaria)
- PCA → Principal Component Analysis (Análisis de Componentes Principales)
- PM → Particulate Matter (Material Particulado)
- PMF → Positive Matrix Factorization (Factorización de Matrices Positivas)
- POC → Primary Organic Carbon (Carbono Orgánico Primario)
- SAE → Scattering Angstrom Exponent (Exponente de Dispersión de Angstrom)
- SD → Standard Deviation (Desviación Estándar)

- SDE → Saharan Dust Event (Intrusión de Polvo Sahariano)
- SOA → Secondary Organic Aerosol (Aerosol Orgánico Secundario)
- SOC → Secondary Organic Carbon (Carbono Orgánico Secundario)
- SSA → Single Scattering Albedo (Albedo de Dispersión Simple)
- TC → Total Carbon (Carbono Total)
- TOC → Total Organic Carbon (Carbono Orgánico Total)
- UBS → Urban Background Site (Entorno Urbano de Fondo)
- WHO → World Health Organization (Organización Mundial de la Salud)
- WIOC → Water Insoluble Organic Carbon (Carbono Orgánico Insoluble en Agua)
- WLS → Weighted Least Squares (Mínimos cuadrados ponderados)
- WSI → Water Soluble Ions (Iones Solubles en Agua)
- WSOC → Water Soluble Organic Carbon (Carbono Orgánico Soluble en Agua)

Nota: Con la finalidad de darle una unificación al texto y a las figuras mostradas, se ha utilizado “.” en lugar de “,” como separador de decimales.

Listado de figuras y tablas

Figura 1. (a) Ubicación de Elche (círculo rojo) en la costa mediterránea y (b) Ubicación de la estación de muestreo (círculo en rojo) en el campus de la Universidad Miguel Hernández (Google Earth, 2024).

Figura 2. Equipos de medición: impactador MOUDI (a) y captador LVS 3.1 (b) (López A.).

Figura 3. Etalómetro AE33 (a) y nefelómetro Aurora 3000 (b) (López A.).

Figura 4. Filtros de las 5 etapas del MOUDI: 2.5, 1.4, 1.0, 0.44, y 0.25 μm (López A.).

Figura 5. Acondicionamiento de filtros (a) y balanzas de precisión (b) (López A.).

Figura 6. Esquema de la técnica ED-XRF (Tech Corp, 2024).

Figura 7. Evolución mensual del WSOC (López-Caravaca et al., 2023).

Figura 8. Contribución porcentual de WSOC en las fuentes obtenidas (López-Caravaca et al., 2023).

Figura 9. Variación temporal de los niveles de cada fuente AS/SOA (rosa), BB (verde), SN (azul), MD (beige), RT (gris) y concentración de WSOC (en marrón) asociada a cada una de ellas (López-Caravaca et al., 2023).

Figura 10. Variabilidad diaria de las concentraciones de WSOC y PM según tamaños (López-Caravaca et al., 2024b).

Figura 11. Distribución de tamaños de WSOC y PM durante días sin eventos (NE) y eventos de contaminación (HPE y SDE) (López-Caravaca et al., 2024b).

Figura 12. Evolución temporal de $\sigma_{\text{WSOC},370}$ y $\sigma_{\text{WIOC},370}$ (López-Caravaca et al., 2024a).

Figura 13. Contribución porcentual de fuentes al valor global de σ_{WSOC} durante los periodos cálido y frío (López-Caravaca et al., 2024a).

Figura 14. Evolución temporal de las fuentes de $\sigma_{\text{WSOC},370}$ (López-Caravaca et al., 2024a).

Figura 15. Coeficientes de correlación de Spearman (ρ) entre WSOC y $\sigma_{\text{BrC},370}$ (azul) y levoglucosano (rosa) (López-Caravaca et al., 2024b).

Tabla 1. Parámetros del análisis de regresión multilineal de $\sigma_{\text{BrC},370}$ (López-Caravaca et al., 2024a).

Resumen

Este estudio ha analizado la evolución temporal y las fuentes de carbono orgánico soluble en agua (WSOC) en partículas submicrométricas en un emplazamiento urbano de Elche (España) a lo largo del año 2021. Para tal fin se monitorizaron filtros de PM_1 ($N = 200$) a partir de los cuales se obtuvieron los siguientes constituyentes químicos: carbono orgánico (OC) y elemental (EC), WSOC, levoglucosano, análisis elemental y iones principales. Se completó el estudio analizando la distribución másica del WSOC en el modo de acumulación utilizando para ello mediciones segregadas por tamaño (0.25, 0.44, 1.0, 1.4 μm) obtenidas gracias a un impactador en cascada tipo MOUDI. Simultáneamente, se caracterizó la absorción y dispersión de la radiación por parte del WSOC. A partir de los resultados de la distribución másica de WSOC también se obtuvo el tamaño con mayor eficiencia de absorción.

Durante el periodo de estudio, las restricciones de tráfico debidas a la COVID-19 dieron lugar a concentraciones de PM_1 y compuestos carbonosos inferiores a las esperadas. La concentración media anual de WSOC fue de $0.95 \mu g \cdot m^{-3}$, con valores máximos durante los meses más fríos. El análisis de fuentes determinó tres fuentes principales de WSOC: quema de biomasa (BB-30.6 %), dominante durante los meses más fríos, el tráfico rodado (RT-23.9 %), se presentó como una fuente bastante estable y la contribución de una fuente relacionada con la formación de aerosoles orgánicos secundarios (SOA-33.8 %), dominante durante el periodo más cálido. Fuentes minoritarias fueron: el polvo mineral (MD-7.4 %) y el nitrato secundario (SN-4.2 %).

Para determinar la contribución de diferentes fuentes a la absorción de luz de WSOC (σ_{WSOC}) se obtuvieron previamente los valores $\sigma_{BrC,\lambda}$. La contribución media del BrC a la absorción total fue de ~ 29 % a 370 nm, revelando una influencia significativa del BrC a la absorción de luz. Asumiendo que la absorción de luz del BrC procedía de WSOC y WIOC, se utilizó un modelo de regresión multilineal (MLR) para estimar σ_{WSOC} y σ_{WIOC} . Los valores medios ($\pm SD$) fueron muy similares para ambos componentes: $\sigma_{WSOC,370} = 1.6 (\pm 0.7) Mm^{-1}$ y $\sigma_{WIOC,370} = 1.9 (\pm 0.7) Mm^{-1}$. Utilizando las fuentes mayoritarias determinadas de WSOC junto con nuevamente un análisis MLR se estimó la contribución de cada una de ellas. Los resultados apuntan a la quema de biomasa como fuente dominante de σ_{WSOC} durante la estación fría, con una contribución de ~ 37 %. Las fuentes de polvo mineral y nitrato secundario, que no se incluyeron en el modelo debido a su baja contribución a la concentración másica de WSOC, representaron un porcentaje significativo de σ_{WSOC} durante este periodo. El aerosol orgánico secundario fue la principal fuente durante la estación cálida (~ 56 %), seguida de las emisiones del tráfico (~ 30 %). Por último, se seleccionó un mes (11 Ene 2021 a 11 Feb 2021) para explorar las diferencias en las distribuciones de tamaño de masa del WSOC en diferentes condiciones meteorológicas y determinar el tamaño más eficiente para la absorción de luz por el WSOC en el modo de acumulación. Se observaron diferencias significativas en las concentraciones de WSOC y en los valores de $\sigma_{ap,\lambda}$ durante los episodios de elevada estabilidad atmosférica en comparación con los días sin eventos. Los aumentos de las concentraciones de WSOC durante estos episodios se asociaron muy probablemente a la producción fotoquímica de compuestos secundarios (en el submodo condensación) y a la absorción de agua (en el submodo droplet). No se detectaron aumentos significativos de los niveles de WSOC durante los eventos de polvo sahariano. El WSOC medido en el corte de tamaño más pequeño (0.25 μm) fue emitido principalmente por la quema de biomasa (BB) y mostró la mayor eficiencia de absorción de luz.

Abstract

This study has analysed the temporal evolution and sources of water-soluble organic carbon (WSOC) in submicrometric particulate matter at an urban site in Elche (Spain) over the year 2021. For this purpose, PM₁ filters (N = 200) were monitored and the following chemical constituents were obtained: organic carbon (OC) and elemental carbon (EC), WSOC, levoglucosan, elemental analysis and main ions. The study was completed by analysing the mass distribution of WSOC in the accumulation mode using size segregated measurements (0.25, 0.44, 1.0, 1.4 μm) obtained with a MOUDI cascade impactor. Simultaneously, the absorption and scattering of solar radiation by the WSOC was characterised. From the results of the WSOC mass distribution, the size with the highest absorption efficiency could also be obtained.

During the study period, traffic restrictions due to COVID-19 resulted in lower than expected concentrations of PM₁ and carbonaceous compounds. The annual average WSOC concentration was 0.95 μg·m⁻³, with maximum values during the coldest months. The source analysis determined three main sources of WSOC: biomass burning (BB-30.6%), dominant during the coldest months, road traffic (RT-23.9%), presented as a rather stable source and the contribution of a source related to secondary organic aerosol formation (SOA-33.8%), dominant during the warmest period. Minority sources were mineral dust (MD-7.4%) and secondary nitrate (SN-4.2%).

To determine the contribution of different sources to the light absorption of WSOC (σ_{WSOC}), the values $\sigma_{\text{BrC},\lambda}$ were previously obtained. The average contribution of BrC to the total aerosol absorption was ~29% at 370 nm, revealing a significant influence of BrC to the light absorption in the study area. Assuming that the light absorption of BrC came from WSOC and WIOC, a multi-linear regression (MLR) model was used to estimate σ_{WSOC} and σ_{WIOC} . The mean values (\pm SD) were very similar for both components: $\sigma_{\text{WSOC},370}=1.6 (\pm 0.7) \text{ Mm}^{-1}$ and $\sigma_{\text{WIOC},370}=1.9 (\pm 0.7) \text{ Mm}^{-1}$. Using the majority sources determined from WSOC together with again MLR analysis the contribution of each of them was estimated. The results point to biomass burning as the dominant source of σ_{WSOC} during the cool season, with a contribution of ~37%. Mineral dust and secondary nitrate sources, which were not included in the model due to their low contribution to the WSOC mass concentration, accounted for a significant percentage of σ_{WSOC} during this period. Secondary organic aerosol was the main source during the warm season (~56%), followed by traffic emissions (~30%). Finally, one month (11 Jan 2021 to 11 Feb 2021) was selected to explore differences in WSOC mass size distributions under different meteorological conditions and to determine the most efficient size for light absorption by WSOC in the accumulation mode. Significant differences in WSOC concentrations and $\sigma_{\text{ap},\lambda}$ values were observed during episodes of high atmospheric stability compared to non-event days. Increases in WSOC concentrations during these episodes were most likely associated with photochemical production of secondary compounds (in the condensation sub-mode) and water absorption (in the droplet sub-mode). No significant increases in WSOC levels were detected during Saharan dust events. WSOC measured at the smallest size cut-off (0.25 μm) was mainly emitted by biomass burning (BB) and showed the highest light absorption efficiency.

1. Introducción

En los últimos tiempos, el interés científico por los aerosoles atmosféricos se ha dirigido hacia sus constituyentes carbonosos. Estos compuestos pueden representar entre el 20 % y el 50 % de la concentración total de partículas en zonas continentales de latitudes medias y llegar hasta el 90 % en bosques tropicales (Molnár et al., 1999; Kanakidou et al., 2005). A su significativa abundancia en la atmósfera y a su composición química específica que los caracteriza, habría que añadir un factor muy importante que aumenta la potencialidad de sus efectos: sus propiedades higroscópicas (Mladenov et al., 2011; Viana et al., 2006). En efecto, la presencia de compuestos orgánicos solubles en agua influye en la higroscopicidad de las partículas atmosféricas y, por tanto, en su capacidad para actuar como núcleos de condensación y formar nubes, lo que tiene un importante impacto sobre el clima (Jacobson et al., 2000; Kanakidou et al., 2005; Asa-Awuku et al., 2009). Destacar también, la gran capacidad de absorción de radiación en el rango UV cercano y visible de algunos de estos compuestos (Laskin et al., 2015; Park y Son, 2017).

Por otra parte, el interés por el estudio de la fracción soluble en agua del aerosol orgánico se debe asimismo a que, una vez inhalado, puede producir efectos adversos específicos y significativos sobre la salud humana (Tuet et al., 2016; Velali et al., 2016).

Estos efectos dependen de la concentración, tamaño y composición química de las partículas atmosféricas que, a su vez, están condicionados por la distribución de fuentes naturales y antropogénicas y las condiciones climáticas del área geográfica considerada.

El carbono total presente en las partículas atmosféricas se clasifica tradicionalmente en carbono elemental (EC), también llamado carbono negro u hollín (BC) y carbono orgánico (OC). Éste, a su vez, se subdivide en carbono orgánico primario (POC) y carbono orgánico secundario (SOC). En función de su solubilidad en agua el OC puede clasificarse, a su vez, en carbono orgánico soluble en agua (WSOC) y carbono orgánico insoluble (WIOC) (Matsumoto et al., 2022).

El WSOC es una compleja mezcla constituida por sustancias orgánicas polares (neutras, ácidas y básicas) de difícil análisis completo (Park and Kim, 2014). Comprende aerosoles primarios, principalmente de la combustión de biomasa y, en gran parte, compuestos orgánicos secundarios formados en la atmósfera en procesos de oxidación fotoquímica de compuestos orgánicos volátiles preexistentes (Decesari et al., 2006; Viana et al., 2008; Sun et al., 2011; Park et al., 2013). El WSOC representa la fracción más oxidada del aerosol orgánico, contribuye de manera significativa (20-70 %) al contenido total de carbono del aerosol atmosférico (Sullivan et al., 2004; Viana et al., 2007; Park and Cho, 2011) y contiene grupos funcionales oxigenados como grupos carboxilo, hidroxilo y carbonilo, etc. Un ejemplo de compuestos WSOC serían el oxalato ($C_2O_4^{2-}$) y el levoglucosano ($C_6H_{10}O_5$).

El WSOC puede ser emitido directamente por las fuentes (primario) o resultar de procesos atmosféricos (secundario) (Hecobian et al., 2010). Las emisiones directas de la quema de biomasa (BB) y aerosoles orgánicos secundarios (SOA) son las dos fuentes más significativas de WSOC. Sin embargo, el WSOC puede liberarse en menor medida a partir de otras fuentes, como las emisiones de vehículos de motor (Xie et al., 2016; Yu y Park, 2021) o el polvo del suelo (Yu et al., 2021). Por lo tanto, las características químicas del WSOC en los aerosoles atmosféricos son

específicas de la ubicación de la zona de estudio y pueden proporcionar información sobre el origen del PM atmosférico.

La contribución del WSOC al contenido total de OC de los aerosoles atmosféricos, por tanto, depende de las fuentes de emisión (Saarikoski et al., 2008), siendo la relación WSOC/OC mayor para las fuentes secundarias que para las primarias. En entornos urbanos europeos, la contribución media de los WSOC al OC total suele variar entre el 20 % y el 70 % para partículas finas (PM_{2.5} y PM₁) (Pio et al., 2007; Viana et al., 2007; Paraskevopoulou et al., 2014; Cesari et al., 2020).

De especial relevancia resulta también el estudio de la distribución por tamaño del WSOC, ya que puede proporcionar información específica sobre las fuentes y los mecanismos de formación de estos compuestos (Huang et al., 2006; Timonen et al., 2008; Park and Kim, 2014). La distribución en masa por tamaños del WSOC suele mostrar un máximo pronunciado en el modo de acumulación (AM) (0.1-1.5 μm), independientemente de las características del lugar de muestreo, de hecho, más del 60 % del WSOC se distribuye en la fracción submicrométrica (Matta et al., 2003; Duarte et al., 2008; Timonen et al., 2008; Bougiatioti et al., 2013; Frka et al., 2018). El WSOC distribuido en el AM está preferentemente asociado a las emisiones de BB y a los procesos de formación de SOA (Yu et al., 2017), mientras que el WSOC en la fracción gruesa procede de aerosoles marinos (Timonen et al., 2008) o de fuentes biogénicas primarias (Yttri et al., 2011).

Se ha demostrado que las concentraciones de WSOC en entornos urbanos suelen ser mayores en invierno que en verano (Viana et al., 2007; Du et al., 2014; Witkowska y Lewandowska, 2016; Frka et al., 2018; Kaskaoutis et al., 2022). Esto puede explicarse teniendo en cuenta que las contribuciones de las emisiones de combustión locales a la carga másica de materiales carbonosos son mayores durante el invierno, como consecuencia del mayor consumo energético y de las malas condiciones de dispersión atmosférica durante esta estación (Park y Cho, 2011). Sin embargo, otros estudios han informado de un patrón estacional diferente. Como ejemplo, Taghvaei et al. (2019) y Snyder et al. (2009), hallaron concentraciones más altas de WSOC durante el verano en Atenas (Grecia) y el Medio Oeste de Estados Unidos, respectivamente, lo que es coherente con la producción fotoquímica de carbono orgánico secundario (SOC).

Desde el punto de vista de la absorción de la radiación, el WSOC se suele utilizar como equivalente del BrC soluble en agua (Liu et al., 2013). El término BrC se ha utilizado para describir el componente de carbono orgánico que absorbe la radiación de manera eficiente en los rangos cercano al ultravioleta y visible (Laskin et al., 2015). La absorción de radiación por el WSOC puede ser comparable a la del carbono elemental (EC) en longitudes de onda ultravioleta (Kirillova et al., 2016; Mo et al., 2021) y tiene un efecto de forzamiento radiativo positivo (Zhou et al., 2022). Por lo tanto, no se puede ignorar la contribución a la absorción de la luz del WSOC en longitudes de onda cortas. Del mismo modo, varios trabajos han demostrado que la absorción de radiación solar por WIOC es comparable e incluso superior a la de WSOC (Huang et al., 2018; Satish et al., 2020; Solemanian et al., 2020; Paraskevopoulou et al., 2023).

Las propiedades de absorción de luz de WSOC o/y BrC pueden depender en gran medida de la fuente (Feng et al., 2013). Esto se debe a la diferente composición química de los cromóforos

(sustancias químicas que tienen electrones capaces de absorber energía en longitudes de onda cortas (UV)) como resultado de las diferentes fuentes de BrC (Huang et al., 2018). La distribución de fuentes de WSOC sigue siendo un reto debido a sus complejos procesos de formación y a la amplia gama de fuentes primarias y secundarias (Mo et al., 2021). La determinación de la contribución de las fuentes a la absorción de luz por WSOC o BrC suele realizarse mediante análisis multivariante (PMF, PCA...) conjuntamente con un análisis MLR (Du et al., 2014., Geng et al., 2020; Solemanian et al., 2020; Ponczek et al., 2022). Las principales fuentes que contribuyen a la absorción de luz por el WSOC son: el BB, principalmente durante la estación fría, los aerosoles orgánicos secundarios y las fuentes relacionadas con las emisiones de vehículos o combustión de combustibles fósiles (Du et al., 2014; Solemanian et al., 2020). Sin embargo, también se han identificado otras fuentes como el SOA biogénico (Zhou et al., 2022), las emisiones primarias de microorganismos/plancton (Geng et al., 2020) o el MD (Jin et al., 2020).

La capacidad de absorción de luz del WSOC de cada fuente puede evaluarse en función del valor de su eficiencia de absorción molar (MAE). La mayoría de los trabajos (Moschos et al., 2018; Geng et al., 2020; Zhou et al., 2022) han informado de que la MAE del WSOC procedente de emisiones de BB es la más elevada, ya que en este caso los cromóforos contribuyen en gran medida a la absorción de luz de los aerosoles atmosféricos (Fan et al., 2016). Sin embargo, el WSOC derivado de combustibles fósiles también puede tener una alta capacidad de absorción de luz (Mo et al., 2021), y algunos estudios han mostrado valores incluso más altos que los del WSOC de la quema de biomasa (Yan et al., 2018). El WSOC secundario suele tener una menor capacidad de absorción de luz, especialmente el WSOC formado a partir de precursores biogénicos (Lambe et al., 2013).

En cuanto a la estacionalidad de la absorción por WSOC, esta depende no sólo de su concentración en masa, sino también de las fuentes imperantes durante cada estación. Por ejemplo, en las zonas urbanas la absorción por WSOC suele ser mayor en invierno debido a la mayor contribución de las emisiones de BB. La relación invierno/verano varía entre 2 y 6 para la mayoría de los entornos urbanos (Moschos et al., 2018; Gilardoni et al., 2020; Solemanian et al., 2020).

2. Objetivos

El objetivo principal de esta tesis es la caracterización del WSOC en partículas submicrométricas en un entorno urbano.

Como objetivos específicos surgen los siguientes:

1. Analizar la evolución temporal de la concentración de WSOC.
2. Identificar y caracterizar las fuentes de WSOC.
3. Cuantificar la contribución de WSOC en la absorción de la radiación y estimar la importancia de cada fuente emisora en el proceso.
4. Determinar el tamaño de partícula más eficiente en la absorción de luz debida al WSOC.

3. Metodología

3.1 Descripción del punto de muestreo

El estudio se realizó en el campus de Elche de la Universidad Miguel Hernández (UMH). El punto de muestreo está situado en la periferia de la ciudad (38°16' N; 0°41' O) a unos 2 km del centro urbano, a 15 km de la costa mediterránea y a 93 m.s.n.m. Elche es una ciudad de tamaño medio en el sureste español, con unos 236000 habitantes (INE, 2022). No existen grandes industrias en la ciudad ni en su entorno emisoras de material particulado (PM), por lo que su principal fuente en el área urbana es el tráfico rodado (Yubero et al., 2015).

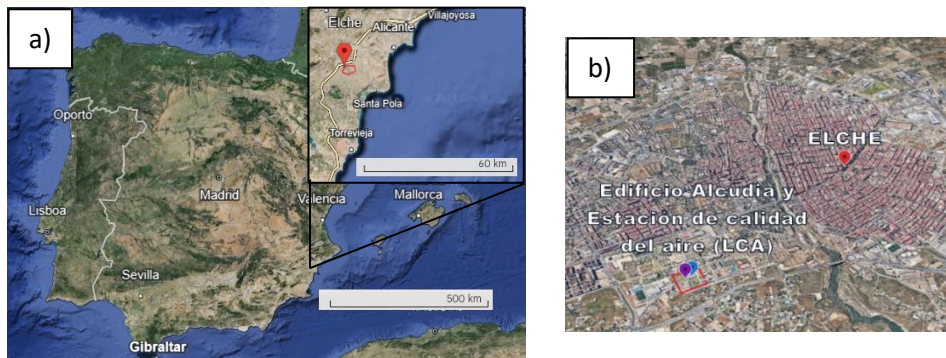


Figura 1. (a) Ubicación de Elche en España y (b) Ubicación de la estación de muestreo (recuadro en rojo) en el campus de la Universidad Miguel Hernández (Google Earth, 2024).

El área de estudio se caracteriza por tener un clima mediterráneo árido, con precipitaciones muy escasas de valores anuales que no superan los $300 \text{ L}\cdot\text{m}^{-2}$ y concentradas durante los meses de otoño y primavera. Los regímenes de brisas marinas (E-SE) son muy frecuentes durante los meses de verano, mientras que durante el invierno el viento procede del noroeste y suroeste. La temperatura media en la ciudad oscila entre $27 \text{ }^\circ\text{C}$ (agosto) y $12 \text{ }^\circ\text{C}$ (enero). La radiación solar es elevada durante la mayor parte del año, con valores medios diarios de 200 y $300 \text{ W}\cdot\text{m}^{-2}$ de abril a septiembre. El número total de horas de sol al año supera las 2800.

El emplazamiento de muestreo es de fondo urbano, con una fuente de tráfico eventual que se debe principalmente a los desplazamientos de los estudiantes y el personal del campus durante la semana laboral. En el entorno cercano al punto de muestreo se ubican casas de campo que utilizan la chimenea como método calefactor en los meses fríos de invierno y realizan quemas de rastrojos entre los meses de octubre a mayo.

El estudio se realizó durante el año 2021, incluyendo el periodo en que estuvieron vigentes ciertas medidas de seguridad que tomó la universidad frente a la COVID-19. Entre ellas, fue relevante la implantación de clases telemáticas que evitaron los desplazamientos de vehículos hasta el campus.

La estación de muestreo, ubicada junto al edificio Alcudia en el interior de la UMH, estaba integrada por dos equipos instalados a 2 m del suelo que recogían simultáneamente el material particulado atmosférico: un captador de bajo volumen (LVS) Derenda 3.1 con un caudal de 2.3

$\text{m}^3 \cdot \text{h}^{-1}$ y que se utilizó para recoger la fracción PM_{10} y un impactador en cascada tipo MOUDI (Micro-Orifice Uniform Deposit Impactor, MS Modelo 131B HFI) que recogía el material particulado fraccionado en 4 etapas (1.4, 1.0, 0.44, 0.25 μm) y operaba a un caudal de $100 \text{ L} \cdot \text{min}^{-1}$. Las muestras de aerosol se recogieron, respectivamente, en filtros de fibra de cuarzo de 47 mm de diámetro y en filtros de membrana de policarbonato (PCTE, Membrana de Policarbonato Track Etched) de 76 mm de diámetro.



Figura 2. Equipos de medición: (a) impactador MOUDI y (b) captador LVS 3.1 (López A.).

La estación se complementaba con dos equipos para medir las propiedades ópticas del aerosol: etalómetro (Magee, AE33) para medir la absorción de luz y nefelómetro (Ecotech, Aurora 3000) utilizado para medir la dispersión de luz.

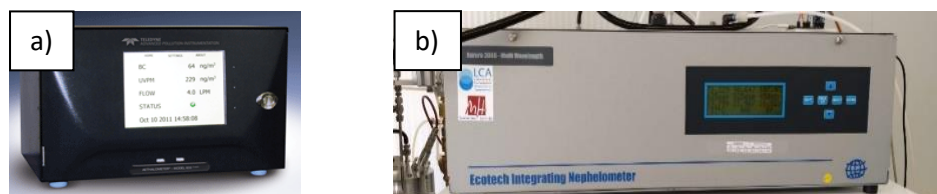


Figura 3. Etalómetro AE33 (a) y nefelómetro Aurora 3000 (b) (López A.).

3.2 Campaña de muestreo

La campaña de muestreo se extendió desde el 10 de diciembre de 2020 al 22 de diciembre de 2021. Se recogieron un total de 209 muestras diarias de PM_{10} y 128 muestras diarias de las 4 etapas del MOUDI. Durante parte de la campaña de muestreo ambos equipos recogieron muestras en paralelo. No obstante, existieron algunas diferencias que se explican a continuación.

3.2.1 Muestreo con LVS 3.1 Derenda

La campaña se inició el 11 de enero de 2021 y finalizó el 22 de diciembre de 2021, con una frecuencia de muestreo diaria (comenzando a las 9:00 h, hora local), durante el primer mes. Pasado ese tiempo, la frecuencia de muestreo pasó a ser de domingo a jueves.

3.2.2 Muestreo con impactador en cascada MOUDI

La campaña de muestreo con el MOUDI se realizó en dos periodos. El periodo de recogida de muestras de invierno comenzó el 10 de diciembre de 2020 hasta el 30 de marzo de 2021 y el periodo de recogida de muestras de los meses cálidos tuvo lugar del 8 de septiembre de 2021 al 28 de octubre de 2021. La frecuencia de muestreo fue análoga a la recogida de muestras con el LVS.



Figura 4. Filtros de las 5 etapas del MOUDI: 2.5, 1.4, 1.0, 0.44, y 0.25 µm (López A.).

3.3 Análisis de muestras

3.3.1 Determinación gravimétrica de la concentración ambiental de aerosol

En las Directivas 2008/50/CE de 21 de mayo de 2008 y 2015/1480/CE de 28 de agosto de 2015, vienen detalladas las principales regulaciones relativas a la *Calidad del aire ambiente y a una atmósfera más limpia en Europa*. Entre otras disposiciones, se especifica el procedimiento para establecer la concentración de material particulado atmosférico según el método gravimétrico, descrito en la norma UNE-EN 12341:2015. Siguiendo la misma, los filtros empleados en este estudio fueron acondicionados en una cámara ambientalmente controlada a una temperatura de $(20 \pm 1 \text{ }^\circ\text{C})$ y una humedad relativa de (45-50 %) durante 48 horas antes de realizar las pesadas. Los filtros de PM_{10} se pesaron utilizando una balanza analítica (Ohaus, modelo AP250D), mientras que los filtros del MOUDI se pesaron empleando una balanza electrónica (Mettler Toledo® XP 105), ambas balanzas tenían una sensibilidad de 10 µg. Cada filtro se pesó tres veces en tres días distintos, antes y después de realizar el muestreo. Una vez pesados, los filtros muestreados se conservaron a 5-8 °C hasta realizar los análisis.

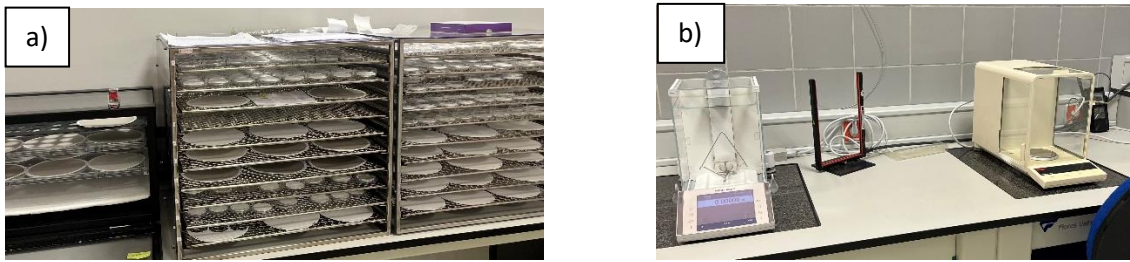


Figura 5. (a) Acondicionamiento de filtros y (b) balanzas de precisión utilizadas (López A.).

Se analizaron las muestras de PM_{10} para la determinación de elementos metálicos, del contenido en carbono orgánico (OC) y carbono elemental (EC), de iones hidrosolubles, levoglucosano y WSOC. Las muestras recogidas en el MOUDI únicamente se analizaron para determinar el contenido de WSOC.

3.3.2 Análisis elemental

Para calcular la composición elemental de las muestras de PM_{10} se utilizó un espectrómetro de fluorescencia de rayos-X por energía dispersiva (ED-XRF) ARL Quant'x (Thermo Fisher Scientific, Reino Unido).

El fundamento de esta técnica no destructiva consiste en irradiar las partículas de aerosol con rayos-X primarios de energía suficiente para extraer electrones de capas internas de los átomos presentes en la muestra. Al perder electrones, los átomos pasan a un estado excitado y cuando electrones de energía superior ocupan el lugar de los electrones expulsados, los átomos vuelven al estado fundamental. Consecuentemente, en esta transición electrónica se emite un fotón, radiación X fluorescente o secundaria. La energía del fotón fluorescente será característica para cada transición energética y cada elemento presenta unas transiciones específicas. De esta manera, se pueden identificar los elementos que componen la muestra a partir de la medición de la energía de la radiación fluorescente emitida (análisis cualitativo) y se puede determinar la concentración de cada elemento midiendo la intensidad o número de fotones por unidad de tiempo (análisis cuantitativo) (Figura 6).

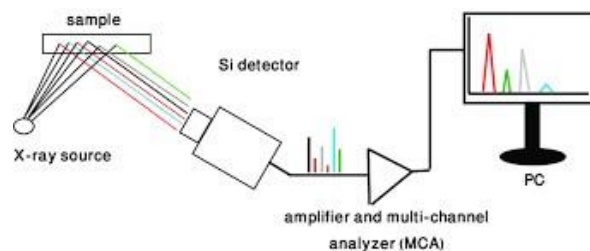


Figura 6. Esquema de la técnica ED-XRF (Tech Corp, 2024).

Los elementos que se han podido cuantificar son: S, K, Ca, Ti, V, Cr, Mn, Fe, Ni, Cu y Zn.

3.3.3 Análisis termo-óptico de transmisión

Para la determinación del contenido de OC y EC de las muestras de PM₁, se utilizó un analizador termo-óptico de transmisión (TOT) (Sunset, Inc.) y el protocolo de análisis EUSAAR-2. Esta técnica requiere un fragmento de filtro de 1.5 cm² para realizar los análisis.

El análisis se divide en dos etapas, la primera ocurre en atmósfera inerte (He) y la segunda en atmósfera oxidante (He + O₂). Mediante las rampas de temperatura que marca el protocolo de análisis y el registro de la variación de transmisión de luz laser a través de la muestra, el equipo es capaz de separar las masas de OC (OC volátil + OC pirolizado) y EC. Mediante los catalizadores adecuados, el equipo transforma el carbono pirolizado en CO₂ y éste en CH₄ que es medido mediante un FID de llama calibrado.

El correcto funcionamiento del equipo se verificó diariamente analizando una muestra de sacarosa de concentración conocida (2.198 µg C·µl⁻¹). Además, mensualmente se realizó una recta de calibrado a partir de distintas disoluciones de sacarosa de concentraciones seleccionadas.

3.3.4 Cromatografía iónica

El contenido en el aerosol de iones solubles en agua se determinó mediante cromatografía iónica.

Previamente, medio filtro captado de PM₁ introducido en 8.5 mL de agua ultrapura se sometió a un baño de ultrasonidos durante 45 minutos. De esta extracción, se obtuvieron tres alícuotas de aproximadamente 2.5 mL, que se utilizaron para el análisis de aniones, cationes y WSOC (apartado 3.3.5).

El otro medio filtro menos el fragmento de 1.5 cm² (utilizado para la determinación del contenido en OC y EC), se empleó para la determinación del contenido en levoglucosano, extraído de la misma manera con 3.5 mL de agua ultrapura.

Las alícuotas resultantes se filtraron con filtros Tracer® de nylon de 25 mm de diámetro y 0.45 µm de diámetro de poro para eliminar los restos de fibras e impurezas del filtro. Filtros “blancos” de referencia fueron analizados de forma análoga a las muestras.

Seguidamente, se utilizaron las alícuotas filtradas para determinar los siguientes componentes por cromatografía iónica:

- **Aniones.** Se ha empleado un cromatógrafo Dionex DX-120 equipado con una columna de intercambio aniónico AS11-HC (4x250 mm) y una columna supresora ARS-300 (4 mm). Como eluyente se ha utilizado una disolución de hidróxido de sodio 15 mM con un flujo de 1 mL·min⁻¹. Se han podido determinar las concentraciones de Cl⁻, NO₃⁻, SO₄²⁻, y C₂O₄²⁻.
- **Cationes.** Se ha utilizado un cromatógrafo Dionex ICS-1100 con una columna analítica CS12A (4x250 mm) y una columna supresora CSRS-300 (4 mm). El eluyente utilizado ha sido ácido metanosulfónico 20 mM con un flujo de 0.8 mL·min⁻¹. Se ha podido cuantificar el contenido de Na⁺, NH₄⁺, K⁺, Mg²⁺ y Ca²⁺ de las muestras.
- **Anhidroazúcares.** Para la determinación de levoglucosano se ha empleado la cromatografía de intercambio aniónica de alta resolución (*High Performance Anion Exchange Chromatography*, HPAEC) acoplada con detección amperométrica pulsada

(*Pulsed Amperometric Detection*, PAD). El cromatógrafo utilizado es Dionex Integrion equipado con un detector electroquímico (electrodo de trabajo de oro) y una columna analítica Dionex Carbopac (PA10 (250 x 4 mm). El perfil de elución empleado fue el siguiente: 18 mM (0-2 min), 200 mM (2-9 min, limpieza de la columna), 18 mM (9-29 min, reequilibración de la columna). El flujo del eluyente NaOH fue de $0.5 \text{ mL} \cdot \text{min}^{-1}$.

3.3.5 Determinación de *Water Soluble Organic Carbon*

Las muestras de PM_{10} se analizaron para determinar el contenido de WSOC utilizando la alícuota de 2.5 mL resultante de la extracción de medio filtro en 8.5 ml de agua ultrapura en un baño de ultrasonidos durante 45 minutos. Los filtros del MOUDI se extrajeron de manera análoga, tomando medio filtro y 5.5 mL de volumen de extracción.

Se utilizó un analizador TOC-L CSH (Shimadzu) para la determinación de los compuestos orgánicos solubles en agua (*Water Soluble Organic Carbon*, WSOC). El instrumento utiliza un método de oxidación catalítica por combustión a $680 \text{ }^\circ\text{C}$. El WSOC se cuantificó como carbono orgánico no purgable (NPOC). Para ello, se diluyó una alícuota filtrada 1:2 con agua ultrapura, se acidificó con HCl 1M (PanReac AppliChem) y se purgó con aire puro para eliminar el carbono inorgánico disuelto y los orgánicos volátiles. Los análisis se realizaron por triplicado y las concentraciones de WSOC se calcularon como el valor medio de las tres mediciones. La calibración se realizó utilizando una solución estándar de hidrogenoftalato de potasio (PanReac AppliChem). Las concentraciones de todas las muestras superaron el límite de detección del equipo.

3.4 Absorción de la luz

Para la determinación de la absorción de luz por los aerosoles atmosféricos ($\sigma_{\text{ap},\lambda}$) se empleó un etalómetro modelo AE33 (Magee Scientific, EE.UU.). En principio el AE33 proporciona valores de atenuación de la luz a causa del PM acumulado en un filtro móvil en siete longitudes de onda diferentes: 370 nm (UV), 470 nm (Azul), 520 nm (Verde), 590 nm (Amarillo), 660 nm (Rojo), 880 nm (IR) y 950 nm (IR). Sin embargo, el valor de atenuación que se obtiene (σ_{ATN}) es superior al verdadero valor de absorción ($\sigma_{\text{ap}} < \sigma_{\text{ATN}}$) debido a un efecto que tiene lugar en el filtro donde se acumula el PM conocido como “efecto de multidispersión”. El efecto se basa en que existe un incremento de la atenuación debido a la multidispersión que sufre la luz al atravesar las fibras que constituyen el filtro donde se deposita el PM. Para corregir este efecto los valores de atenuación son divididos por un factor (H^*) que depende del tipo de filtro utilizado en el AE33, en nuestro caso su valor vale 1.76 (Savadkoobi et al. 2023). Una vez conocido el valor de σ_{ap} se puede obtener el valor de concentración de BC para cada λ .

El instrumento funcionó a un caudal de aire constante de $3.9 \text{ L} \cdot \text{min}^{-1}$. La resolución temporal fue de 1 min. Posteriormente se calcularon las medias diarias de σ_{ap} y carbono negro (*Black Carbon*, BC) a 880 nm. Los datos se distribuyeron uniformemente a lo largo del año. El Exponente de Angstrom de Absorción (*Absorption Angstrom Exponent*, AAE) se obtuvo a partir de σ_{ap} mediante la ecuación (1):

$$AAE = - \frac{\ln \frac{\sigma_{\text{ap}}(\lambda_1)}{\sigma_{\text{ap}}(\lambda_2)}}{\ln \frac{\lambda_1}{\lambda_2}} \quad (1)$$

dónde $\lambda_1 = 370$ nm y $\lambda_2 = 950$ nm.

Este parámetro informa sobre la composición química de las partículas que están absorbiendo. Cuando el BC es el componente absorbente dominante del aerosol, el valor de AAE es cercano a 1, mientras que cuando hay una notable influencia de polvo mineral o/y BrC suelen tener valores de AAE significativamente superiores a 1.

3.4.1 Absorción de la luz por BrC

Para determinar la contribución de BrC a la absorción de la luz (σ_{BrC}) para cada longitud de onda, se utilizó la metodología descrita en Kaskaoutis et al. (2021), denominada “modelo BrC”. Este enfoque se basa en el supuesto de que la absorción de la luz no se ve influida por el MD, por tanto, con el fin de evitar el efecto de la absorción de luz por el MD transportado con frecuencia hasta la zona de estudio desde el norte de África, se eliminaron de la base de datos los días que se identificaron bajo la influencia de una intrusión sahariana. Según la ecuación (2), el coeficiente de absorción total medido ($\sigma_{ap,\lambda}$) puede tener dos contribuciones: la absorción por BC y la absorción por BrC.

$$\sigma_{ap\lambda} = \sigma_{BC\lambda} + \sigma_{BrC\lambda} \quad (2)$$

Esta metodología se basa en asumir que el BC es el único componente absorbente a $\lambda = 880$ nm y que su dependencia espectral para el resto de longitudes de onda es función de λ^{-1} . La contribución de BrC para cada longitud de onda se estimó posteriormente según la ecuación (2) a partir de las desviaciones entre los valores de σ_{ap} medidos para cada λ y los obtenidos en función de λ^{-1} . Este procedimiento se ha utilizado ampliamente para determinar el valor de $\sigma_{BrC\lambda}$ a partir de mediciones del etalómetro (Ran et al., 2016; Nicolás et al., 2018; Gilardoni et al., 2020; Pani et al., 2021).

3.4.2 Absorción de la luz por WSOC

Alternativamente, el coeficiente de absorción de BrC también puede determinarse mediante análisis espectrofotométrico de los extractos acuosos de muestras de PM sin la interferencia de BC y otras partículas insolubles en agua (Hecobian et al., 2010). La fracción de OC soluble en metanol (MSOC) muestra valores de $\sigma_{BrC\lambda}$ más altos que la OC soluble en agua (WSOC), ya que el metanol (a diferencia del agua) puede extraer cromóforos con mayores pesos moleculares y características de absorción más altas (Zhang et al., 2013). Sobre esta base, la extracción con agua permite determinar la absorción del BrC soluble en agua (WSBrC), mientras que la extracción con metanol es un enfoque alternativo para medir la absorción total de luz del BrC. Hoy en día, el uso de los coeficientes de absorción de BrC y/o WSBrC determinados mediante análisis espectrofotométrico es el procedimiento más empleado para medir la absorción de luz por BrC (Du et al., 2014; Soleimanian et al., 2020; Paraskevopoulou et al., 2023).

En el presente estudio no se pudo utilizar la metodología descrita anteriormente debido a que la muestra era insuficiente, por ello, se optó por un análisis MLR para estimar la absorción por WSBrC (σ_{WSOC}). Para ello, asumimos que las concentraciones máscas de BrC eran las mismas que las de OC (Pani et al., 2021). La ecuación (3) del modelo es la siguiente:

$$y = b_0 + b_1x_1 + b_2x_2 + \dots + b_kx_k + \varepsilon \quad (3)$$

dónde y son los datos de salida que debe predecir el modelo (en este trabajo, $\sigma_{BrC,\lambda}$), x_i son las variables de entrada independientes (en el presente estudio, las concentraciones máscas de

WSOC y WIOC), b_i son las constantes de regresión lineal, b_0 es la intersección de y (término constante) y ϵ es el término residual. En este caso, el valor de la intersección es cero, ya que la absorción de luz por BrC es la suma de la de WSOC y WIOC. Los coeficientes de regresión del modelo corresponden a los valores MAE (en $\text{m}^2 \cdot \text{g}^{-1}$) de los componentes carbonosos. La contribución relativa de cada componente químico se estimó entonces a partir de los coeficientes de regresión lineal multiplicados por sus concentraciones máxicas. No obstante, debe tenerse en cuenta que el cálculo de los valores MAE según el procedimiento descrito por Pani et al. (2021) se basa en el supuesto de que toda la fracción orgánica presenta propiedades de absorción de la luz. Dado que una fracción de OC no absorbe luz, el uso de este enfoque que considera una concentración de BrC límite superior subestimaré la eficiencia de absorción de la masa. Por lo tanto, el MAE real para el BrC será seguramente superior a los valores presentados aquí (Yang et al., 2009). Del mismo modo, la aplicación del análisis MLR para estimar los valores MAE_{WSOC} y MAE_{WIOC} proporcionará límites inferiores para estos parámetros. Este procedimiento se describe en Izhar et al. (2020). Los autores informaron de una buena correlación ($R^2=0.72$) entre σ_{WSOC} estimado por este método y la medida por extracción acuosa a $\lambda=365$ nm, aunque la absorción estimada por WSBrC fue 1.8 veces la obtenida en extractos acuosos. Gilardoni et al. (2020) obtuvieron el mismo factor al comparar los coeficientes de absorción del BrC soluble en metanol con las mediciones del etalómetro.

Por último, con el fin de cuantificar las fuentes de absorción de luz por WSOC, los factores PMF se acoplaron con el análisis MLR.

3.5 Datos meteorológicos e identificación de eventos

Los parámetros meteorológicos y los niveles de ozono (O_3) fueron obtenidos a partir una estación perteneciente a la red regional, ubicada a 2.5 km al sudeste del centro de la ciudad. Para la determinación del espesor de la capa límite planetaria (*planetary boundary layer*, PBL) se utilizó el modelo Global Data Assimilation System (GDASI) de NOAA Air Resources Laboratory (<https://www.ready.noaa.gov/READYamet.php>).

La identificación de episodios de polvo sahariano (*Saharian dust episodes*, SDE) están basados en los resultados del modelo de predicción BSCDREAM8b (<https://www.bsc.es/tech-transfer/services/mineral-dust>). Además, se utilizó el modelo de análisis de retro trayectorias HYSPLIT (Draxler y Rolph, 2015) para confirmar que el origen de las masas de aire era el norte de África. Se obtuvieron las retro trayectorias de los cuatro días anteriores al muestreo, a las 12:00 UTC a 1500 m.s.n.m. La identificación de estos eventos se confirmó mediante el análisis de series temporales de material particulado tanto en el punto de muestreo como en las estaciones regionales de fondo de la zona de estudio.

3.6 Identificación de fuentes: *Positive Matrix Factorization*

La PMF es una herramienta avanzada de análisis factorial multivariante utilizada para identificar la distribución de fuentes de contaminantes medioambientales. La teoría matemática y los principios del modelo se describen en detalle en Paatero y Tapper (1994) y Paatero (1997). A

modo de resumen, la PMF descompone la matriz de concentración de contaminantes en una matriz de perfil de factores (f) y una matriz de contribución de factores (g) según la ecuación (4):

$$X_{ij} = \sum_{k=1}^p g_{ik} f_{kj} + e_{ij} \quad (4)$$

Dónde X_{ij} representa la concentración de contaminante de la muestra i de especie química j . g_{ik} es la contribución del factor k -ésimo a la muestra i y f_{kj} es el perfil del factor k . e_{ij} representa los residuos. En la PMF, g_{ik} y f_{kj} se limitan a un valor mayor o igual que 0.

La PMF utiliza un método de mínimos cuadrados ponderados para minimizar la función objetivo Q , ecuación (5), dónde s_{ij} es la incertidumbre de la muestra i . La solución de la PMF es la que tiene el valor más bajo de Q .

$$Q = \sum_{i=1}^n \sum_{j=1}^m \frac{e_{ij}^2}{s_{ij}^2} \quad (5)$$

Este análisis se ha realizado utilizando el software EPA PMF v. 5.0 (Norris et al., 2014). Para ejecutar el modelo, los valores de concentración por debajo del límite de detección se sustituyeron por la mitad del límite de detección y los valores que faltaban se sustituyeron por el valor medio de la especie (Polissar et al., 1998).

4. Resultados y discusión

Los resultados y su discusión en este estudio han sido divididos en dos partes. La primera expone un análisis relativo a la concentración y fuentes de WSOC y la segunda hace referencia a su capacidad de absorción de luz. Ambas partes se presentan distinguiendo la caracterización del WSOC en la fracción PM_{10} y por distribución de tamaños dentro del modo de acumulación.

Estos resultados, que resuelven los objetivos iniciales planteados, están incluidos y estructurados en los siguientes tres artículos que conforman esta tesis:

- 1- *“Sources of water-soluble organic carbon in fine particles at a southern European urban background site”*. Trabajo que incluye resultados referentes a la concentración y fuentes de WSOC en la fracción PM_{10} . (Sección 4.1.1).
- 2- *“Characterization of water-soluble organic carbon absorption at an urban background site in the south-eastern Iberian Peninsula”*. Estudio que aborda la absorción de la radiación por parte del WSOC. (Sección 4.2.1).
- 3- *“WSOC in accumulation mode aerosols: distribution and relationship with BrC light absorption at an urban background site”*. Artículo que detalla la caracterización (concentración y absorción) del WSOC por fracciones de tamaño submicrométricas. (Secciones 4.1.2 y 4.2.2).

4.1 Concentración y fuentes de WSOC

4.1.1 WSOC en PM_{10}

La concentración media de WSOC obtenida en el ambiente urbano de Elche en la fracción PM_{10} fue $0.95 \mu\text{g}\cdot\text{m}^{-3}$, valor que se sitúa en la parte inferior del intervalo de valores registrados en zonas urbanas europeas. El valor medio de PM_{10} fue de $7.6 \mu\text{g}\cdot\text{m}^{-3}$, por lo que el WSOC representa el 12.5 % del PM_{10} . Por su parte, el ratio WSOC/OC obtenido (0.46) indica que prácticamente la mitad del OC es soluble.

La variabilidad temporal del WSOC se muestra en la figura 7. Los valores mensuales más elevados se registran a finales del otoño y durante el invierno. La mayor concentración media mensual ($1.43 \mu\text{g}\cdot\text{m}^{-3}$) se alcanzó en diciembre y fue en parte debido a un episodio de BB ocurrido a finales de este mes. Los niveles diarios de WSOC aumentaron significativamente bajo este tipo de eventos, de hecho, la concentración máxima diaria registrada durante el periodo de estudio ($2.8 \mu\text{g}\cdot\text{m}^{-3}$) se alcanzó un día en el que hubo actividades de quema de biomasa. Esto muestra que los niveles de WSOC en PM_{10} pueden presentar variaciones importantes en función de las fuentes de emisión.

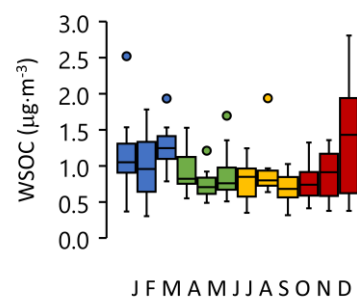


Figura 7. Evolución mensual del WSOC (López-Caravaca et al., 2023).

Gracias a la utilización de la técnica PMF se han identificado cinco fuentes de PM_{10} . Las fuentes identificadas y su contribución porcentual al valor medio anual de PM_{10} han sido: la quema de biomasa (BB-16.9%), polvo mineral (MD-19.1 %), tráfico rodado (RT-7.0 %) y dos fuentes de

carácter secundario, una dominada por el sulfato de amonio (AS-33.8%) y otra por el nitrato secundario (SN-23.3%).

El porcentaje de la contribución de WSOC en cada fuente puede verse en la figura 8. Como puede apreciarse destacan las contribuciones en la fuente secundaria (AS) y en la fuente relacionada con la quema de biomasa. Debe indicarse que, aunque existen evidencias en la bibliografía sobre la naturaleza secundaria del WSOC, no se ha podido identificar una fuente asociada exclusivamente a la formación de aerosoles orgánicos secundarios (SOA), muy probablemente porque no se analizaron trazadores específicos de la formación de SOA, como los ácidos dicarboxílicos distintos del oxalato. Sin embargo, podemos decir que la formación de SOA se asocia/relaciona principalmente con la fuente AS. Para llegar a esta afirmación se utilizó el O_3 (utilizado como trazador de SOA). La concentración de O_3 únicamente correlacionó significativamente con la fuente AS justificando así la identificación de AS con SOA.

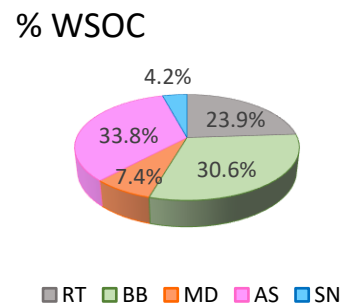


Figura 8. Contribución porcentual de WSOC en las fuentes obtenidas (López-Caravaca et al., 2023).

La contribución media mensual del WSOC (en marrón) a la concentración másica de cada fuente puede verse en la figura 9.

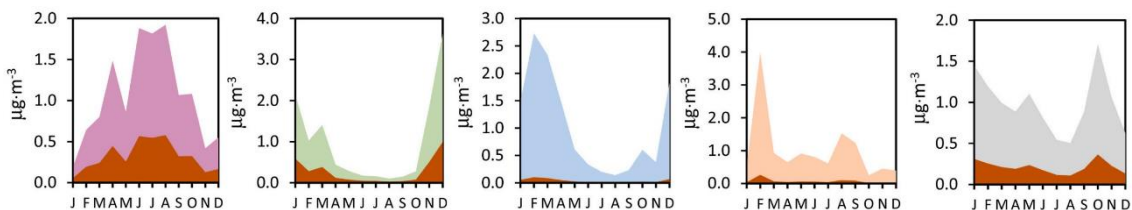


Figura 9. Variación temporal de los niveles de cada fuente AS/SOA (rosa), BB (verde), SN (azul), MD (beige), RT (gris) y concentración de WSOC (en marrón) asociada a cada una de ellas (López-Caravaca et al., 2023).

Como puede apreciarse, las altas concentraciones registradas durante finales de otoño y principios de invierno mostradas en la figura 7 se debieron al WSOC emitido durante las quemadas de biomasa. Destacar los elevados valores de WSOC procedente de la fuente SOA durante los meses más cálidos y una contribución casi constante del emitido por el tráfico.

La obtención del ratio WSOC/OC relativo a cada fuente determinó que el valor más elevado se registró en la fuente SOA (~0.55), lo cual indica que el 55 % del OC emitido por esta fuente es soluble.

4.1.2 Distribución másica

Como se indicó anteriormente se realizó una campaña durante el invierno para caracterizar la distribución másica del WSOC (32 muestras diarias). La distribución abarca el denominado modo de acumulación en cuatro tamaños: 0.25, 0.44, 1.0 y 1.4 μm . La mayor concentración de PM se encontró en la fracción $PM_{1.4}$. Por el contrario, la concentración máxima de WSOC ($0.23 \mu\text{g}\cdot\text{m}^{-3}$) se obtuvo en la fracción de tamaño más pequeña ($0.25 \mu\text{m}$). Este tamaño está incluido en el

denominado “modo de condensación” el cual constituye un submodo del de acumulación. Las contribuciones porcentuales de WSOC a los niveles de PM también fueron mayores en las fracciones de tamaño más pequeño, con valores superiores al 14 %. En la mayoría de emplazamientos europeos las concentraciones máximas de WSOC en el modo acumulación se registraron en los intervalos de tamaño comprendidos entre ~ 0.2 y $\sim 0.6 \mu\text{m}$, independientemente del tipo de emplazamiento y del periodo de medición. Por lo tanto, la concentración máxima de WSOC en el área de estudio se encuentra en el rango inferior de este intervalo.

Se evidenció que, en algunos intervalos de tamaño, se registró una diferencia significativa entre los valores medios y la mediana en las concentraciones de PM y WSOC. Concretamente, se observaron diferencias notables entre las concentraciones media y mediana en la etapa de $1.4 \mu\text{m}$ para el PM y en la etapa de $0.25 \mu\text{m}$ para WSOC. Estos resultados apuntan a que la ocurrencia de episodios de PM puede tener un impacto significativo en los niveles de PM y WSOC en estos rangos de tamaño. La figura 10 muestra las series temporales de concentraciones de PM y WSOC segregadas por tamaño durante el periodo de estudio para hacer evidenciar tales impactos.

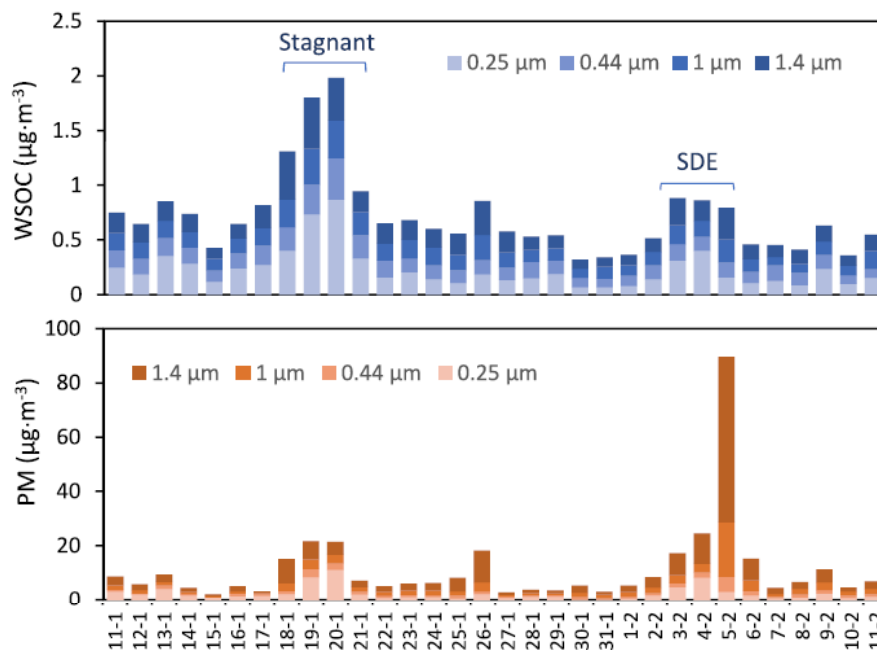


Figura 10. Variabilidad diaria de las concentraciones de WSOC y PM según tamaños (López-Caravaca et al., 2024b).

Al principio de la segunda semana de muestreo, las concentraciones de WSOC aumentaron significativamente en todas las fracciones de tamaño. Para los rangos de tamaño más pequeños, los niveles de WSOC fueron casi tres veces superiores a los registrados durante la semana anterior debido a un episodio de alta estabilidad atmosférica (HPE-Stagnant) que tuvo lugar entre el 18 y el 20 de enero. Cerca del final del periodo de medida, las concentraciones de WSOC pero sobre todo las de PM en sus tamaños más grandes aumentaron considerablemente. En este caso, el aumento se debió a un episodio de polvo sahariano (SDE) que tuvo lugar entre el 3 y el 5 de febrero. La figura 11 muestra de forma más detallada la influencia de HPE y SDE en las concentraciones de WSOC y PM por tamaños. Se observa que durante el HPE el incremento en las concentraciones de WSOC para todos los tamaños es mayor que durante la SDE. De hecho,

los niveles medios durante los días sin evento (NE) y SDE fueron muy similares para todos los rangos de tamaño. Los aumentos en los niveles de WSOC en los tamaños más grandes (submodo droplet) se debieron probablemente a la absorción de agua por partículas en modo acumulación en condiciones de alta HR ambiental (condiciones típicas de estos episodios de elevada estabilidad ambiental), mientras que en los más pequeños (submodo condensación) están asociados con la producción diurna fotoquímica de WSOC.

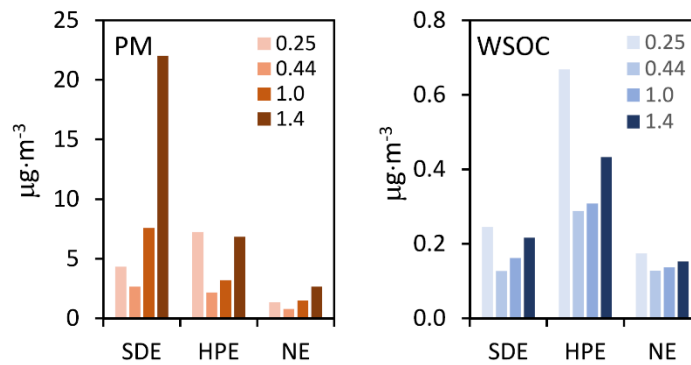


Figura 11. Distribución de tamaños de WSOC y PM durante días sin eventos (NE) y eventos de contaminación (HPE y SDE) (López-Caravaca et al., 2024b).

En cuanto a la distribución de PM, se observa que es la fracción de mayor tamaño (1.4 μm) la más influenciada por la SDE. Es conocido que este tipo de fenómenos de transporte en las costas mediterráneas occidentales tiene una mayor incidencia en los tamaños más gruesos del PM.

4.2 Absorción de la luz por WSOC

4.2.1 σ_{WSOC} en PM_1 : caracterización y fuentes

Siguiendo la metodología descrita en la sección 3.4.1 se determinó a partir $\sigma_{\text{ap},\lambda}$ las contribuciones de $\sigma_{\text{BrC},\lambda}$ y $\sigma_{\text{BrC},\lambda}$. El valor de $\sigma_{\text{BrC},\lambda}$ es clave para determinar su eficiencia de absorción másica (MAE) y obtener el valor de σ_{WSOC} . Al no conocer la concentración ($\mu\text{g}\cdot\text{m}^{-3}$) de BrC, el valor de MAE se calculó a partir del valor de concentración másica de OC, según:

$$\text{MAE}_{\text{BrC},\lambda} = \sigma_{\text{BrC},\lambda} / [\text{OC}]$$

El valor de MAE para $\lambda=370$ nm fue de $1.9 \text{ m}^2\cdot\text{g}^{-1}$. Sin embargo, este valor constituye una cota inferior del verdadero valor de MAE_{BrC} al estar el BrC incluido en OC.

Para estimar la absorción por WSOC (σ_{WSOC}), se utilizó la técnica MLR. Dado que en este caso no se cumplía el supuesto de homocedasticidad, se utilizó una generalización del modelo (mínimos cuadrados ponderados, WLS) para resolver este problema. Partimos de la premisa de que la absorción por BrC es debida a la absorción por parte de WSOC más la correspondiente a los compuestos orgánicos insolubles (WIOC) con capacidad de absorber la radiación solar. Los resultados se presentan en la tabla 1. Los coeficientes normalizados fueron casi los mismos para el WSOC y el WIOC, lo que indica una contribución similar de ambos componentes. Los valores MAE ($\lambda=370$ nm) fueron $1.72 \text{ m}^2\cdot\text{g}^{-1}$ para el WSOC y $1.70 \text{ m}^2\cdot\text{g}^{-1}$ para el WIOC, lo que sugiere que ambos componentes absorben la luz UV prácticamente con la misma eficiencia.

Tabla 1. Parámetros del análisis de regresión multilineal de $\sigma_{\text{BrC},370}$ (López-Caravaca et al., 2024a).

	Coefficientes no normalizados	Std. error	Coefficientes normalizados	p-valor	R ²
WSOC	1.72	0.57	0.43	0.003	0.75
WIOC	1.70	0.53	0.45	0.002	

Las contribuciones medias anuales (\pm SD) obtenidas a partir del modelo fueron: $\sigma_{\text{WSOC},370}=1.6$ (± 0.7) Mm^{-1} y $\sigma_{\text{WIOC},370}=1.9$ (± 1.1) Mm^{-1} , lo que indica que la absorción de luz por componentes orgánicos insolubles en agua contribuyó significativamente a σ_{BrC} . Este resultado muestra que la absorción de luz por BrC se subestimaría en gran medida si se utilizara WSOC como sustituto de BrC, lo cual sucede en algunas ocasiones.

La figura 12 muestra los valores medios mensuales de la absorción por WSOC y WIOC ($\lambda=370$ nm). Ambas absorciones presentan una similar estacionalidad con valores máximos en invierno y mínimos durante el periodo estival (patrón típico de zonas urbanas). La razón más probable de los valores más altos de σ_{WSOC} durante los meses fríos es el aumento de las emisiones de la quema de biomasa, además de las mayores concentraciones de WSOC registradas. Por otro lado, la combustión de combustibles fósiles y la BB son fuentes dominantes de WIOC y las contribuciones de estas fuentes a los niveles de PM_{10} son mayores durante el periodo frío, (lo que explica los mayores valores de σ_{WIOC} registrados durante el otoño y el invierno). El valor mínimo de σ_{WSOC} durante el verano (1.3 Mm^{-1}) frente al 1.9 Mm^{-1} registrado durante el invierno puede explicarse considerando que el SOA (que es el mayor contribuyente al WSOC durante esta estación) está compuesto principalmente por cromóforos incoloros de bajo peso molecular. No obstante, la pérdida de cromóforos durante los meses cálidos no fue tan elevada como la observada en otras zonas urbanas, donde la relación invierno/verano fue superior al valor obtenido en el presente estudio.

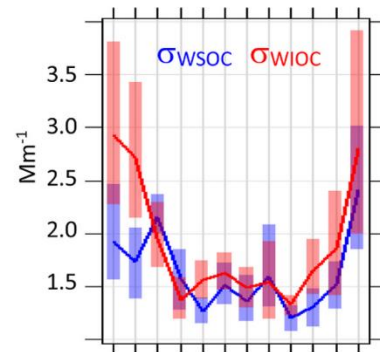


Figura 12. Evolución temporal de $\sigma_{\text{WSOC},370}$ y $\sigma_{\text{WIOC},370}$ (López-Caravaca et al., 2024a).

La contribución de las diferentes fuentes a la absorción de luz por WSOC se estimó a partir de las fuentes de WSOC obtenidas previamente. No obstante, dado que el modelo MLR puede ser muy sensible a la elección de las especies incluidas en el análisis, sólo se consideró incluir las fuentes mayoritarias de WSOC (ver figura 8), es decir: SOA, RT y BB. La contribución de los factores SN y MD a las concentraciones de WSOC fue inferior al 10 %, por lo tanto, los intentos de incluir estos factores en el modelo dieron como resultado eficiencias de absorción de masa poco realistas y coeficientes de regresión estadísticamente no significativos para la absorción. En la aplicación del análisis MLR, $\sigma_{\text{WSOC},370}$ fue la variable dependiente y las tres fuentes consideradas (F_i) fueron las variables independientes:

$$\sigma_{\text{WSOC},370}=b_0+b_1F_1+b_2F_2+b_3F_3+\varepsilon$$

En este caso, b_i representa la eficiencia de absorción de masa de cada componente, mientras que ε es el término residual y b_0 la intersección en el eje Y. El término b_0 (ordenada en el origen) tiene en cuenta los componentes no incluidos en el modelo (SN y MD). La contribución relativa

de cada factor se estimó a partir de los coeficientes de regresión lineal multiplicados por sus concentraciones máxicas. El modelo se aplicó independientemente para los meses de otoño-invierno (periodo frío) y para los de primavera-verano (periodo cálido). El modelo fue capaz de explicar el 52 % de la variación total de la absorción de luz por WSOC durante la estación cálida y un 70 % para la estación fría.

La contribución media de cada fuente a $\sigma_{\text{WSOC},370}$ durante ambos periodos se muestra en la figura 13. Tráfico (~31 %) y SOA (~56 %) fueron las principales fuentes que contribuyeron a la absorción de luz por WSOC en el periodo cálido, mientras que el BB fue la fuente dominante (~37 %) durante la estación fría. Durante esta estación, las fuentes no consideradas en el modelo contribuyeron significativamente a la absorción por WSOC (~27 %). Esto puede explicarse considerando que las condiciones de alta estabilidad atmosférica que favorecen la formación de nitrato secundario son más frecuentes durante el invierno. La importante contribución de SN a σ_{WSOC} apunta a la formación de compuestos orgánicos absorbentes de luz que contienen nitrógeno bajo altas concentraciones de nitrato.

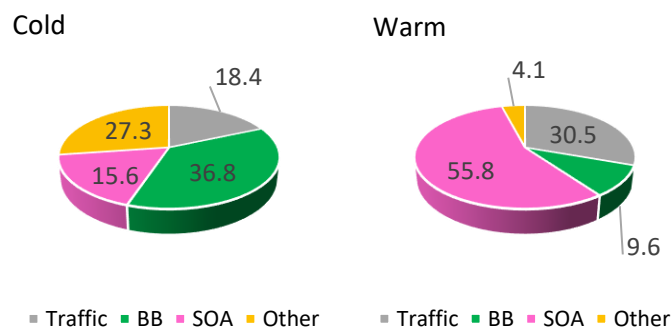


Figura 13. Contribución porcentual de fuentes al valor global de σ_{WSOC} durante los periodos cálido y frío (López-Caravaca et al., 2024a).

La figura 14 por su parte presenta las contribuciones mensuales de cada fuente a σ_{WSOC} . Los valores de $\sigma_{\text{WSOC}}(\text{BB})$ fueron más elevadas durante los meses de invierno y otoño debido a las mayores emisiones procedentes de la quema de biomasa. El valor medio registrado en diciembre (~1.8 Mm^{-1}) podría atribuirse a las actividades de quema de biomasa cerca del lugar de muestreo. La variabilidad temporal de σ_{WSOC} procedente del tráfico rodado fue más suave que las de $\sigma_{\text{WSOC}}(\text{BB})$ y $\sigma_{\text{WSOC}}(\text{SOA})$. Durante el verano $\sigma_{\text{WSOC}}(\text{SOA})$ fue la más alta, con un valor medio estacional de ~1.0 Mm^{-1} . Esto es lógico ya que el SOA es la fuente predominante de WSOC durante este periodo.

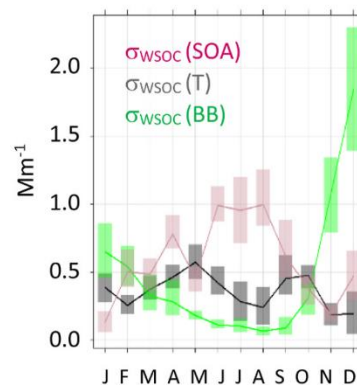


Figura 14. Evolución temporal de las fuentes de $\sigma_{\text{WSOC},370}$ (López-Caravaca et al., 2024a).

Las contribuciones medias anuales ($\pm\text{SD}$) calculadas por el modelo ($\lambda=370$ nm) fueron: $\sigma_{\text{WSOC}}(\text{BB})= 0.42 (\pm 0.57) \text{ Mm}^{-1}$, $\sigma_{\text{WSOC}}(\text{SOA}) = 0.46 (\pm 0.36) \text{ Mm}^{-1}$ y $\sigma_{\text{WSOC}}(\text{RT}) = 0.35 (\pm 0.25) \text{ Mm}^{-1}$.

4.2.2 Eficiencia de la absorción según tamaño

Este apartado tiene como objetivo establecer la relación entre σ_{BrC} y la distribución másica de WSOC en el modo acumulación para determinar en qué tamaño, dentro de este modo, se presenta la mayor eficiencia de absorción de la luz debida al WSOC. En este caso se ha tenido que trabajar con el valor de σ_{BrC} en vez de con σ_{WSOC} (que hubiese sido lo deseable). La razón de ello es en que los filtros utilizados por el impactador no se pudo determinar el valor de OC, por lo que fue imposible conocer la contribución de WIOC y proceder como en el apartado anterior para la obtención de σ_{WSOC} .

La contribución del BrC a la absorción de la luz para cada longitud de onda se estimó a partir de las diferencias entre los valores medidos de σ_{ap} y los calculados para el BC según lo explicado en el apartado 3.4.1 de la metodología.

Para determinar el tamaño más eficiente para la absorción de luz por WSOC, se realizó una correlación de Spearman entre $\sigma_{\text{BrC},370}$ y las concentraciones de WSOC segregadas por tamaño (N=29) (ver figura 15). Aunque las correlaciones fueron estadísticamente significativas para todos los rangos de tamaño, ρ fue mayor para las concentraciones de WSOC en la fase de impactación de $0.25 \mu\text{m}$ ($\rho \sim 0.9$). Este resultado indica que la capacidad de absorción de radiación por parte del WSOC depende en cierta medida de su distribución de tamaño, y que las partículas pequeñas de WSOC son las más eficientes en términos de absorción de luz. Para entender este resultado debemos tener en cuenta que el WSOC emitido por diferentes fuentes pueden no tener la misma eficiencia de absorción ya que la absorción de luz del WSOC puede verse afectada por la fuente cromófora. En este sentido, el BB se ha identificado como una fuente importante de WSOC con alta capacidad de absorción de luz.

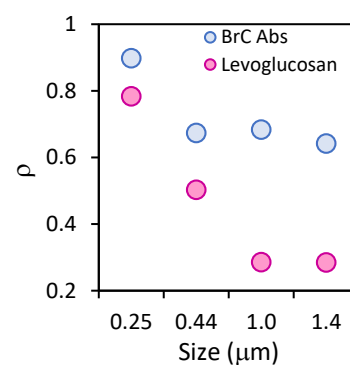


Figura 15. Coeficientes de correlación de Spearman (ρ) entre WSOC y $\sigma_{\text{BrC},370}$ (azul) y levoglucosano (rosa) (López-Caravaca et al., 2024b).

Hemos visto cómo durante el periodo de estudio, las emisiones de BB fueron de las fuentes más importantes de WSOC lo que sugiere que el WSOC emitido por esta fuente podría haberse distribuido principalmente en los rangos de tamaños más pequeños. Esta hipótesis se confirma al realizar la correlación entre el levoglucosano (trazador típico de la fuente BB) y la concentración de WSOC según tamaño (N=12) (ver puntos rosas en la figura 15). Sólo se encontró una correlación estadísticamente significativa (p -valor < 0.01) entre el levoglucosano y la concentración de WSOC en la etapa de $0.25 \mu\text{m}$ ($\rho=0.78$). Este resultado indica que el WSOC en este tamaño es emitido principalmente por la fuente BB y muestra la mayor capacidad de absorción de luz.

5. Conclusiones

A continuación, se presentan las principales conclusiones obtenidas en el presente trabajo:

- La reducción del tráfico impuesta durante el periodo de muestreo repercutió de manera significativa en las concentraciones de PM_{10} y compuestos carbonosos monitorizados registrándose valores inferiores a los esperables para un entorno urbano.
- Además de determinar la existencia de las tradicionales fuentes de WSOC (BB, SOA y RT) se verificó la existencia de dos fuentes minoritarias (MD y SN) en el área de estudio que demostraron tener una relevancia mayor a la esperada durante los meses más fríos en la absorción de la radiación.
- La contribución media del BrC fue de un ~29 % respecto de la absorción total, subrayando la significativa influencia de este componente en el proceso en el área de estudio ya que rara vez se supera el 40 % dentro de entornos urbanos.
- El WSOC distribuido en el modo de acumulación demostró ser sensible a eventos de elevada estabilidad atmosférica registrándose incrementos notables sobre todo en los tamaños más pequeños. Sin embargo, durante el transcurso de eventos saharianos la variación no fue significativa.
- La emisión de WSOC por parte de la fuente BB parece haberse distribuido prioritariamente en el rango de tamaño inferior dentro del modo de acumulación y mostró tener la mayor capacidad de absorción de la radiación.
- Siguiendo en la línea de recientes estudios se ha concluido que la absorción de la luz por BrC estaría subestimada si se usa como equivalente la absorción por parte WSOC. De hecho, se ha podido determinar el relevante papel en el proceso de WIOC, con valores muy similares a los de WSOC.

5. Conclusions

The main conclusions obtained in this work are presented below:

- The reduction in traffic imposed during the sampling period had a significant impact on the concentrations of PM_{10} and carbonaceous compounds monitored, registering values lower than those expected for an urban environment.
- In addition to determining the existence of the traditional WSOC sources (BB, SOA and RT), the existence of two minority sources (MD and SN) in the study area was verified, which proved to be more relevant than expected during the coldest months in the absorption of radiation.
- The average contribution of BrC was ~29% of the total absorption, underlining the significant influence of this component on the process in the study area as it rarely exceeds 40% within urban environments.
- The WSOC distributed in the accumulation mode proved to be sensitive to events of high atmospheric stability with noticeable increases especially at the smaller sizes. However, during the course of Saharan events the variation was not significant.
- The WSOC emission from the BB source seems to have been primarily distributed in the lower size range within the accumulation mode and showed to have the highest absorption capacity of the radiation.
- In line with recent studies, it has been concluded that the light absorption by BrC is underestimated if the absorption by WSOC is used as an equivalent. In fact, it has been possible to determine the relevant role in the WIOC process, with values very similar to those of WSOC.

6. Referencias

- Asa-Awuku, A., Engelhart, G.J., Lee, B.H., Pandis, S.N., Nenes, A., 2009. Relating CCN activity, volatility, and droplet growth kinetics of β -caryophyllene secondary organic aerosol. *Atmos. Chem. Phys.* 9, 795–812.
- Bougiatioti, A., Zampas, P., Koulouri, E., Antoniou, M., Theodosi, C., Kouvarakis, G., Saarikoski, S., Mäkelä, T., Hillamo, R., Mihalopoulos, N., 2013. Organic, elemental and water-soluble organic carbon in size segregated aerosols, in the marine boundary layer of the Eastern Mediterranean. *Atmos. Environ.* 64, 251–262.
- Cesari, D., Merico, E., Dinoi, A., Gambaro, A., Morabito, E., Gregoris, E., Barbaro, E., Feltracco, M., Alebić-Juretić, A., Odorčić, D., Kontošić, D., Mifka, B., Contini, D., 2020. An inter-comparison of size segregated carbonaceous aerosol collected by low-volume impactor in the port-cities of Venice (Italy) and Rijeka (Croatia). *Atmos. Pollut. Res.* 11, 10, 1705–1714.
- Decesari, S., Mircea, M., Cavalli, F., Fuzzi, S., Moretti, F., Tagliavini, E., Facchini, M.C., 2007. Source attribution of water-soluble organic aerosol by nuclear magnetic resonance spectroscopy. *Environ. Sci. Technol.* 41, 2479–2484.
- Draxler, R.R., Rolph, G.D., 2015. HYSPLIT (HYbrid Single-Particle Lagrangian Integrated Trajectory) Model Access via NOAA ARL READY Website. <http://ready.arl.noaa.gov/HYSPLIT.php>.
- Du, Z., He, K., Cheng, Y., Duan, F., Ma, Y., Liu, J., Zhang, X., Zheng, M., Weber, R., 2014. A yearlong study of water-soluble organic carbon in Beijing I: sources and its primary vs. secondary nature. *Atmos. Environ.* 92, 514–521.
- Duarte, R., Mieiro, C.L., Penetra, A., Pio, C.A., Duarte, A.C., 2008. Carbonaceous materials in size-segregated atmospheric aerosols from urban and coastal-rural areas at the Western European Coast. *Atmos. Res.* 90, 253–263.
- Ealo, M., Alastuey, A., Pérez, N., Ripoll, A., Querol, X., Pandolfi, M., 2018. Impact of aerosol particle sources on optical properties in urban, regional and remote areas in the north-western Mediterranean. *Atmos. Chem. Phys.* 18, 1149–1169.
- Feng, Y., Ramanathan, V., Kotamarthi, V.R., 2013. Brown carbon: a significant atmospheric absorber of solar radiation? *Atmos. Chem. Phys.* 13, 8607–8621.
- Frka, S., Grgić, I., Turšič, J., Gini, M.I., Eleftheriadis, K., 2018. Seasonal variability of carbon in humic-like matter of ambient size-segregated water-soluble organic aerosols from urban background environment. *Atmos. Environ.* 173, 239–247.
- Geng, X., Mo, Y., Li, J., Zhong, G., Tang, J., Jiang, H., Ding, X., Malik, R.N., Zhang, G., 2020. Source apportionment of water-soluble brown carbon in aerosols over the northern South China Sea: Influence from land outflow, SOA formation and marine emission. *Atmos. Environ.* 229, 117484.
- Gilardoni, S., Massoli, P., Marinoni, A., Mazzoleni, C., Freedman, A., Lonati, G., De Iuliis, S., Gianelle, V., 2020. Spatial and temporal variability of carbonaceous aerosol absorption in the Po Valley. *Aerosol Air Qual. Res.* 20, 2624–2639.

- Hecobian, A., Zhang, X., Zheng, M., Frank, N., Edgerton, N.E.S., Weber, R.J., 2010. Water-soluble organic aerosol material and the light-absorption characteristics of aqueous extracts measured over the Southeastern United States. *Atmos. Chem. Phys.* 10, 5965–5977.
- Huang, R.J., Yang, L., Cao, J., Chen, Y., Chen, Q., Li, Y., Duan, J., Zhu, C., Dai, W., Wang, K., Lin, C., Ni, H., Corbin, J.C., Wu, Y., Zhang, R., Tie, X., Hoffmann, T., O'Dowd, C., Dusek, U., 2018. Brown carbon aerosol in urban Xi'an, Northwest China: the composition and light absorption properties. *Environ. Sci. Technol.* 52, 6825–6833.
- Huang, X.F., Yu, J.Z., He, L.Y., Yuan, Z., 2006. Water-soluble organic carbon and oxalate in aerosols at a coastal urban site in China: size distribution characteristics, sources, and formation mechanisms. *J. Geophys. Res.* 111, D22212.
- Izhar, S., Gupta, T., Panday, A.K., 2020. Improved method to apportion optical absorption by black and brown carbon under the influence of haze and fog at Lumbini, Nepal, on the Indo-Gangetic Plains. *Environ. Pollut.* 263, 114640.
- Jacobson, M. C., Hansson, H.-C., Noone, K. L., and Charlson, R. J., 2000. Organic atmospheric aerosols: review and state of the science. *Rev. Geophys.* 38, 267–294.
- Jin, Y., Yan, C., Sullivan, A.P., Liu, Y., Wang, X., Dong, H., Chen, S., Zeng, L., Collett, J.L., Mei Zheng, M., 2020. Significant contribution of primary sources to water-soluble organic carbon during spring in Beijing, China. *Atmosphere* 11, 395.
- Kanakidou, M., Seinfeld, J.H., Pandis, S.N., Barnes, I., Dentener, F.J., Facchini, M.C., Van Dingenen, R., Ervens, B., Nenes, A., Nielsen, C.J., Swietlicki, E., Putaud, J.P., Balkanski, Y., Fuzzi, S., Horth, J., Moortgat, G.K., Winterhalter, R., Myhre, C.E.L., Tsigaridis, K., Vignati, E., Stephanou, E.G., Wilson, J., 2005. Organic aerosol and global climate modelling: a review. *Atmos. Chem. Phys.* 5, 1053–1123.
- Kaskaoutis, D.G., Grivas, G., Oikonomou, K., Tavernaraki, P., Papoutsidaki, K., Tsagkaraki, M., Stavroulas, I., Zarmpas, P., Paraskevopoulou, D., Bougiatioti, A., Liakakou, E., Gavrouzou, M., Dumka, U.C., Hatzianastassiou, N., Sciare, J., Gerasopoulos, E., Mihalopoulos, N., 2022. Impacts of severe residential wood burning on atmospheric processing, water-soluble organic aerosol and light absorption, in an inland city of Southeastern Europe. *Atmos. Environ.* 280, 119139.
- Kaskaoutis, D.G., Grivas, G., Stavroulas, I., Bougiatioti, A., Liakakou, E., Dumka, U.C., Gerasopoulos, E., Mihalopoulos, N., 2021. Apportionment of black and brown carbon spectral absorption sources in the urban environment of Athens, Greece, during Winter. *Sci. Total Environ.* 801, 149739.
- Kirillova, E. N., Marinoni, A., Bonasoni, P., Vuillermoz, E., Facchini, M. C., Fuzzi, S., Decesari, S., 2016. Light absorption properties of brown carbon in the high Himalayas. *J. Geophys. Res.: Atmospheres* 121, 9621–9639.
- Laskin, A., Laskin, J., Nizkorodov, S.A., 2015. Chemistry of atmospheric brown carbon. *Chem. Rev.* 115, 4335–4382.
- López-Caravaca, A., Crespo, J., Galindo, N., Yubero, E., Juárez, N., Nicolás, J.F., 2023. Sources of water-soluble organic carbon in fine particles at a southern European urban background site. *Atmos. Environ.* 306, 119844.

- López-Caravaca, A., Crespo, J., Galindo, N., Yubero, E., Clemente, A., Castañer, R., Nicolás, J.F., 2024a. Characterization of water-soluble organic carbon absorption at an urban background site in the south-eastern Iberian Peninsula. *Atmos. Environ.* 324, 120435.
- López-Caravaca, A., Crespo, J., Galindo, N., Yubero, E., Juárez, N., Nicolás, J.F., 2024b. WSOC in accumulation mode aerosols: Distribution and relationship with BrC light absorption at an urban background site. *Atmos. Pollut. Res.* 15, 102133.
- Liu, J., Bergin, M., Guo, H., King, L., Kotra, N., Edgerton, E., Weber, R.J., 2013. Size resolved measurements of brown carbon in water and methanol extracts and estimates of their contribution to ambient fine-particle light absorption. *Atmos. Chem. Phys.* 13, 12389–12404.
- Matsumoto, K., Kodama, S., Sakata, K., Watanabe, Y., 2022. Atmospheric deposition fluxes and processes of the water-soluble and water-insoluble organic carbon in central Japan. *Atmos. Environ.* 271, 118913.
- Matta, E., Facchini, M.C., Decesari, S., Mircea, M., Cavalli, F., Fuzzi, S., Putaud, J.-P. Dell'Acqua, A., 2003. Mass closure on the chemical species in size-segregated atmospheric aerosol collected in an urban area of the Po Valley, Italy. *Atmos. Chem. Phys.* 3, 623–637.
- Mladenov, N., Alados-Arboledas, L., Olmo, F.J., Lyamani, H., Delgado, A., Molina, A., Reche, I., 2011. Applications of optical spectroscopy and stable isotope analyses to organic aerosol source discrimination in an urban area. *Atmos. Environ.* 45, 1960–1969.
- Mo, Y., Li, J., Cheng, Z., Zhong, G., Zhu, S., Tian, C., Chen, Y., Zhang, G., 2021. Dual carbon isotope-based source apportionment and light absorption properties of water-soluble organic carbon in PM_{2.5} over China. *J. Geophys. Res.: Atmospheres*, 126, e2020JD033920.
- Molnár, A., Mészáros, E., Hansson, H.C., Karlsson, H., Gelencsér, A., Kiss, G.Y., Krivácsy, Z., 1999. The importance of organic and elemental carbon in the fine atmospheric aerosol particles. *Atmos. Environ.* 33, 2745–2750.
- Moschos, V., Kumar, N. K., Daellenbach, K. R., Baltensperger, U., Prévôt, A. S. H., El Haddad, I., 2018. Source apportionment of brown carbon absorption by coupling ultraviolet–visible spectroscopy with aerosol mass spectrometry, *Environ. Sci. Tech. Lett.* 5, 302–308.
- Nicolás, J.F., Castañer, R., Crespo, J., Yubero, E., Galindo, N., C. Pastor, C., 2018. Seasonal variability of aerosol absorption parameters at a remote site with high mineral dust loads. *Atmos. Res.* 210, 100–109.
- Norris, G., Duvall, R., Brown, S., Bai, S., 2014. EPA Positive Matrix Factorization (PMF) 5.0 Fundamentals and User Guide. U.S. Environmental Protection Agency Office of Research and Development, Washington DC, 20460 (i-124, EPA/600/R-14/108, April).
- Paatero, P., 1997. Least Squares Formulation of Robust, Non-Negative Factor Analysis, *Chemom. Intell. Lab. Syst.* 37, 23–35.
- Paatero, P., Tapper, U., 1994. Positive Matrix Factorization: a non-negative factor model with optimal utilization of error estimates of data values. *Environmetrics* 5, 111–126.

- Pani, S.K., Lin, N-H., Griffith, S.M., Chantara, S., Lee, C-T., Thepnuan, D., Tsai, Y.I., 2021. Brown carbon light absorption over an urban environment in northern peninsular Southeast Asia. *Environ. Pollut.* 276, 116735.
- Paraskevopoulou, D., Kaskaoutis, D.G., Grivas, G., Bikkina, S., Tsagkaraki, M., Vrettou, I.M., Tavernaraki, K., Papoutsidaki, K., Stavroulas, I., Liakakou, E., Bougiatioti, A., Oikonomou, K., Gerasopoulos, E., Mihalopoulos, N., 2023. Brown carbon absorption and radiative effects under intense residential wood burning conditions in Southeastern Europe: New insights into the abundance and absorptivity of methanol-soluble organic aerosols. *Sci. Total Environ.* 860, 160434.
- Paraskevopoulou, D., Liakakou, E., Gerasopoulos, E., Theodosi, C., Mihalopoulos, N., 2014. Long-term characterization of organic and elemental carbon in the PM_{2.5} fraction: the case of Athens, Greece. *Atmos. Chem. Phys.* 14, 13313–13325.
- Park S, Schauer J, Cho S., 2013. Sources and their contributions to two water-soluble organic carbons observed at a roadway site. *Atmos. Environ.* 77, 348–357.
- Park, S.S., Cho, S.Y., 2011. Tracking sources and behaviors of water-soluble organic carbon in fine particulate matter measured at an urban site in Korea. *Atmos. Environ.* 45, 60–72.
- Park, S.S., Kim, J.H., 2014. Possible sources of two size-resolved water-soluble organic carbon fractions at a roadway site during fall season. *Atmos. Environ.* 94, 134–143.
- Park, S.S., Son, S.C., 2017. Relationship between carbonaceous components and aerosol light absorption during winter at an urban site of Gwangju, Korea. *Atmos. Res.* 185, 73–83.
- Pio, C.A., Legrand, M., Oliveira, T., Afonso, J., Santos, C., Caseiro, A., Fialho, P., Barata, F., Puxbaum, H., Sánchez-Ochoa, A., Kasper-Giebl, A., Gelencsér, A., Preunkert, S., Schock, M., 2007. Climatology of aerosol composition (organic versus inorganic) at nonurban sites on a west-east transect across Europe. *J. Geophys. Res.* 112, D23S02.
- Polissar, A.V., Hopke, P.K., Paatero, P., Malm, W.C., Sisler, J.F., 1998. Atmospheric aerosol over Alaska: 2. Elemental composition and sources. *J. Geophys. Res.* 103, 19045–19057.
- Ponczek, M., Franco, M.A., Carbone, S., Rizzo, L.V., Monteiro dos Santos, D., Morais, F.G., Duarte, A., Barbosa, H., Artaxo, P., 2022. Linking the chemical composition and optical properties of biomass burning aerosols in Amazonia. *Environ. Sci.: Atmos.* 2, 252–269.
- Ran, L., Deng, Z.Z., Wang, P.C., Xia, X.A., 2016. Black carbon and wavelength-dependent aerosol absorption in the North China Plain based on two-year aethalometer measurements. *Atmos. Environ.* 142, 132–144.
- Saarikoski, S., Timonen, H., Saarnio, K., Aurela, M., Järvi, L., Keronen, P., Kerminen, V.-M., Hillamo, R., 2008. Sources of organic carbon in fine particulate matter in northern European urban air. *Atmos. Chem. Phys.* 8, 6281–6295.
- Satish, R., Rastogi, N., Singh, A., Singh, D., 2020. Change in characteristics of water-soluble and water-insoluble brown carbon aerosols during a large-scale biomass burning. *Environ. Sci. Pollut. R.* 27, 33339–33350.

- Savadkoohi, M., Pandolfi, M.C., Niemi, J.V., Mooibroek, D., Gloria Titos, G., Green, D.C., Tremper, A.H., Hueglin, C., Liakakou, E., Mihalopoulos, M., Stavroulas, I., Artiñano, B., Coz, E., Alados-Arboledas, L., Beddows, D., Riffault, V., De Brito, J.F., Bastian, S., Baudic, A., Costabile, F., Chazeau, B., Gómez-Amo, J.L., Estellés, V., Matos, V., van der Gaag, E., Gille, G., Luoma, K., Manninen, H.E., Norman, M., Silvergren, S., Petit, J-E., Putaud, J-P., Rattigan, O.V., Timonen, H., Tuch, T., Merkel, M., Weinhold, K., Vratolis, S., Vasilescu, J., Favez, O., Harrison, R.M., Lag, P., Wiedensohler, A., Hopke, P.H., Petäjä, T., Querol, X., 2023. The variability of mass concentrations and source apportionment analysis of equivalent black carbon across urban Europe. *Environ. Inter.* 178, 108081.
- Snyder, D.C., Rutte, A.P., Collins, R., Worley, C., Schauer, J.J., 2009. Insights into the origin of water-soluble organic carbon in atmospheric fine particulate matter. *Aerosol Sci. Technol.* 43 (11), 1099–1107.
- Soleimanian, E., Mousavi, A., Taghvaei, S., Shafer, M.M., Sioutas, C., 2020. Impact of secondary and primary particulate matter (PM) sources on the enhanced light absorption by brown carbon (BrC) particles in central Los Angeles. *Sci. Total Environ.* 705, 135902.
- Sullivan, A.P., Weber, R.J., Clements, A.L., Turner, J.R., Bae, M.S., Schauer, J.J., 2004. A method for on-line measurement of water-soluble organic carbon in ambient aerosol particles: results from an urban site. *Geophys. Res. Lett.* 31, L13105.
- Sun, Y., Zhang, Q., Zheng, M., Ding, X., Edgerton, E.S., Wan, X., 2011. Characterization and source apportionment of water-soluble organic matter in atmospheric fine particles (PM_{2.5}) with high-resolution aerosol mass spectrometry and GC/MS. *Environ. Sci. Technol.* 45, 4854–4861.
- Taghvaei, S., Sowlat, M.H., Diapouli, E., Manousakas, M.I., Vasilatou, V., Eleftheriadis, K., Sioutas, C., 2019. Source apportionment of the oxidative potential of fine ambient particulate matter (PM_{2.5}) in Athens, Greece. *Sci. Total Environ.* 653, 1407–1416.
- Timonen, H., Saarikoski, S., Tolonen-Kivimäki, O., Aurela, M., Saarnio, K., Petäjä, T., Aalto, P.P., Kulmala, M., Pakkanen, T., Hillamo, R., 2008. Size distributions, sources and source areas of water-soluble organic carbon in urban background air. *Atmos. Chem. Phys.* 8, 5635–5647.
- Tuet, W.Y., Fok, S., Verma, V., Tagle Rodriguez, M.S., Grosberg, A., Champion, J.A., Ng, N.L., 2016. Dose-dependent intracellular reactive oxygen and nitrogen species (ROS/RNS) production from particulate matter exposure: comparison to oxidative potential and chemical composition. *Atmos. Environ.* 144, 335–344.
- Velali, E., Papachristou, E., Pantazaki, A., Choli-Papadopoulou, T., Planou, S., Koura, A., Manoli, E., Besis, A., Voutsas, D., 2016. Redox activity and in vitro bioactivity of the water-soluble fraction of urban particulate matter in relation to particle size and chemical composition. *Environ. Pollut.* 208, 774–786.
- Viana, M., Chi X., Maenhaut, W., Querol, A., Alastuey, A., Mikuška, P., Večeřa, Z., 2006. Organic and elemental carbon concentrations in carbonaceous aerosols during summer and winter sampling campaigns in Barcelona, Spain, *Atmos. Environ.*, 40, 2180–2193.
- Viana, M., Maenhaut, W., ten Brink, H.M., Chi, X., Weijers, E., Querol, X., Alastuey, A., Mikuška, P., Večeřa, Z., 2007. Comparative analysis of organic and elemental carbon concentrations in carbonaceous aerosols in three European cities. *Atmos. Environ.* 41(28), 5972–5983.

- Viana, M., López, J.M., Querol, X., Alastuey, A., García-Gacio, D., Blanco-Heras, G., López-Mahía, P., Piñero-Iglesias, M., Sanz, M.J., Sanz, F., Chi, X., Maenhaut, W., 2008. Tracers and impact of open burning of rice Straw residues on PM in Eastern Spain. *Atmos. Environ.* 42, 1941–1957.
- Witkowska, A., Lewandowska, A.U., 2016. Water soluble organic carbon in aerosols (PM₁, PM_{2.5}, PM₁₀) and various precipitation forms (rain, snow, mixed) over the southern Baltic Sea station. *Sci. Total Environ.* 573, 337–346.
- Xie, M., Mladenov, N., Williams, M.W., Neff, J.C., Wasswa, J., Hannigan, M.P., 2016. Water soluble organic aerosols in the Colorado Rocky Mountains, USA: composition, sources and optical properties. *Sci. Rep.* 6, 1–12.
- Yang, M., Howell, S.G., Zhuang, J., Huebert, B.J. 2009. Attribution of aerosol light absorption to black carbon, brown carbon, and dust in China – interpretations of atmospheric measurements during EAST-AIRE. *Atmos. Chem. Phys.* 9, 2035–2050.
- Yttri, K.E., Simpson, D., Stenström, K., Puxbaum, H., Svendby, T., 2011. Source apportionment of the carbonaceous aerosol in Norway – quantitative estimates based on ¹⁴C, thermal-optical and organic tracer analysis. *Atmos. Chem. Phys.* 11, 9375–9394.
- Yu G., Zhang Y., Cho S.Y., Park S., 2017. Influence of haze pollution on water-soluble chemical species in PM_{2.5} and size-resolved particles at an urban site during fall. *J. Environ. Sci.* 57:370-382.
- Yu, G.H., Park, S., 2021. Chemical characterization and source apportionment of PM_{2.5} at an urban site in Gwangju, Korea. *Atmos. Pollut. Res.* 112, 101192.
- Yu, Q., Chen, J., Qin, W., Cheng, S., Zhang, Y., Sun, Y., Xin, K., Ahmad, M., 2021. Characteristics, primary sources and secondary formation of water-soluble organic aerosols in downtown Beijing. *Atmos. Chem. Phys.* 21, 1775–1796.
- Yubero, E., Galindo, N., Nicolás, J.F., Crespo, J., Calzolari, G., Lucarelli, F., 2015. Temporal variations of PM₁ major components in an urban street canyon. *Environ. Sci. Pollut. Res.* 22, 13328–13335.
- Zhang, X., Lin, Y.-H., Surratt, J. D., & Weber, R. J., 2013. Sources, composition and absorption Ångström exponent of light-absorbing organic components in aerosol extracts from the Los Angeles Basin. *Environ. Sci. Technol.* 47(8), 3685–3693.
- Zhou, Y., Chen, J., Fan, F., Feng, Y., Wang, S., Fu, Q., Feng, J., 2022. Deconvolving light absorption properties and influencing factors of carbonaceous aerosol in Shanghai. *Sci. Total Environ.* 839, 156280.

7. Anexos

Anexo I: El material particulado

El aerosol atmosférico, también llamado material particulado (PM), se define como el conjunto de partículas sólidas y/o líquidas (a excepción del agua pura) presentes en suspensión en la atmósfera (Seinfeld y Pandis, 2006). Estas partículas se distinguen por su emisión desde diversas fuentes, su transformación a través de variados procesos atmosféricos, una corta vida en la atmósfera y la desaparición a través de múltiples vías de eliminación. Asimismo, los aerosoles exhiben composiciones complejas y varían considerablemente en forma y tamaño, en un amplio rango que va desde los 10 nm hasta las 100 μm . Esas particularidades explican su distribución no homogénea a lo largo de todo el planeta con unas propiedades fisicoquímicas muy variadas.

El interés científico por el PM se basa en su influencia sobre la salud humana y el medio ambiente. Varios estudios han demostrado la relación entre la contaminación del aire por PM y un aumento en la mortalidad humana (Pope y Dockery, 2006). La inhalación es la principal vía de exposición a los aerosoles, los cuales pueden causar daño en células u órganos al alcanzar el sistema respiratorio y cardiovascular. El tamaño de las partículas en suspensión es crucial para determinar sus efectos en la salud humana. Partículas con un diámetro entre 2.5 y 10 μm (fracción torácica) pueden alcanzar la región tráqueo-bronquial. Partículas con diámetros inferiores a 2.5 μm (fracción respirable) alcanzan la región alveolar y las de menos de 0.1 μm , (partículas ultrafinas) incluso pueden acceder al torrente sanguíneo (Cassee et al., 2013), siendo potencialmente las más peligrosas por su capacidad para la translocación a órganos (Kreyling, 2006) y causar inflamación (Samet et al., 2009). Además, las fracciones ultrafinas pueden contener elementos orgánicos o trazas de metales pesados, actuando como vectores para la penetración de estos contaminantes cancerígenos y el desarrollo de enfermedades en distintas partes del cuerpo humano (Daher et al., 2013).

Por otra parte, la presencia de los aerosoles en la atmósfera puede provocar cambios en el balance radiativo terrestre y en la estabilidad atmosférica, como consecuencia de su capacidad de absorber y dispersar la radiación solar (efecto directo) y de servir de núcleos de formación de nubes, afectando a las precipitaciones (efecto indirecto). Otros efectos que puede tener el material particulado de la atmósfera es la contaminación de suelos, aguas subterráneas e incluso interferir en el crecimiento vegetal por deposición seca o húmeda, como también afectar a las edificaciones o monumentos (erosión, degradación) y a la seguridad vial, marítima o aérea (visibilidad).

Las partículas atmosféricas pueden ser emitidas por una gran variedad de fuentes de origen natural o antropogénico. Las partículas de origen natural son las predominantes. Respecto a los mecanismos de formación, las partículas pueden ser directamente emitidas como tales a la atmósfera (partículas primarias) o bien ser generadas en la atmósfera por transformaciones de gases precursores para formar nuevas partículas por condensación, o interacción entre un gas y una partícula atmosférica para dar lugar a un nuevo aerosol por adsorción o coagulación (partículas secundarias).

Los mecanismos de formación y crecimiento de las partículas condicionan su distribución por tamaños. En función de su diámetro, se clasifican en cuatro grupos o modas características:

- Moda de nucleación ($d < 0.02 \mu\text{m}$).

- Moda “Aitken” ($0.02 \mu\text{m} < d < 0.1 \mu\text{m}$).
- Moda de acumulación ($0.1 \mu\text{m} < d < 1 \mu\text{m}$). Dentro de esta moda se pueden distinguir dos submodas: condensación ($0.1 \mu\text{m} < d < 0.5 \mu\text{m}$) y “droplet” ($0.5 \mu\text{m} < d < 1 \mu\text{m}$).
- Moda gruesa ($d > 1 \mu\text{m}$).

Generalmente, la granulometría, composición química y distribución del material particulado suelen estar condicionados inicialmente por el foco emisor.

De forma general, los procesos de combustión a altas temperaturas y las reacciones atmosféricas producen partículas finas, mientras que los procesos mecánicos contribuyen a la emisión de partículas gruesas. Así mismo, las principales fuentes de partículas primarias pertenecientes a la moda fina serían las relacionadas con el transporte, combustión de combustibles fósiles, quema de biomasa e industrias de metales no férricos y otras industrias. Por otro lado, entre las fuentes de partículas primarias pertenecientes a la moda gruesa destacan la resuspensión de material particulado por acción eólica, la resuspensión de material particulado por tráfico rodado, la vegetación y el aerosol marino.

Además, cabe mencionar la existencia de fenómenos naturales tales como las intrusiones de masas de aire africano, episodios de elevada estabilidad atmosférica, volcanes o las precipitaciones que pueden alterar la concentración de material particulado atmosférico en suspensión en la región en que se producen.

En cuanto al marco regulatorio comunitario, el control de material particulado y otros contaminantes atmosféricos queda regido a través de la Directiva 2008/50/CE, del Parlamento Europeo y el consejo de 21 de mayo de 2008, relativa a la calidad del aire ambiente y a una atmósfera más limpia en Europa. A nivel nacional, es el Real Decreto 102/2011, de 28 de enero, relativo a la mejora de la calidad del aire, el que define los criterios de calidad de aire respecto a diversos contaminantes atmosféricos, acorde con lo dispuesto en la ley 34/2007, de 15 de noviembre, de calidad del aire y protección de la atmósfera. Este real decreto fue modificado posteriormente por el Real Decreto 678/2014, por el Real Decreto 39/2017 y por el Real Decreto 34/2023 para incluir y actualizar distintas normas medioambientales. En el Real Decreto 818/2018, de 6 de julio, se recogen las medidas para la reducción de emisiones nacionales de determinados contaminantes atmosféricos (Ministerio para la Transición Ecológica y el Reto Demográfico, 2024).

Referencias

Cassee, F.R., Heroux, M.E., Gerlofs-Nijland, M.E., Kelly, F.J., 2013. Particulate matter beyond mass: recent health evidence on the role of fractions, chemical constituents and sources of emission. *Inhal. Toxicol.* 25, 802–812.

Daher, N., Saliba, N.A., Shihadeh, A.L., Jaafar, M., Baalbaki, R., Sioutas, C., 2013. Chemical composition of size-resolved particulate matter at near-freeway and urban background sites in the greater Beirut area. *Atmos. Environ.* 80, 96-106.

Kreyling, W.G., 2006. Translocation and accumulation of nanoparticles in secondary target organs after uptake by various routes of intake. *Toxicol. Lett.* 164S, S1–S324.

Pope III, C.A., Dockery, D.W., 2006. Health effects of fine particulate air pollution: lines that connect. *J. Air Waste Manage. Assoc.* 56, 709–742.

Samet, J.M, Avila-Tang, E., Boffetta, P., Hannan, L.M., Olivo-Marston, S., Thun, M.J., Rudin, C.M., 2009. Lung Cancer in Never Smokers: Clinical Epidemiology and Environmental Risk Factors. 2009. Clin. Cancer Res. 15 (18), 5626–5645.

Seinfeld, J.H. and Pandis, S.N., 2006. Atmospheric Chemistry and Physics: From Air Pollution to Climate Change. 2nd Edition, John Wiley & Sons, New York.

Anexo II: La absorción de la radiación por aerosoles

El carbono negro -*Black Carbon*- (BC), el carbono marrón -*Brown Carbon*- (BrC) y el polvo mineral son los principales componentes absorbentes de luz de los aerosoles atmosféricos (Andreae y Gelencsér, 2006). El BC es el componente de aerosol que más luz absorbe con un forzamiento radiativo efectivo estimado de $+0.11 \text{ W/m}^2$ (IPCC, 2021). El BC es un producto de la combustión incompleta de combustibles fósiles, biocombustibles y biomasa, y muestra una débil dependencia con la longitud de onda (Kirchstetter et al., 2004). El BrC absorbe eficazmente la luz en la región visible (Andreae y Gelencsér, 2006; Laskin et al., 2015). Estudios recientes estiman que su contribución al forzamiento radiativo es muy significativa (Brown et al., 2018; Zhang et al., 2020). El BrC puede emitirse a partir de la combustión de biomasa, pero también de otras fuentes como los materiales biogénicos. Además, los aerosoles orgánicos secundarios también pueden ser una fuente de BrC (Moosmüller et al., 2009). En cuanto al polvo mineral, puede absorber luz en la misma región que el BrC debido a su contenido en óxidos de hierro.

La absorción de luz por el material particulado (PM) puede cuantificarse mediante el coeficiente de absorción (σ_{ap}). Los valores de σ_{ap} registrados en la literatura dependen en gran medida del tipo de entorno. En las estaciones de montaña, se suelen observar valores bajos de BC y σ_{ap} cuando el lugar de muestreo se encuentra por encima de la capa límite planetaria, principalmente durante la estación fría (Joshi et al., 2020). De hecho, en condiciones de troposfera libre, σ_{ap} suele estar por debajo de 3 Mm^{-1} ($\lambda = 550 \text{ nm}$). Por otro lado, en zonas urbanas con elevada densidad de tráfico, se registran altas concentraciones de BC y PM fino, por lo que suelen presentar elevados valores de σ_{ap} . En concreto, en España, los valores se sitúan en el intervalo $15\text{-}25 \text{ Mm}^{-1}$ para longitudes de onda en el visible medio (Titos et al., 2012; Segura et al., 2016). La variación estacional de σ_{ap} en entornos urbanos se caracteriza por presentar máximos en invierno y mínimos en verano (Nepomuceno et al., 2014). Por el contrario, en entornos de montaña los máximos se registran comúnmente en el periodo estival (Andrews et al., 2011).

La medición de los coeficientes de absorción a diferentes longitudes de onda es importante ya que la dependencia espectral de σ_{ap} está relacionada con sus propiedades físicas y químicas (Segura et al., 2016). El exponente Angstrom (AAE) describe la dependencia espectral de σ_{ap} . Los valores de AAE cercanos a la unidad indican una débil dependencia de la longitud de onda de la absorción de la luz y se asocian a la absorción por BC. Alternativamente, valores de AAE de ~ 2 apuntan a la presencia de aerosoles procedentes de quema de biomasa (Kirchstetter et al., 2004). Cuando hay aerosoles de polvo mineral, los valores de AAE también son superiores a 1 (Collaud-Coen et al., 2004). En general, se obtienen valores de AAE más bajos en verano y más altos durante el invierno. Posiblemente, los máximos de AAE observados en invierno se deban

a una mayor contribución al PM de fuentes como la quema de biomasa y el polvo mineral (Ealo et al., 2016; Huerta-Viso et al., 2020).

Referencias

Andreae, M. O. and Gelencsér, A., 2006. Black carbon or brown carbon? The nature of light-absorbing carbonaceous aerosols, *Atmos. Chem. Phys.*, 6, 3131–3148.

Andrews, E., Ogren, J.A., Bonasoni, P., Marinoni, A., Cuevas, E., Rodriguez, S., Sun, J.Y., Jaffe, D.A., Fischer, E.V., Baltensperger, U., Weingartner, E., Coen, M.C., Sharma, S., Macdonald, A.M., Leaitch, W.R., Lin, N.H., Laj, P., Arsov, T., Kalapov, I., Jefferson, A., Sheridan, P., 2011. Climatology of aerosol radiative properties in the free troposphere. *Atmos. Res.* 102, 365393.

Brown, H., Liu, X., Feng, Y., Jiang, Y., Wu, M., Lu, Z., Wu, C., Murphy, S., and Pokhrel, R., 2018. Radiative effect and climate impacts of brown carbon with the Community Atmosphere Model (CAM5), *Atmos. Chem. Phys.*, 18, 17745–17768.

Collaud-Coen, M., Weingartner, E., Schaub, D., Hueglin, C., Corrigan, C., Henning, S., Schwikowski, M., Baltensperger, U., 2004. Saharan dust events at the Jungfraujoch: detection by wavelength dependence of the single scattering albedo and first climatology analysis. *Atmos. Chem. Phys.* 4, 2465–2480.

Ealo, M., Alastuey, A., Ripoll, A., Pérez, N., Cruz-Minguillón, M., Querol, X., Pandolfi, M., 2016. Detection of Saharan dust and biomass burning events using near-real-time intensive aerosol optical properties in the north-western Mediterranean. *Atmos. Chem. Phys.* 16, 12567–12586.

Huerta-Viso, A., Crespo, J., Galindo, N., Yubero, E., Nicolás J.F., 2020. Saharan Dust Events over the Valencian Community (Eastern Iberian Peninsula): Synoptic Circulation Patterns and Contribution to PM₁₀ Levels. *Aerosol and Air Qual. Res.* 20, 2519–2528.

IPCC, 2021. IPCC Climate Change 2021-The Physical Science Basis. Contribution of Working Group I to the Sixth Assessment Report of the Intergovernmental Panel on Climate Change. Cambridge University Press, Cambridge, United Kingdom and New York, NY, USA, pp. 817–922.

Joshi, H., Manish, N., Liji, D., Tarun, G., Mukunda, G., Suresh, B., 2020. Absorption characteristics of aerosols over the central Himalayas and its adjacent foothills. *Atmos. Res.* 233, 104718.

Kirchstetter, T., Novakov, W., Hobbs, P.V., 2004. Evidence that the spectral dependence of light absorption by aerosols is affected by organic carbon. *J. Geophys. Res.* 109, D221208.

Laskin, A., Laskin, J., Nizkorodov, S.A., 2015. Chemistry of atmospheric brown carbon. *Chem. Rev.* 115, 4335–4382.

Moosmüller, H., Chakrabarty, R.K., Arnott, W.P., 2009. Aerosol light absorption and its measurement: a review. *J. Quant. Spectrosc. Radiat. Transfer* 110 (11), 844–878.

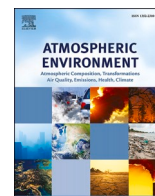
Nepomuceno, S., Wagner, F., Silva, A., 2014. Multiyear Measurements of the Aerosol Absorption Coefficient Near the Surface in a Small-Sized Urban Area in Portugal. *Adv. Meteorol.* 24.

Park, S., Kim, S.W., Lin, N.H., Pani, S.K., Sheridan, P.J., Andrews, E., 2019. Variability of aerosol optical properties observed at a polluted marine (gosan, korea) and a high-altitude mountain (lulin, Taiwan) site in the Asian continental Outflow. *Aerosol Air Qual. Res.* 19, 1272–1283.

Segura, S., Estellés, V., Esteve, A.R., Marcos, C.R., Utrillas, M.P., Martínez-Lozano, J.A., 2016. Multiyear in-situ measurements of atmospheric aerosol absorption properties at an urban coastal site in western Mediterranean. *Atmos. Environ.* 129, 18–26.

Zhang, A., Wang, Y., Zhang, Y., Weber, R.J., Song, Y., Ke, Z., Zou, Y., 2020. Modeling the global radiative effect of brown carbon: a potentially larger heating source in the tropical free troposphere than black carbon. *Atmos. Chem. Phys.* 20, 1901–1920.

Anexo III: Artículos publicados



Sources of water-soluble organic carbon in fine particles at a southern European urban background site

A. López-Caravaca, J. Crespo, N. Galindo, E. Yubero, N. Juárez, J.F. Nicolás*

Atmospheric Pollution Laboratory (LCA), Department of Applied Physics, Miguel Hernández University, Avenida de La Universidad S/N, 03202, Elche, Spain

HIGHLIGHTS

- Sources and monthly evolution of WSOC was analysed at an urban background site.
- WSOC exhibited higher levels during the colder months when BB source peaked.
- A source related to SOA formation is the responsible for a third of the WSOC.
- Average WSOC to OC ratio was 0.46 and it was fairly steady throughout the year.

ARTICLE INFO

Keywords:

PM₁
WSOC
PMF
WSOC/OC ratio

ABSTRACT

In this study, the temporal evolution and sources of water-soluble organic carbon (WSOC) in submicron particles at an urban background site in Elche (Spain) were investigated. Measurements of PM₁ (N = 200) were carried out over one year (2021). Samples were analysed for organic carbon (OC), elemental carbon (EC), WSOC, levoglucosan, elements and major ions. A positive matrix factorization (PMF) analysis was performed in order to identify the sources of WSOC on an annual and a monthly basis. During the study period, traffic restrictions due to COVID-19 led to lower concentrations of PM₁ and carbonaceous compounds than expected. The WSOC annual average mass concentration was 0.95 $\mu\text{g}\cdot\text{m}^{-3}$, with maximum values during the colder months. The apportionment results indicate that the biomass burning (BB) source contributed 30.63% to WSOC levels, road traffic (RT) accounted for 23.90% of the WSOC, while the contribution of a source related to secondary organic aerosol formation (ammonium sulfate-AS) was 33.80%. Minor sources of WSOC were: soil dust (SD) and secondary nitrate (SN), which contributed 7.44% and 4.22%, respectively, to WSOC concentrations. The WSOC/OC ratio did not exhibit significant variations during the study period, since source contributions were similar for WSOC and OC. The highest values of this ratio were recorded in summer, due to the higher contribution from the AS source to WSOC concentrations.

1. Introduction

Organic carbon (OC) can be divided into water-soluble organic carbon (WSOC) and water-insoluble organic carbon. WSOC is a complex mixture of compounds likely containing oxygenated functional groups such as carboxyl, hydroxyl and carbonyl groups (Saxena and Hildemann, 1996) and comprises typically 20–70% of OC (Pio et al., 2007). Water-solubility affects the chemical and physical properties of aerosols, which are key factors in determining their effects on human health and the environment. Water-soluble organic compounds modify the hygroscopicity of aerosols and their ability to act as cloud condensation nuclei, thus having an important impact on both the Earth's albedo and climate

(Asa-Awuku et al., 2009; Kanakidou et al., 2005). The impact of WSOC on climate is not limited to its influence on cloud formation, but also to its light absorbing properties in the UV–visible region (Laskin et al., 2015; Park and Son, 2017). Additionally, there is significant interest in the measurement of the water-soluble fraction of the organic aerosol since, once inhaled, it can cause specific adverse effects on human health (Tuet et al., 2016; Velali et al., 2016).

WSOC can be emitted directly from sources (primary emissions) or result from atmospheric processes (secondary sources) (Hecobian et al., 2010). Direct emissions from biomass burning (BB) and secondary organic aerosol (SOA) formation have been recognized as the two most significant sources of WSOC (Saxena and Hildemann, 1996; Decesari

* Corresponding author. Laboratory of Atmospheric Pollution, Miguel Hernández University, Av. de la Universidad s/n, Edif. Alcudia, 03202, Elche, Spain.
E-mail address: j.nicolas@umh.es (J.F. Nicolás).

et al., 2006; Jin et al., 2020). However, WSOC can be released to a lesser extent from other sources such as motor vehicle emissions (Xie et al., 2016; Yu and Park, 2021) or soil dust (Yu et al., 2021). Therefore, the chemical features of WSOC in atmospheric aerosols are specific of the location of the study area and can provide information on the origin of atmospheric PM.

WSOC mass size distributions usually show a pronounced maximum in the accumulation mode ($\sim 0.5 \mu\text{m}$), independently of the characteristics of the sampling site, as shown in the works by Bougiatioti et al. (2013) (marine background), Matta et al. (2003), Timonen et al. (2008) and Frka et al. (2018) (urban background), or Duarte et al. (2008) (urban and coastal rural areas). A higher contribution of WSOC in the submicron fraction has been reported under broad anthropogenic pollution conditions (Turšič et al., 2006). In general, more than 60% of WSOC is distributed in the submicron fraction, as reported in the mentioned studies.

A number of previous works have shown that WSOC concentrations in urban environments are usually higher in winter than in summer (Viana et al., 2007; Du et al., 2014; Witkowska and Lewandowska, 2016; Frka et al., 2018; Kaskaoutis et al., 2022). This can be explained considering that the contributions from local combustion emissions to the mass loading of carbonaceous materials are greater during winter, as a consequence of increased energy consumption and poor atmospheric dispersion conditions during this season (Park and Cho, 2011). However, other studies have reported a different seasonal pattern. For instance, Taghvaei et al. (2019) and Snyder et al. (2009), found higher WSOC concentrations during summer in Athens (Greece) and the Mid-western United States, respectively, which is consistent with the photochemical production of secondary organic carbon (SOC).

Despite the importance and abundance of WSOC, data on the water-soluble fraction of the atmospheric organic aerosol are scarce in urban areas of the Western Mediterranean basin (Matta et al., 2003; Viana et al., 2007; Duarte et al., 2008; Mladenov et al., 2011), especially in the PM₁ fraction. With the aim of addressing this knowledge gap, this paper presents the results of the WSOC content in PM₁ during a year-long campaign at an urban background station (UBS) in southern Europe. WSOC measurements were completed with the chemical analysis of inorganic ions, metals, OC, elemental carbon (EC) and levoglucosan from the filter samples. The goals of this study are to explore the seasonal variation of WSOC and evaluate its sources by using the PMF technique. Also, the contribution from primary and secondary sources is assessed. In addition, the results of this work will serve as a basis for further research focusing on light absorption properties of WSOC.

2. Methodology

2.1. Monitoring site and sampling

The monitoring station was placed at the campus of the Miguel Hernández University of Elche (UMH) (38°16' N; 0°41' W; 93 m.a.s.l.). The city is located in the southeast of the Iberian Peninsula, close to the Mediterranean Sea. A description of the urban features of Elche and its climate can be found in Nicolás et al. (2020). The station is located in a well-ventilated area on the outskirts of the city, and can be considered as an urban background site. The sampling campaign was carried out throughout the year 2021. Twenty-four hour PM₁ samples were collected onto quartz fibre filters by means of a Derenda 3.1 low volume sampler ($2.3 \text{ m}^3 \cdot \text{h}^{-1}$). PM masses were determined by gravimetric analysis in an environmentally controlled chamber (temperature of $20 \pm 1 \text{ }^\circ\text{C}$ and relative humidity of $50 \pm 5\%$). The sampling frequency was approximately four times a week. During the study period, 200 PM₁ samples were collected. The number of samples per season was similar: winter (59), spring (49), summer (40) and autumn (52). Seasons are defined as winter (January–March), spring (April–June), summer (July–September) and autumn (October–December).

2.2. Analytical procedures

PM₁ samples were analysed for major and trace elements, OC and EC, inorganic ions, levoglucosan and WSOC. In the elemental analysis, minimum detection limits (MDL) were determined as described in Giannoni et al. (2015). For the remaining techniques, MDL were calculated as 2σ . Analytical procedures are briefly described next.

Elemental analysis was performed by Energy Dispersive X-Ray Fluorescence (ED-XRF) using an ARL Quant'x Spectrometer (Thermo Fisher Scientific, UK) with a Si(Li) detector. A detailed description of this procedure is reported in Chiari et al. (2018). In this work, the concentrations of selected metals (K, Ca, Ti, V, Fe and Zn) are presented. Other trace metals (Ni, Mn, Cr, Ni and Cu) showed concentrations frequently below the detection limits of the measurement technique and are not used in the present study.

After the elemental analysis, half of each filter was extracted with ultrapure water using an ultrasonic bath. The water extracts were then analysed to determine the concentrations of ions and WSOC. Ion chromatography (IC) was used to determine major anions (Cl^- , SO_4^{2-} , NO_3^- , $\text{C}_2\text{O}_4^{2-}$) and cations (Na^+ , NH_4^+ , Mg^{2+} , K^+ , Ca^{2+}). For a complete description of this technique, see Galindo et al. (2018). The percentage of valid data was higher than 75% for all ions except Cl^- , Mg^{2+} and Na^+ . (These ions have not been used in the subsequent statistical analysis). For the determination of WSOC levels, a TOC-L CSH analyser (Shimadzu) was used. The instrument uses a $680 \text{ }^\circ\text{C}$ combustion catalytic oxidation method. In the present study, WSOC was quantified as the non-purgeable organic carbon (NPOC). For this, an aliquot of the water extract was diluted 1:2 with ultrapure water, acidified with 1 M HCl (PanReac AppliChem) and purged with pure air in order to remove dissolved inorganic carbon and volatile organics. Analyses were run in triplicate and WSOC concentrations were calculated as the average value of the three measurements. Calibration was conducted using a standard solution of potassium hydrogen phthalate (PanReac AppliChem). Concentrations of all samples were above the MDL.

Organic and elemental carbon were measured on 1.5-cm^2 punches taken from the remaining half of the quartz-fibre filter by means of a Thermal-Optical Carbon Aerosol Analyser (Sunset Laboratory, Inc.) according to the EUSAAR-2 protocol. All samples had OC and EC concentrations above the MDL.

High performance anion-exchange chromatography (HPAEC) coupled with pulsed amperometric detection (PAD) was used to quantify levoglucosan in PM₁ samples. For this, the remaining portion of each filter was extracted ultrasonically with ultrapure water. The HPAEC-PAD used here was a Thermo Scientific Dionex Integriion ion chromatograph and an electrochemical detector with a gold working electrode (Galindo et al., 2021). The separation was carried out on a Dionex Carpac PA10 analytical column ($250 \times 4 \text{ mm}$). NaOH at a flow rate of 0.5 mL min^{-1} was used as a carrier solvent. The gradient was: 18 mM (0–2 min), 200 mM (2–9 min; column cleaning), 18 mM (9–29 min; equilibration). The percentage of valid data was 72%.

Summary statistics of PM₁ components, with the exception of carbonaceous compounds, are presented in Table S1 (Supplementary material).

2.3. Meteorological data

Meteorological parameters and ozone (O_3) levels were obtained from a station belonging to the regional network, located approximately 2.5 km to the southeast of the city centre. The Global Data Assimilation System (GDAS1) model from the NOAA Air Resources Laboratory (<http://www.ready.noaa.gov/READYamet.php>) was used for the determination of the planetary boundary layer (PBL) height. Seasonal averages of the main meteorological variables are shown in Table S2 (Supplementary material).

The identification of Saharan dust episodes (SDE) was based on the results of the predictive model BSCDREAM8b (<https://ess.bsc.es/bsc->

dust-daily-forecast). Moreover, a backtrajectory analysis (HYSPLIT model, Draxler and Rolph, 2015) was used to confirm the north-African origin of air masses. Four-day back-trajectories ending at the sampling point at 1500 m a.s.l were obtained at 12:00 UTC for these days. The identification of these events was confirmed by PM time series analysis both at the sampling site and at regional background stations within the study area. This procedure is based on a method for the identification and quantification of the contribution of SDE in Spain and Portugal (Querol et al., 2006).

2.4. Source apportionment by PMF

The PMF model (Paatero and Tapper, 1994) was applied to the whole data set with the aim of identifying both the profiles of the main aerosol sources and their contribution to PM₁ mass concentrations. The EPA PMF v. 5.0 software was used.

Input data were prepared using the procedure suggested by Polissar et al. (1998). PMF results for a varying number of factors (from 4 to 7) were systematically explored in order to find out the most reasonable solution. For this, Q values (i.e., values reached by the objective function which is minimized by the model), distribution of residuals, G-space plots, physical sense of source profiles and contributions were considered. Different uncertainty analyses, including the Bootstrap (BS), Displacement (DISP) and BS-DISP (Bootstrap + Displacement) tests, were performed to further validate the PMF results. Further details on the use of this model can be found elsewhere (Clemente et al., 2021; Galindo et al., 2021).

3. Results

3.1. General characteristics of PM₁ and carbonaceous species

Because of the COVID-19 restrictions and recommendations, the attendance of the students to the university campus during the study period was significantly lower than that during the pre-pandemic period, particularly during the first months of 2021. Therefore, traffic within and in the vicinity of the sampling site was also reduced. The impact of mobility restrictions due the COVID-19 lockdown on PM levels and composition in Elche can be found in Clemente et al. (2022). An important decrease in the concentrations of PM₁ (35%) and carbonaceous components (30% and 60% for OC and EC, respectively) was observed as a consequence of traffic restrictions during this period.

3.1.1. Monthly variation of the concentrations of PM₁ and carbonaceous components

Table 1 shows summary statistics of the levels of PM₁ and carbonaceous components, as well as the WSOC to OC ratio, during 2021. It is assumed that measured concentrations were lower than expected due to mobility restrictions, since traffic has been identified as a major source of PM₁ in urban areas (Squizzato et al., 2016; Brines et al., 2019). In fact, the average PM₁ concentration was lower than the value obtained in a previous work at an UBS in the same city (9.2 µg·m⁻³; Galindo et al., 2013) and significantly lower than those reported for other urban areas in Spain (Mogo et al., 2006; Titos et al., 2014). Another reason that could

Table 1
Statistics of PM₁, OC, EC, WSOC (in µg·m⁻³) and the WSOC/OC ratio at the urban background site in Elche.

	PM ₁	OC	EC	WSOC	WSOC/OC
Mean	7.60	2.11	0.37	0.95	0.46
SD	6.10	1.05	0.20	0.40	0.10
P5	2.39	1.09	0.15	0.41	0.30
Median	6.10	1.86	0.33	0.85	0.47
P95	17.23	3.87	0.78	1.75	0.62
Skewness ^a	3.80	2.56	1.97	1.32	-0.04

^a Skewness ~0 denotes a normal distribution; SD: Standard Deviation.

explain the levels of PM₁ measured during the study period is the low impact of SDE, especially during summer on PM₁. Although these episodes have a greater impact on the coarse fraction, an increase in PM₁ concentrations has also been observed when the study area is under the influence of Saharan dust (Galindo et al., 2020).

The monthly evolution of PM₁ concentrations is presented in Fig. 1a. Maximum monthly levels were measured during late autumn and winter, which is in agreement with the results of previous works (Squizzato et al., 2016; Majewski et al., 2018). The highest PM₁ levels were reached in February due to the occurrence of a stagnation episode and two Saharan dust events.

Average OC and EC concentrations in PM₁ were significantly lower than the values found at other urban background environments in Europe (Squizzato et al., 2016; Majewski et al., 2018). The low levels of EC, which is considered as a reliable motor vehicle tracer in urban areas, underline the special traffic conditions during the sampling period. In previous works performed at a traffic site in the same city, OC and EC concentrations were notably higher than those observed in the present study, particularly for EC (Yubero et al., 2015; Galindo et al., 2019). The contribution of carbonaceous components to PM₁ concentrations during the sampling period was 33%, while at the traffic site OC and EC accounted for 47% of the total PM₁ mass concentration. The results of the chemical mass closure method used to reconstruct PM₁ mass concentrations are shown in Fig. S1 (Supplementary material).

Temporal variations of OC (Fig. 1b) and EC concentrations (Fig. 1c) showed minimum values during spring and summer months. The same seasonal cycle has been described for EC in other works, which can be attributed to less effective dispersion conditions during the cold period (Squizzato et al., 2016). In the case of OC, the observed monthly variability can also be explained considering that the partitioning of semi-volatile organic compounds into the condensed phase is favoured by the lower winter temperatures (Yubero et al., 2014).

As regards WSOC, the number of works dealing with the water-soluble organic content of the PM₁ fraction in urban and suburban environments is scarce. In fact, most published data on WSOC concentrations refer to PM_{2.5} (e.g. Viana et al., 2007; Pio et al., 2007; Snyder et al., 2009; Sciare et al., 2011; Park et al., 2012). Table 2 presents average levels of WSOC in PM₁ measured at urban background stations in Europe. Concentrations in the PM_{2.5} fraction are not shown here, since a significant portion of the WSOC mass is found in the super-micron size range (Duarte et al., 2008; Timonen et al., 2008; Bougiatioti et al., 2013; Witkowska and Lewandowska, 2016), and thus data would not be comparable.

The average WSOC concentration measured in Elche (0.95 µg·m⁻³) was similar to that found in Helsinki (excluding BB episodes); nevertheless, it was approximately half of the values registered in Ljubljana and Mainz, and much lower than the levels reached in Bologna. Thus, WSOC concentrations at our sampling point were in the lower range of previously reported values for European urban background areas.

The temporal variability of WSOC levels (Fig. 1d) was similar to that displayed by OC, with maximum values during late autumn and winter. The highest monthly concentration (1.43 µg·m⁻³-median value) was reached in December due to a BB episode occurring at the end of the month. In fact, daily WSOC levels significantly increased under these events, which contributes to explain the seasonal variability shown in Fig. 1d. The maximum daily concentration (2.8 µg·m⁻³) was measured on a day with biomass burning activities in the study area. WSOC levels in PM₁ may show important variations depending on emission sources. Thus, Timonen et al., 2008, reported WSOC concentrations at an UBS in Finland ranging from 0.58 µg·m⁻³, in air masses originating from the clean arctic, to 4.3 µg·m⁻³, when PM was transported from wild land fire areas.

The small standard deviation of the WSOC/OC ratio suggests a similar contribution from sources to both WSOC and OC. The average value of this ratio (0.46) was between the ratios found in urban areas where traffic is the main pollution source and the higher values observed

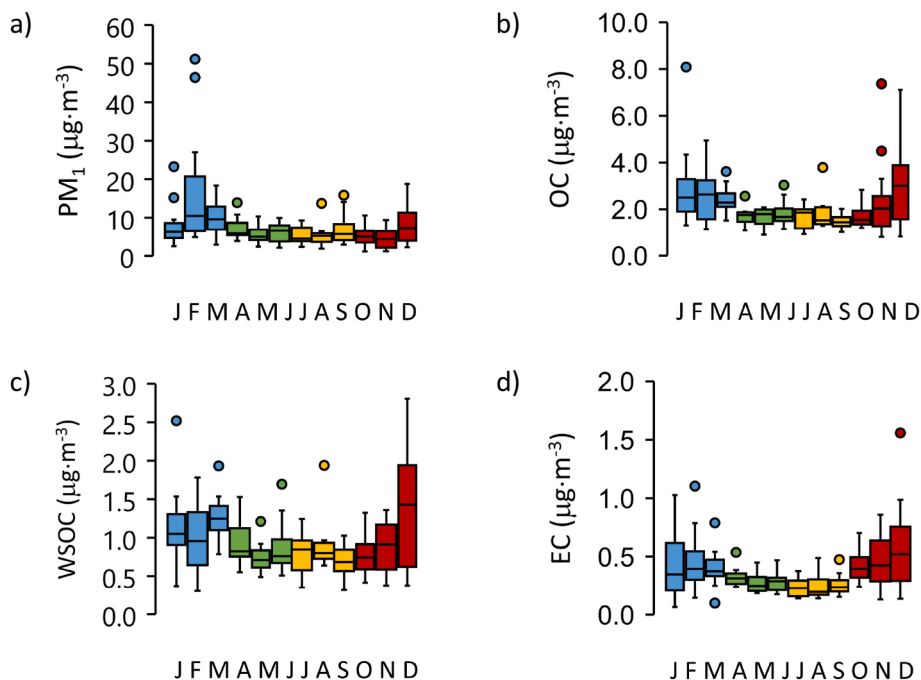


Fig. 1. Monthly evolution of: a) PM₁, b) OC, c) EC and d) WSOC. The upper and lower edges of the box represent the 75th and 25th percentiles, respectively, and the whiskers are the maximum and minimum values. The line inside the box plot represents the median value. Dots are outlier values.

Table 2

WSOC mean concentrations (µg·m⁻³) obtained at different urban stations in Europe.

Site	Size	WSOC ^a	Period	Reference
Helsinki (Finland)	PM ₁	1.5 (0.85) ^b	Annual	Saarikoski et al. (2008)
Ljubljana (Slovenia)	d < 1.0 µm	3.7–0.45–1.4–1.4	W–S–Su–A	Frka et al. (2022)
Mainz (Germany)	d < 0.9 µm	1.82	A	Voliotis et al., 2017
Bologna (Italy)	d < 1.2 µm	4.11–1.14 ^c	W + A–S + Su	Matta et al. (2003)

W (Winter); S (Spring); Su (Summer); A (Autumn).

^a Obtained from the sum of the concentration from each impactor stage, (with the exception of Helsinki).

^b Excluding two major biomass burning episodes.

^c Median values.

at rural sites or forest areas (Park and Cho, 2011; Li et al., 2010). The WSOC/OC ratio distribution was normal (Table 1), and therefore average and median values were nearly the same. Monthly variations of WSOC concentrations and the WSOC/OC ratio are discussed in the next section.

3.2. Sources of WSOC

3.2.1. General characterization of sources

Five factors were identified using the PMF model. This solution showed the highest stability, with ≥96% of the BS factors mapped to the base factors. Additionally, no factor swapping or decrease in Q was observed in DISP. In the BS-DISP uncertainty method, 92% of the BS resamplings were accepted and there was a 0.1% decrease in Q with just 1–3 swaps for some of the factors at the lowest dQmax. The sources identified have been named as ammonium sulfate (AS), biomass burning (BB), secondary nitrate (SN), soil dust (SD) and road traffic (RT). The correlation between measured and modelled PM₁ concentrations was quite good (R² = 0.70).

Fig. 2 shows the monthly evolution of the percentage contribution

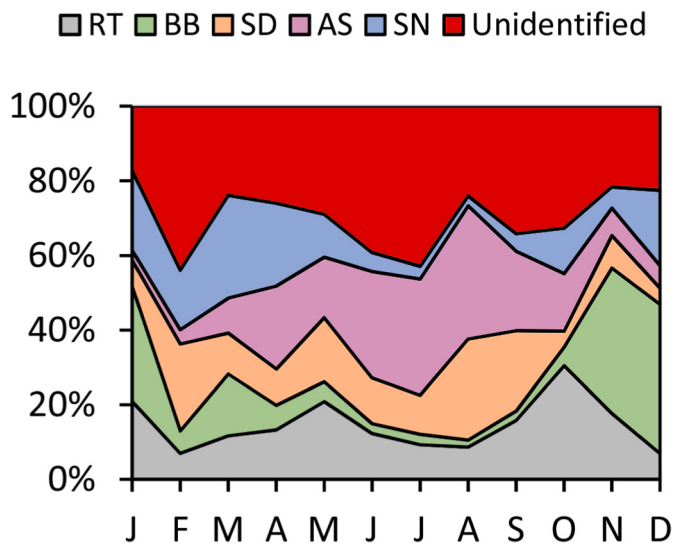


Fig. 2. Monthly evolution of percentage contribution of the different PMF factors to the mean measured PM₁ concentration.

from the sources obtained using the PMF model. The percentage contribution of the identified factors to the mean PM₁ concentration was ~70%. Significant contributions from AS were observed during the warmer period, while BB accounted for around 40% of the PM₁ mass during late autumn.

Fig. 3 shows the chemical profiles of the identified PM₁ sources and their temporal evolution. The bars show the composition profile, whereas the blue squares indicate the percentage of the total mass explained by each factor. The figures on the right side present the temporal variability of each factor, as well as the average monthly contribution of WSOC to the mass concentration of each factor (in brown).

Factor 1 was dominated by sulfate and ammonium (called ammonium sulfate factor). This factor contributed 33.76% to the mean

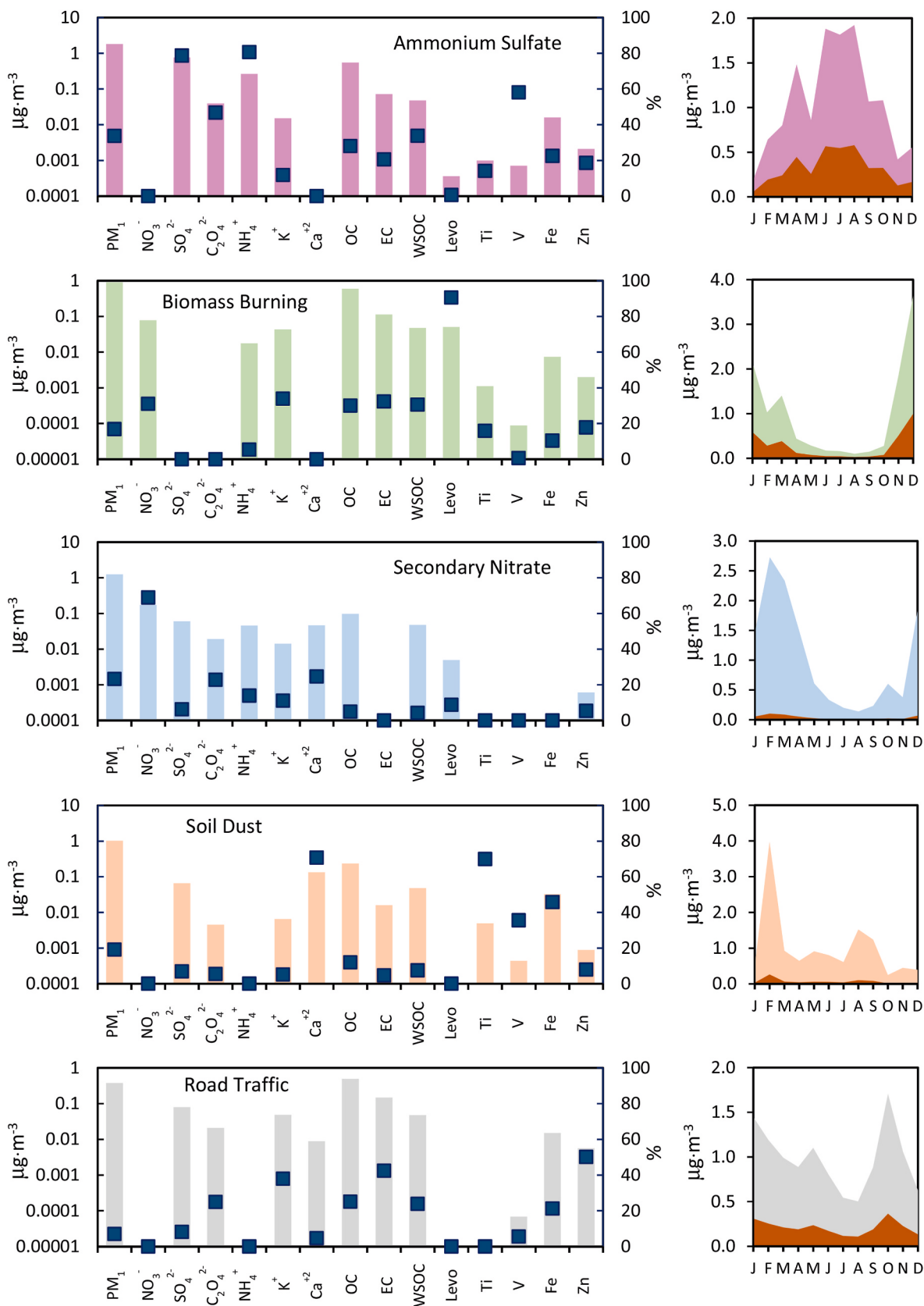


Fig. 3. Chemical profiles of the identified PMF factors. The plots on the right side show temporal variations of PM₁ and WSOC levels (in brown) associated with each factor.

modelled concentration of PM₁. The seasonal evolution of this source was the same as that previously described for (NH₄)₂SO₄ in the study area. Concentrations were maxima in summer since the oxidation rate of SO₂ to H₂SO₄ is highest during this season due to higher temperatures and solar radiation (Nicolás et al., 2009). The high contribution of V suggests that this source also includes emissions from oil combustion (Theodosi et al., 2018), being the PMF analysis unable to distinguish between both sources.

Factor 2 was identified as a biomass burning source. This factor accounted for only 16.87% of the average PM₁ concentration and explained a large fraction of BB tracers such as K⁺ (34.00%) and levoglucosan (90.56%). NO₃⁻ and OC are generally associated with this source as well (Sharma et al., 2016). The OC/EC ratio in the BB factor was 5.3, which is within the upper range of ratios reported for other southern European cities (Amato et al., 2016). This may be explained by a higher proportion of secondary organic aerosols in the study area (Clemente et al., 2021). The BB source showed a marked seasonal cycle, with maximum values during the coldest months. The highest WSOC concentrations during winter were associated with this factor.

The third factor was identified as secondary nitrate, and accounted for 69.00% of NO₃⁻. The contribution from this source to the average PM₁ concentration was 23.32%. Nitrate in this source is related to the formation of secondary nitrate particles through reactions of nitric acid with ammonia and soil particles. The SN source showed a clear maximum in winter and early spring when NO₃⁻ is principally as NH₄NO₃ in the PM₁ fraction (Galindo et al., 2013). Maximums NH₄NO₃ concentrations during the coldest months are due to the higher frequency of atmospheric stagnation episodes and the lower temperatures that favor its formation.

Factor 4 represents the soil dust source. This factor explained 69.88% of the Ti mass concentration, which suggests that it includes mineral dust from North Africa. As reported in previous works performed in the same study region, Ti can be used as a tracer of Saharan dust (Galindo et al., 2020). In fact, in the graph showing the temporal evolution of this source, it can be clearly observed that the maximum concentration was reached in February, coinciding with two intense Saharan dust events in the study area. This source contributed 19.10% to the average PM₁ concentration during the study period. This contribution was slightly higher than that determined by the chemical mass closure method (see Fig. S1).

The last factor was identified as the road traffic source. This factor accounted for 7.03% of the average PM₁ mass concentration. This source explained large fractions of typical road traffic tracers such as EC (42.45%), a marker of tailpipe exhaust emissions (Sharma et al., 2014; Megido et al., 2016) or Zn (50.19%), usually linked to particles emitted from tyre wear (Grigoratos and Martini, 2014; Pant and Harrison, 2013).

As mentioned above, Fig. 3 also displays average monthly WSOC concentrations for each of the identified sources. These temporal variations help understand the seasonal trend in WSOC levels shown in Fig. 1. Thus, the high concentrations registered during late autumn and early winter were due to BB emissions.

Although there are evidences in the literature on the secondary nature of WSOC, a factor exclusively associated with Secondary Organic Aerosol (SOA) formation could not be identified, most likely because specific tracers of SOA formation, such as dicarboxylic acids other than oxalate, were not analysed (Xie et al., 2016). Nevertheless, previous works have used ozone as a marker of SOA formation (Saarikoski et al., 2008). The relationship between O₃ and SOA is most likely due to the fact that they originate through synchronized photochemical reactions from the same volatile organic compounds (Tohidi et al., 2022). To provide insights into this question, correlations between O₃ concentrations and the contribution from each factor were calculated (Table S3, Supplementary material). The only source that was significantly correlated with ozone ($p_{\text{Spearman}} = 0.730$; $p\text{-value} < 0.05$) was AS. The presence of oxalate in this source also supports that SOA formation was primarily associated with this factor (Saarikoski et al., 2008).

Another feature of the AS factor is that the relationship between the concentration of WSOC explained by this source and relative humidity (RH) was different depending on the season of the year. This suggests different formation mechanisms during the warm and cold periods. Fig. S2 shows the relationship between WSOC concentrations in the AS source and RH during spring-summer and autumn-winter. Data were grouped in 10% RH bins from HR < 50% (bin 1) to HR > 90% (bin 6). The number of days within each RH interval is also shown. During the warm season, a rise in WSOC concentrations as RH increased was not observed. Instead, concentrations were approximately the same for all RH bins (with the exception of bin 5). In contrast, during autumn and winter, WSOC levels increased as RH became higher. In fact, a strong correlation between WSOC concentrations and RH was obtained ($R^2 = 0.90$; $p\text{ value} < 0.05$) during the cold season. Differences between SOA formation pathways in summer and winter have been reported in other works (Galindo et al., 2019; Xiang et al., 2017). The most likely explanation is that aqueous-phase chemistry is a major pathway for SOA formation in winter, while during the warm season SOA is predominantly generated through gas-phase photochemical reactions.

3.2.2. Source contributions to WSOC

The correlation between measured and modelled WSOC concentrations is shown in Fig. 4, while the contribution of each source to the average modelled WSOC concentration is presented in Fig. 5.

The AS factor was the source that contributed most to the average WSOC concentration (33.8%). The BB and RT factors also accounted for a significant fraction of WSOC levels. The remaining sources contributed less than 10% to the average WSOC concentration. Comparison of the percentage contributions from the 3 main factors with those obtained in other similar studies (Table 3) reveals a high contribution from the BB and RT sources to WSOC levels in the study area. On the other hand, the contribution from the AS source was lower than those found at other urban areas.

The mean monthly contribution of each source to WSOC levels is presented in Fig. 6. The main conclusions that can be drawn from this figure are: a) the BB source was the main contributor to WSOC during late autumn and early winter, accounting for more than 50% of the total mass concentration in that period; b) during the warm season, WSOC was primarily associated with secondary processes (AS). The contribution from this source was higher than 65% during summertime and c) the contribution from the road traffic factor was relatively constant throughout the year, except in October, when it reached its maximum

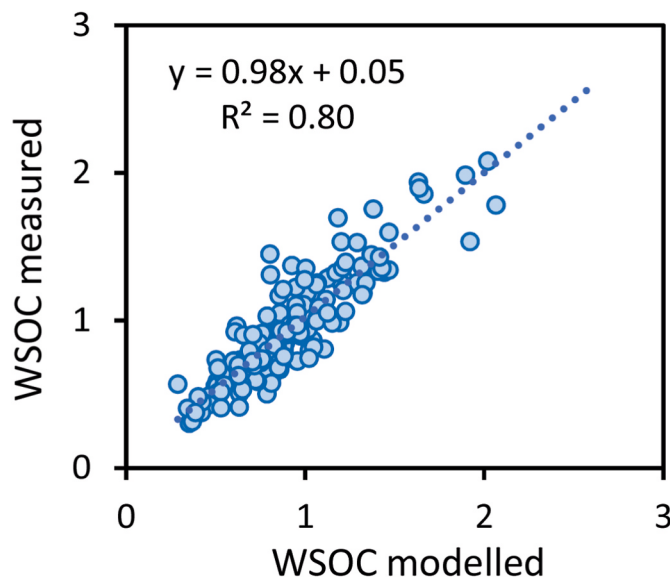


Fig. 4. PMF modelled versus measured WSOC concentrations.

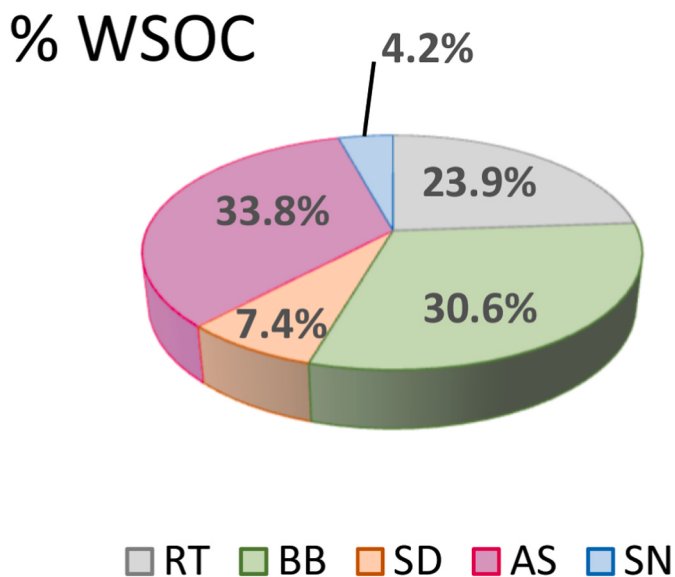


Fig. 5. Percentage contribution of WSOC to each source.

Table 3
Contributions of AS, BB and Traffic sources to WSOC at different sites.

Site	AS	BB	Traffic	Reference
Gwangju ^a (Korea)-Road site	51.3/30.5	11.6/19.9	19.0/14.8	Park et al. (2015)
Helsinki (Finland)-UBS	50.5	17.3	12.9	Saarikoski et al. (2008)
Beijing (China)-Urban site	53.7 ^b	39.0	6.0 ^c	Du et al. (2014)
Elche (Spain)-UBS	33.8	30.6	23.9	This study

^a Contribution of: Hydrophilic WSOC/Hydrophobic WSOC.

^b Contribution of AS and Oxalate sources.

^c Mixed primary source.

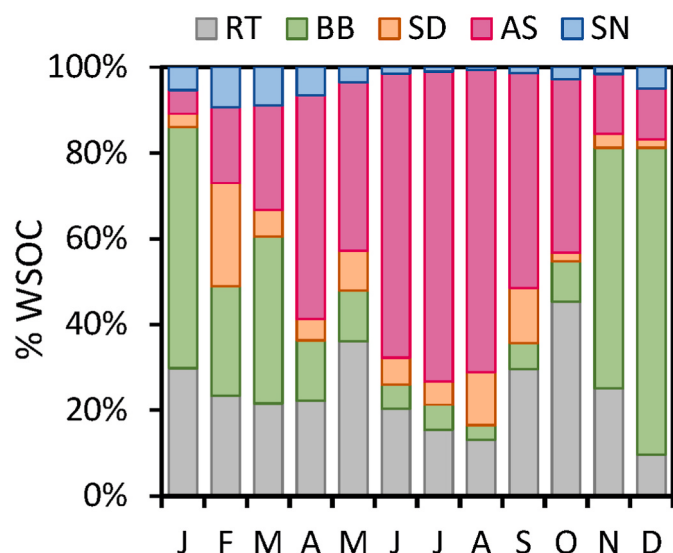


Fig. 6. Monthly percentage contribution from each source to WSOC levels.

value.

If the SD, BB and RT factors are considered to be associated with primary emissions (Jin et al., 2020), and the remaining factors with secondary aerosol formation processes, it can be concluded that WSOC came mainly from primary sources during autumn and winter (~75%),

while during the summer and spring seasons secondary formation accounted for ~65% and ~57%, respectively, of the measured WSOC concentration. It is important to mention that, although BB emissions has been considered as a primary source of WSOC, this is not straightforward since the formation mechanisms of biomass burning-related WSOC are still not well understood. Indeed, it is possible that the solubility of organic aerosol in biomass burning plumes could be increased by aging processes (Timonen et al., 2013). Thus, the increase of WSOC levels under BB influence does not necessarily imply a primary origin of WSOC (Du et al., 2014).

3.2.3. Ratio WSOC/OC

The low seasonal variability of the WSOC to OC ratio (Fig. 7) indicates that source contributions to both WSOC and OC were similar during the study period (Saarikoski et al., 2008), as can be checked in Fig. 2. Additionally, a high Spearman correlation coefficient between daily WSOC and OC concentrations was obtained ($\rho = 0.859$; $p\text{-value} < 0.001$).

The lowest WSOC/OC ratio was observed in early winter, specifically in February (0.405- median value), which indicates a higher contribution from water-insoluble organic components during that period. In order to provide insights into the seasonal variability of the WSOC/OC ratio, Table 4 shows the average WSOC/OC ratio for each of the sources identified with the PMF model.

WSOC/OC ratios were higher for secondary than for primary sources. The ratio for the SD source was unexpectedly low, since it has been reported that long-range transport allows for more photochemical processing of aerosols leading to more oxidized and therefore more water-soluble OC (Saarikoski et al., 2008). As can be seen in Fig. 6, the largest contribution from the AS factor to WSOC levels was reached in summer, which could explain the increase of the WSOC/OC ratio observed during this season in Fig. 7. Even so, the WSOC/OC ratio obtained during summer in the study area (0.48) was lower than those reported for other urban sites in Europe. For instance, Szidat et al. (2009) found a ratio of 0.53 in Göteborg (Sweden), while the WSOC/OC ratio in Athens (Greece) was ~0.71 (Paraskevopoulou et al., 2014). This could be due to the significant contribution from the Soil Dust (SD) source to PM₁ concentrations during August and September (~12.5%, see Fig. 6), since the lowest WSOC/OC ratio was obtained for this source.

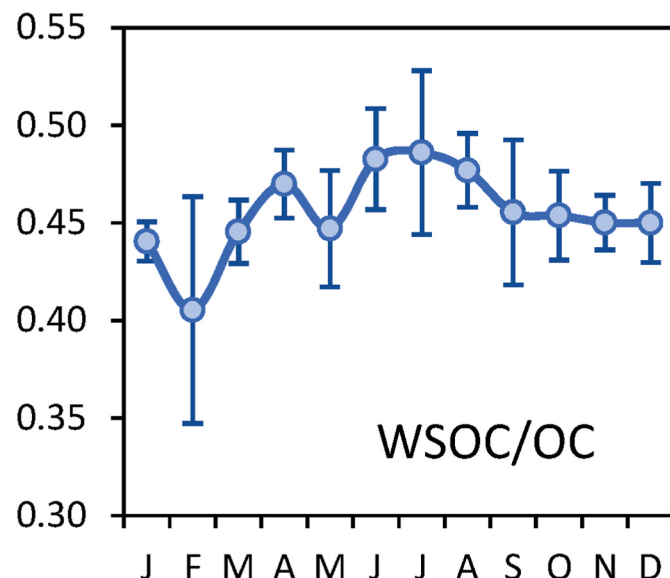


Fig. 7. Monthly evolution of the WSOC to OC ratio.

Table 4
Average WSOC/OC ratios for the six identified sources.

Source	WSOC/OC
AS	0.545
BB	0.461
SN	0.487
SD	0.283
RT	0.433

4. Conclusions

Two hundred PM₁ samples were collected during 2021 at the campus of the University of Elche and analysed for chemical characterisation. Due to mobility recommendations given by local and university authorities during the study period, the concentrations of PM₁ and the associated carbonaceous components (OC and EC) were lower than expected for an urban background environment. For this reason, WSOC average levels were found to be low compared to those measured at other urban background sites in Europe.

The seasonal evolution of WSOC concentrations was analysed on the basis of the WSOC source apportionment performed using the PMF model. BB was identified as the main contributor to WSOC levels during the cold season, while during summer the AS factor accounted for the largest fraction of the WSOC. This source is most likely associated with secondary organic aerosol formation. The traffic source registered a small contribution to the annual average of PM₁ during the study period. Nevertheless, it accounted for a significant fraction of the total WSOC. The average contribution of these three sources to the annual average WSOC concentration was nearly 90%.

The contribution of each of the identified sources to OC and WSOC concentrations was very similar; for this reason, the WSOC/OC ratio was fairly constant throughout the year, with an average value of 0.46. Slightly higher values were measured in summer due to a higher contribution from the AS source to WSOC levels.

CRedit authorship contribution statement

A. López-Caravaca: Formal analysis, Investigation, Visualization, Writing – original draft, Writing – review & editing. **J. Crespo:** Funding acquisition, Project administration, Conceptualization. **N. Galindo:** Writing – review & editing, Supervision. **E. Yubero:** Supervision, Writing – review & editing. **N. Juárez:** Formal analysis, Investigation. **J. F. Nicolás:** Writing – original draft, Supervision, Funding acquisition, Project administration, Investigation.

Declaration of competing interest

The authors declare that they have no known competing financial interests or personal relationships that could have appeared to influence the work reported in this paper.

Data availability

Data will be made available on request.

5. Acknowledgements

This work was supported by the Spanish Ministry of Science, Innovation and Universities (COSMOS Project, ref. RTI 2018-098639-B-I00). A. López-Caravaca thanks the Spanish Ministry of Science and Innovation for a predoctoral grant (PRE 2019-089098).

Appendix A. Supplementary data

Supplementary data to this article can be found online at <https://doi.org/10.1016/j.atmosenv.2023.119844>.

References

- Amato, F., Alastuey, A., Karanasiou, A., Lucarelli, F., Nava, S., Calzolari, G., Severi, M., Becagli, S., Gianelle, V., Colombi, C., Alves, C., Custódio, D., Nunes, T., Cerqueira, M., Pio Eleftheriadis, K., Diapouli, E., Reche, C., Minguillón, M.C., Vratolis, S., Harrison, R.M., Querol, X., 2016. AIRUSE-LIFE+: a harmonized PM speciation and source apportionment in five southern European cities. *Atmos. Chem. Phys.* 16, 3289–3309.
- Asa-Awuku, A., Engelhart, G.J., Lee, B.H., Pandis, S.N., Nenes, A., 2009. Relating CCN activity, volatility, and droplet growth kinetics of β -caryophyllene secondary organic aerosol. *Atmos. Chem. Phys.* 9, 795–812.
- Bougiatioti, A., Zampas, P., Koulouri, E., Antoniou, M., Theodosi, C., Kouvarakis, G., Saarikoski, S., Mäkelä, T., Hillamo, R., Mihalopoulos, N., 2013. Organic, elemental and water-soluble organic carbon in size segregated aerosols, in the marine boundary layer of the Eastern Mediterranean. *Atmos. Environ.* 64, 251–262.
- Brines, M., Dall'Osto, M., Amato, F., Minguillón, M.C., Karanasiou, A., Grimalt, J.O., Alastuey, A., Querol, X., van Drooge, B.L., 2019. Source apportionment of urban PM₁ in Barcelona during SAPUSS using organic and inorganic components. *Environ. Sci. Pollut. Res.* 26, 32114–32127.
- Chiari, M., Yubero, E., Calzolari, G., Lucarelli, F., Crespo, J., Galindo, N., Nicolás, J.F., Giannoni, M., Nava, S., 2018. Comparison of PIXE and XRF analysis of airborne particulate matter samples collected on Teflon and quartz fibre filters. *Nucl. Instrum. Methods B* 417, 128–132.
- Clemente, A., Yubero, E., Galindo, N., Crespo, J., Santacatalina, M., Carratalá, A., 2021. Quantification of the impact of port activities on PM₁₀ levels at the port-city boundary of a Mediterranean city. *J. Environ. Manag.* 281, 111842.
- Clemente, A., Yubero, E., Nicolás, J.F., Caballero, S., Crespo, J., Galindo, N., 2022. Changes in the concentration and composition of urban aerosols during the COVID-19 lockdown. *Environ. Res.* 203, 111788.
- Decesari, S., Fuzzi, S., Facchini, M.C., Mircea, M., Emblico, L., Cavalli, F., Maenhaut, W., Chi, X., Schkolnik, G., Falkovich, A., Rudich, Y., Claeys, M., Pashynska, V., Vas, G., Kourtev, I., Vermeylen, R., Hoffer, A., Andreae, M.O., Tagliavini, E., Moretti, F., Artaxo, P., 2006. Characterization of the organic composition of aerosols from Rondônia, Brazil, during the LBA-SMOCC 2002 experiment and its representation through model compounds. *Atmos. Chem. Phys.* 6, 375–402.
- Draxler, R.R., Rolph, G.D., 2015. HYSPLIT (HYbrid Single-Particle Lagrangian Integrated Trajectory) Model Access via NOAA ARL READY Website. <http://ready.arl.noaa.gov/HYSPLIT.php>.
- Du, Z., He, K., Cheng, Y., Duan, F., Ma, Y., Liu, J., Zhang, X., Zheng, M., Weber, R., 2014. A yearlong study of water-soluble organic carbon in Beijing I: sources and its primary vs. secondary nature. *Atmos. Environ.* 92, 514–521.
- Duarte, R., Miegro, C.L., Penetra, A., Pio, C.A., Duarte, A.C., 2008. Carbonaceous materials in size-segregated atmospheric aerosols from urban and coastal-rural areas at the Western European Coast. *Atmos. Res.* 90, 253–263.
- Frka, S., Grgić, I., Tursić, J., Gini, M.I., Eleftheriadis, K., 2018. Seasonal variability of carbon in humic-like matter of ambient size-segregated water-soluble organic aerosols from urban background environment. *Atmos. Environ.* 173, 239–247.
- Frka, S., Sala, M., Brodnik, H., Štefane, B., Kroflič, A., Grgić, I., 2022. Seasonal variability of nitroaromatic compounds in ambient aerosols: mass size distribution, possible sources and contribution to water-soluble brown carbon light absorption. *Chemosphere* 299, 134381.
- Galindo, N., Gil-Moltó, J., Varea, M., Chofre, C., Yubero, E., 2013. Seasonal and interannual trends in PM levels and associated inorganic ions in southeastern Spain. *Microchem. J.* 110, 81–88.
- Galindo, N., Yubero, E., Nicolás, J.F., Varea, M., Clemente, A., 2018. Day-night variability of PM₁₀ components at a Mediterranean urban site during Winter. *Air Qual. Atmos. Health* 11, 1251–1258.
- Galindo, N., Yubero, E., Clemente, A., Nicolás, J.F., Navarro-Selma, B., Crespo, J., 2019. Insights into the origin and evolution of carbonaceous aerosols in a Mediterranean urban environment. *Chemosphere* 235, 636–642.
- Galindo, N., Yubero, E., Clemente, A., Nicolás, J.F., Varea, M., Crespo, J., 2020. PM events and changes in the chemical composition of urban aerosols: a case study in the western Mediterranean. *Chemosphere* 244, 125520.
- Galindo, N., Clemente, A., Yubero, E., Nicolás, J.F., Crespo, J., 2021. PM₁₀ chemical composition at a residential site in the western Mediterranean: estimation of the contribution of biomass burning from levoglucosan and its isomers. *Environ. Res.* 196, 110394.
- Giannoni, M., Calzolari, G., Chiari, M., Lucarelli, F., Mazzinghi, A., Nava, S., Ruberto, C., 2015. Feasibility study of ED-XRF analysis of atmospheric particulate matter samples collected with high time resolution. *X Ray Spectrom.* 44, 282–288.
- Grigoratos, T., Martini, G., 2014. Non-exhaust Traffic Related Emissions - Brake and Tyre Wear PM. JRC Science and Policy Reports, European Commission.
- Hecobian, A., Zhang, X., Zheng, M., Frank, N., Edgerton, N.E.S., S, E., Weber, R.J., 2010. Water-soluble organic aerosol material and the light-absorption characteristics of aqueous extracts measured over the Southeastern United States. *Atmos. Chem. Phys.* 10, 5965–5977.
- Jin, Y., Yan, C., Sullivan, A.P., Liu, Y., Wang, X., Dong, H., Chen, S., Zeng, L., Collett, J.L., Mei Zheng, M., 2020. Significant contribution of primary sources to water-soluble organic carbon during spring in Beijing, China. *Atmosphere* 11, 395.

- Kanakidou, M., Seinfeld, J.H., Pandis, S.N., Barnes, I., Dentener, F.J., Facchini, M.C., Van Dingenen, R., Ervens, B., Nenes, A., Nielsen, C.J., Swietlicki, E., Putaud, J.P., Balkanski, Y., Fuzzi, S., Horth, J., Moortgat, G.K., Winterhalter, R., Myhre, C.E.L., Tsigaridis, K., Vignati, E., Stephanou, E.G., Wilson, J., 2005. Organic aerosol and global climate modelling: a review. *Atmos. Chem. Phys.* 5, 1053–1123.
- Kaskaoutis, D.G., Grivas, G., Oikonomou, K., Tavarnarakis, P., Papoutsidakis, K., Tsagkaraki, M., Stavroulas, I., Zampas, P., Paraskevopoulou, D., Bougiatioti, A., Liakakou, E., Gavrouzou, M., Dumka, U.C., Hatzianastassiou, N., Sciare, J., Gerasopoulos, E., Mihalopoulos, N., 2022. Impacts of severe residential wood burning on atmospheric processing, water-soluble organic aerosol and light absorption, in an inland city of Southeastern Europe. *Atmos. Environ.* 280, 119139.
- Laskin, A., Laskin, J., Nizkorodov, S.A., 2015. Chemistry of atmospheric brown carbon. *Chem. Rev.* 115, 4335–4382.
- Li, L., Wang, W., Feng, J., Zhang, D., Li, H., Gu, Z., Wang, B., Sheng, G., Fu, J., 2010. Composition, source, mass closure of PM_{2.5} aerosols for four forests in eastern China. *J. Environ. Sci.* 22 (3), 405–412.
- Majewski, G., Rogula-Kozłowska, W., Rozbicka, K., Rogula-Kopiec, P., Mathews, P., Brandyk, A., 2018. Concentration, chemical composition and origin of PM₁: results from the first long-term measurement campaign in Warsaw (Poland). *Aerosol Air Qual. Res.* 18, 636–654.
- Matta, E., Facchini, M.C., Decesari, S., Mircea, M., Cavalli, F., Fuzzi, S., Putaud, J.-P., Dell'Acqua, A., 2003. Mass closure on the chemical species in size-segregated atmospheric aerosol collected in an urban area of the Po Valley, Italy. *Atmos. Chem. Phys.* 3, 623–637.
- Megido, L., Negral, L., Castrillón, L., Marañón, E., Fernández-Nava, Y., Suárez-Peña, B., 2016. Traffic tracers in a suburban location in northern Spain: relationship between carbonaceous fraction and metals. *Environ. Sci. Pollut. Res.* 23, 8669–8678.
- Mladenov, N., Alados-Arboledas, L., Olmo, F.J., Lyamani, H., Delgado, A., Molina, A., Reche, I., 2011. Applications of optical spectroscopy and stable isotope analyses to organic aerosol source discrimination in an urban area. *Atmos. Environ.* 45, 1960–1969.
- Mogo, S., Cachorro, V.E., Sorribas, M., 2006. Optical and chemical properties of atmospheric PM fractions related with air masses in the central Iberian Peninsula. *Opt. Pura Apl.* 39, 331–340.
- Nicolás, J.F., Galindo, N., Yubero, E., Pastor, C., Esclapez, R., Crespo, J., 2009. Aerosol inorganic ions in a semi-arid region on the southeastern Spanish Mediterranean coast. *Water Air Soil Pollut.* 201, 149–159.
- Nicolás, J.F., Lucarelli, F., Galindo, N., Yubero, E., Crespo, J., Calzolari, G., Nava, S., 2020. Impact of traffic flows and meteorological events on the hourly elemental composition of fine and coarse particles at an urban site. *Aerosol Air Qual. Res.* 20, 991–1001.
- Pant, P., Harrison, R.M., 2013. Estimation of the contribution of road traffic emissions to particulate matter concentrations from field measurements: a review. *Atmos. Environ.* 77, 78–97.
- Paraskevopoulou, D., Liakakou, E., Gerasopoulos, E., Theodosi, C., Mihalopoulos, N., 2014. Long-term characterization of organic and elemental carbon in the PM_{2.5} fraction: the case of Athens, Greece. *Atmos. Chem. Phys.* 14, 13313–13325.
- Park, S.S., Cho, S.Y., 2011. Tracking sources and behaviors of water-soluble organic carbon in fine particulate matter measured at an urban site in Korea. *Atmos. Environ.* 45, 60–72.
- Park, S.S., Cho, S.Y., Kim, K.W., Lee, K.-H., Jung, K., 2012. Investigation of organic aerosol sources using fractionated water-soluble organic carbon measured at an urban site. *Atmos. Environ.* 55, 64–72.
- Park, S.S., Cho, S.Y., Bae, M.S., 2015. Source identification of water-soluble organic aerosols at a roadway site using a positive matrix factorization analysis. *Sci. Total Environ.* 533, 410–421.
- Park, S.S., Son, S.C., 2017. Relationship between carbonaceous components and aerosol light absorption during winter at an urban site of Gwangju, Korea. *Atmos. Res.* 185, 73–83.
- Paatero, P., Tapper, U., 1994. Positive Matrix Factorization: a non-negative factor model with optimal utilization of error estimates of data values. *Environmetrics* 5, 111–126.
- Pio, C.A., Legrand, M., Oliveira, T., Afonso, J., Santos, C., Caseiro, A., Fialho, P., Barata, F., Puxbaum, H., Sánchez-Ochoa, A., Kasper-Giebl, A., Gelencsér, A., Preunkert, S., Schock, M., 2007. Climatology of aerosol composition (organic versus inorganic) at nonurban sites on a west-east transect across Europe. *J. Geophys. Res.* 112, D23S02.
- Polissar, A.V., Hopke, P.K., Paatero, P., Malm, W.C., Sisker, J.F., 1998. Atmospheric aerosol over Alaska: 2. Elemental composition and sources. *J. Geophys. Res.* 103 (D15), 19045–19057.
- Querol, X., Alastuey, A., Pey, J., Escudero, M., Castillo, S., Gonzalez, A., Pallares, M., Jiménez, S., Cristóbal, A., Ferreira, F., Marques, F., Monjarino, J., Cuevas, E., Alonso, S., Artiñano, B., Salvador, P., de la Rosa, J., 2006. Spain and Portugal Methodology for the identification of natural African dust episodes in PM₁₀ and PM_{2.5}, and justification with regards to the exceedances of the PM₁₀ daily limit value. In: Ministerio de Medio Ambiente, Medio Rural y Marino (Spain) and Ministério do Ambiente. Ordenamento do Território e Desenvolvimento Regional (Portugal), p. 32.
- Saarikoski, S., Timonen, H., Saarnio, K., Aurela, M., Järvi, L., Kerminen, P., Kerminen, V.-M., M., V., Hillamo, R., 2008. Sources of organic carbon in fine particulate matter in northern European urban air. *Atmos. Chem. Phys.* 8, 6281–6295.
- Saxena, P., Hildemann, L., 1996. Water-soluble organics in atmospheric particles: a critical review of the literature and application of thermodynamics to identify candidate compounds. *J. Atmos. Chem.* 24, 57–109.
- Sciare, J., d'Argouges, O., Sarda-Estève, R., Gaimoz, G., Dolgorouky, C., Bonnaire, N., Favez, O., Bonsang, B., Gros, V., 2011. Large contribution of water-insoluble secondary organic aerosols in the region of Paris (France) during wintertime. *J. Geophys. Res.* 116, D22203.
- Sharma, S.K., Mandal, T.K., Saxena, M., Sharma, R.A., Datta, A., Saud, T., 2014. Variation of OC, EC, WSOC and trace metals of PM₁₀ in Delhi, India. *J. Atmos. Sol. Terr. Phys.* 113, 10–22.
- Sharma, S.K., Sharma, A., Saxena, M., Choudhary, N., Masiwal, R., Mandal, T.K., Sharma, C., 2016. Chemical characterization and source apportionment of aerosol at an urban area of Central Delhi, India. *Atmos. Pollut. Res.* 7, 110–121.
- Snyder, D.C., Rutte, A.P., Collins, R., Worley, C., Schauer, J.J., 2009. Insights into the origin of water-soluble organic carbon in atmospheric fine particulate matter. *Aerosol Sci. Technol.* 43 (11), 1099–1107.
- Squizzato, S., Masiol, M., Agostini, C., Visin, F., Formenton, G., Harrison, R.M., Rampazzo, G., 2016. Factors, origin and sources affecting PM₁ concentrations and composition at an urban background site. *Atmos. Res.* 180, 262–273.
- Szidat, S., Ruff, M., Perron, N., Wacker, L., Synal, H.-A., Hallquist, M., Shannigrahi, A.S., Yttri, K.E., Dye, C., Simpson, D., 2009. Fossil and non-fossil sources of organic carbon (OC) and elemental carbon (EC) in Göteborg, Sweden. *Atmos. Chem. Phys.* 9, 1521–1535.
- Taghvaei, S., Sowlat, M.H., Diapouli, E., Manousakas, M.I., Vasilatou, V., Eleftheriadis, K., Sioutas, C., 2019. Source apportionment of the oxidative potential of fine ambient particulate matter (PM_{2.5}) in Athens, Greece. *Sci. Total Environ.* 653, 1407–1416.
- Theodosi, C., Tsagkaraki, M., Zampas, P., Grivas, G., Liakakou, E., Paraskevopoulou, D., Lianou, M., Gerasopoulos, E., Mihalopoulos, N., 2018. Multi-year chemical composition of the fine-aerosol fraction in Athens, Greece, with emphasis on the contribution of residential heating in wintertime. *Atmos. Chem. Phys.* 18, 14371–14391.
- Timonen, H., Saarikoski, S., Tolonen-Kivimäki, O., Aurela, M., Saarnio, K., Petäjä, T., Aalto, P.P., Kulmala, M., Pakkanen, T., Hillamo, R., 2008. Size distributions, sources and source areas of water-soluble organic carbon in urban background air. *Atmos. Chem. Phys.* 8, 5635–5647.
- Timonen, H., Carbone, S., Aurela, M., Saarnio, K., Saarikoski, S., Ng, N.L., Canagaratna, M.R., Kulmala, M., Kerminen, V.M., Worsnop, D.R., Hillamo, R., 2013. Characteristics, sources and water-solubility of ambient submicron organic aerosol in springtime in Helsinki, Finland. *J. Aerosol Sci.* 56, 61–77.
- Titos, G., Lyamani, H., Pandolfi, M., Alastuey, A., Alados-Arboledas, L., 2014. Identification of fine (PM₁) and coarse (PM₁₀₋₁) sources of particulate matter in an urban environment. *Atmos. Environ.* 89, 593–602.
- Tohidi, R., Altuwajjiri, A., Pirhadi, M., Sioutas, C., 2022. Quantifying ambient concentrations of primary and secondary organic aerosol in central Los Angeles using an integrated approach coupling source apportionment with regression analysis. *Atmos. Environ.* 268, 118807.
- Tuet, W.Y., Fok, S., Verma, V., Tagle Rodriguez, M.S., Grosberg, A., Champion, J.A., Ng, N.L., 2016. Dose-dependent intracellular reactive oxygen and nitrogen species (ROS/RNS) production from particulate matter exposure: comparison to oxidative potential and chemical composition. *Atmos. Environ.* 144, 335–344.
- Turšič, J., Podkrajšek, B., Grgič, I., Ctyroky, P., Berner, A., Dusek, U., Hitznerberger, R., 2006. Chemical composition and hygroscopic properties of size-segregated aerosol particles collected at the Adriatic coast of Slovenia. *Chemosphere* 63, 1193–1202.
- Velali, E., Papachristou, E., Pantazaki, A., Choli-Papadopoulou, T., Planou, S., Koura, A., Manoli, E., Besis, A., Voutsas, D., 2016. Redox activity and in vitro bioactivity of the water-soluble fraction of urban particulate matter in relation to particle size and chemical composition. *Environ. Pollut.* 208, 774–786.
- Viana, M., Maenhaut, W., ten Brink, H.M., Chi, X., Weijers, E., Querol, X., Alastuey, A., Mikuska, P., Vecera, Z., 2007. Comparative analysis of organic and elemental carbon concentrations in carbonaceous aerosols in three European cities. *Atmos. Environ.* 41 (28), 5972–5983.
- Voliotis, A., Prokes, R., Lammel, G., Samara, C., 2017. New insights on humic-like substances associated with wintertime urban aerosols from central and southern Europe: size-resolved chemical characterization and optical properties. *Atmos. Environ.* 166, 286–299.
- Witkowska, A., Lewandowska, A.U., 2016. Water soluble organic carbon in aerosols (PM₁, PM_{2.5}, PM₁₀) and various precipitation forms (rain, snow, mixed) over the southern Baltic Sea station. *Sci. Total Environ.* 573, 337–346.
- Xiang, P., Zhou, X., Duan, J., Tan, J., He, K., Yuan, C., Ma, Y., Zhang, Y., 2017. Chemical characteristics of water-soluble organic compounds (WSOC) in PM_{2.5} in Beijing, China: 2011–2012. *Atmos. Res.* 183, 104–112.
- Xie, M., Mladenov, N., Williams, M.W., Neff, J.C., Wasswa, J., Hannigan, M.P., 2016. Water soluble organic aerosols in the Colorado Rocky Mountains, USA: composition, sources and optical properties. *Sci. Rep.* 6, 1–12.
- Yu, Q., Chen, J., Qin, W., Cheng, S., Zhang, Y., Sun, Y., Xin, K., Ahmad, M., 2021. Characteristics, primary sources and secondary formation of water-soluble organic aerosols in downtown Beijing. *Atmos. Chem. Phys.* 21, 1775–1796.
- Yu, G.H., Park, S., 2021. Chemical characterization and source apportionment of PM_{2.5} at an urban site in Gwangju, Korea. *Atmos. Pollut. Res.* 112, 101192.
- Yubero, E., Galindo, N., Nicolás, J.F., Lucarelli, F., Calzolari, G., 2014. Carbonaceous aerosols at an industrial site in Southeastern Spain. *Air Qual. Atmos. Health* 7, 263–271.
- Yubero, E., Galindo, N., Nicolás, J.F., Crespo, J., Calzolari, G., Lucarelli, F., 2015. Temporal variations of PM₁ major components in an urban street canyon. *Environ. Sci. Pollut. Res.* 22, 13328–13335.



Characterization of water-soluble organic carbon absorption at an urban background site in the south-eastern Iberian Peninsula

A. López-Caravaca, J. Crespo, N. Galindo, E. Yubero, A. Clemente, R. Castañer, J.F. Nicolás*

Atmospheric Pollution Laboratory (LCA), Department of Applied Physics, Miguel Hernández University, Avenida de la Universidad S/N, 03202, Elche, Spain

HIGHLIGHTS

- Sources of WSOC absorption was analysed at an urban background site in the southeast of the Iberian Peninsula.
- BrC accounted for 29% of the total aerosol absorption at 370 nm, with similar contributions from WSOC and WIOC.
- Marked seasonal variation of WSOC absorption, with higher levels during the cold season when BB emissions are highest.

ARTICLE INFO

Keywords:

WSOC absorption
MLR
BrC
Sources
Carbonaceous aerosol

ABSTRACT

Measurements of absorption coefficients ($\sigma_{\text{ap},\lambda}$) and carbonaceous components (OC, EC, WSOC and levoglucosan) in PM_{10} were conducted at an urban background site in southeastern Spain throughout 2021. The main goal of this research was to determine the contribution from different sources to WSOC light absorption (σ_{WSOC}). For this, $\sigma_{\text{BrC},\lambda}$ values were previously obtained. The mean contribution of BrC to total aerosol absorption was $\sim 29\%$ at 370 nm, revealing a significant influence of BrC to light absorption in the study area. Assuming that BrC light absorption was from WSOC and WIOC, a multilinear regression (MLR) model was used to estimate σ_{WSOC} and σ_{WIOC} . Average values (mean \pm SD) were very similar for both components: $\sigma_{\text{WSOC},370} = 1.6 (\pm 0.7) \text{ Mm}^{-1}$ and $\sigma_{\text{WIOC},370} = 1.9 (\pm 0.7) \text{ Mm}^{-1}$. Finally, the PMF technique coupled with MLR analysis was used to identify the sources of WSOC light absorption and estimate their contribution. Our findings point to biomass burning as the dominant source of σ_{WSOC} during the cold season, with a contribution of $\sim 37\%$. The Mineral Dust and Secondary Nitrate sources, that were not included in the model due to their low contribution to WSOC mass concentrations, accounted for a significant percentage of σ_{WSOC} during this period. Secondary organic aerosol was the major source during the warm season ($\sim 56\%$), followed by traffic emissions ($\sim 30\%$).

1. Introduction

Based on the water solubility, organic carbon (OC) can be divided into water-soluble organic carbon (WSOC) and water-insoluble organic carbon (WIOC). The contribution of WSOC to the total OC content of atmospheric aerosols depends on emission sources (Saarikoski et al., 2008), being the WSOC/OC ratio higher for secondary than for primary sources. In European urban environments, the average contribution of WSOC to total OC usually varies between 20% and 70% for fine particles ($\text{PM}_{2.5}$ and PM_{10}) (Cesari et al., 2020; López-Caravaca et al., 2023; Paraskevopoulou et al., 2014; Viana et al., 2007).

WSOC is usually used as a proxy of water-soluble brown carbon (Liu et al., 2013). The term brown carbon (BrC) has been used to describe the

organic carbon component that absorbs radiation efficiently in the near-UV and visible ranges (Laskin et al., 2015). Radiation absorption by WSOC can be comparable to that by elemental carbon (EC) at ultraviolet wavelengths (Kirillova et al., 2016; Mo et al., 2021) and has a positive radiative forcing effect (Zhou et al., 2022). Therefore, the contribution to light absorption of WSOC at low wavelengths cannot be ignored. Similarly, previous works have shown that solar radiation absorption by WIOC is comparable and even higher than that by WSOC (Huang et al., 2018; Paraskevopoulou et al., 2023; Satish et al., 2020; Soleimanian et al., 2020).

The light absorption properties of WSOC or BrC can be highly source-dependent (Feng et al., 2013). This is due to the different chemical composition of chromophores as a result of different sources of BrC

* Corresponding author. Laboratory of Atmospheric Pollution, Miguel Hernández University, Av. de la Universidad s/n, Edif. Alcudia, 03202, Elche, Spain.
E-mail address: j.nicolas@umh.es (J.F. Nicolás).

(Huang et al., 2018). Source apportionment of WSOC still remains a challenge because of its complex formation processes and wide range of primary and secondary sources (Mo et al., 2021). The determination of the contribution of sources to light absorption by WSOC or BrC is usually performed by multivariate analysis (PMF, PCA ...) coupled with multilinear regression (MLR) analysis (Du et al., 2014; Geng et al., 2020; Ponczek et al., 2022; Soleimanian et al., 2020). An important characteristic of the PMF/PCA factors is that these take into account the internal mixing of atmospheric particles (Ealo et al., 2018) and its main advantage is the convolution between emission strength and subsequent atmospheric dispersion/processing (Brito et al., 2018). The main sources that contribute to light absorption by WSOC are: biomass burning (BB), primarily during the cold season, secondary organic aerosols (SOA), and sources related to vehicle or fossil fuel combustion emissions (Du et al., 2014; Soleimanian et al., 2020). However, other sources such as biogenic SOA (Zhou et al., 2022), microorganism/plankton primary emissions (Geng et al., 2020) or mineral dust (MD) (Jin et al., 2020) have also been identified.

The light absorption capacity of WSOC for each source can be evaluated as a function of the Mass Absorption Efficiency (MAE) value. MAE is a critical optical parameter for evaluating the light absorption ability (Bond and Bergstrom, 2006). Most works (Geng et al., 2020; Moschos et al., 2018; Zhou et al., 2022) have reported that the MAE of WSOC from BB emissions is highest, since chromophores from BB strongly contribute to the light absorption of atmospheric aerosols (Fan et al., 2016). However, the fossil-derived WSOC may also have a high light absorption capacity (Mo et al., 2021), and some studies have shown even higher values than those of biomass burning WSOC (Yan et al., 2018). Secondary WSOC usually has a lower light absorption capacity, especially WSOC formed from biogenic precursors (Lambe et al., 2013).

Regarding the seasonality of absorption by WSOC, it depends not only on its mass concentration but also on its sources during each season. For instance, in urban areas absorption by WSOC is usually higher in winter due to the larger contribution from BB emissions. The winter/summer ratio varies between 2 and 6 for most urban environments (Moschos et al., 2018; Gilardoni et al., 2020; Soleimanian et al., 2020).

This paper is the second of a two-part series aimed at investigating the sources and absorption properties of WSOC in the Western Mediterranean area. The motivation of this study is the lack of works on this topic in the Mediterranean region. The main goals of the present work are: (1) to estimate the relative contribution of WSOC to BrC absorption in PM₁ and (2) to determine the contribution from different sources to WSOC light absorption. For this, the PMF technique coupled with the MLR model was used. PMF factors were previously identified by López-Caravaca et al. (2023).

2. Methodology

2.1. Monitoring site and measurements

Two hundred daily samples of PM₁ were collected during 2021 at the campus of the Miguel Hernández University of Elche (38°16' N; 0°41' W; 93 m.a.s.l), a medium size city (~190,000 inhabitants) located in southeastern Spain. The monitoring site was located in a well-ventilated area on the outskirts of the city and can be considered as an urban background site (UBS). Traffic in the surroundings of the sampling site is primarily due to commuting of students and university staff to the campus. A description of the urban features of Elche and its climate can be found in Nicolás et al. (2020).

PM₁ samples were collected onto quartz fibre filters by means of a Derenda 3.1 low volume sampler (2.3 m³·h⁻¹). PM masses were determined by gravimetric analysis in an environmentally controlled chamber (temperature of 20 ± 1 °C and relative humidity of 50 ± 5%). The sampling frequency was approximately four times a week. PM₁ samples were analysed for EC, OC, levoglucosan and WSOC. Concurrently, measurements of σ_{ap,λ} were performed. Light absorption measurements

are described in section 2.3. The number of daily data of σ_{ap,λ} was 260. The number of simultaneous measurements of absorption optical properties and aerosol chemical composition was 160. These data were evenly distributed throughout the year. Seasons are defined in the text as: winter (January–March), spring (April–June), summer (July–September) and autumn (October–December).

2.2. Chemical analysis

Organic and elemental carbon were measured on 1.5 cm² punches of the quartz-fibre filters by means of a Thermal-Optical Carbon Aerosol Analyser (Sunset Laboratory, Inc.) according to the EUSAAR-2 protocol. All samples had OC and EC concentrations above the MDL.

Samples were extracted with ultrapure water in an ultrasonic bath for 45 min and filtered through nylon syringe filters (0.45 μm). The determination of WSOC levels was performed using a TOC-L CSH analyser (Shimadzu), whereas levoglucosan was analysed by high performance anion-exchange chromatography (HPAEC) coupled with pulsed amperometric detection (PAD). For this, a Thermo Scientific Dionex Integriion ion chromatograph and an electrochemical detector with a gold working electrode were used. Details on the analytical procedures can be found in López-Caravaca et al. (2023).

2.3. Light absorption measurements

Measurements of σ_{ap,λ} and black carbon (BC) at 880 nm were performed using an Aethalometer model AE33 (Magee Scientific, USA). The Aethalometer provides the absorption coefficients at seven wavelengths (370, 470, 520, 590, 660, 880 and 950 nm). To obtain aerosol absorption coefficients from aerosol attenuation coefficients, the harmonization factor for M8060 filter tape (H* factor = 1.76) was used (Savadkoobi et al., 2023). The instrument operated at a constant air flow rate of 3.9 L·m⁻¹. The time resolution was 1 min. Daily averages were subsequently calculated. The Absorption Angstrom Exponent (AAE) was obtained from σ_{ap} using equation (1):

$$AAE = \frac{\ln \frac{\sigma_{ap}(\lambda_1)}{\sigma_{ap}(\lambda_2)}}{\ln \frac{\lambda_1}{\lambda_2}} \quad (1)$$

where λ₁ = 370 nm and λ₂ = 950 nm.

2.3.1. Determination of σ_{BrC,λ}

For the determination of σ_{BrC,λ} those days under the influence of mineral dust (MD) transported from North Africa were removed from the database in order to avoid the effect of light absorption by MD. According to equation (2), the total measured absorption coefficient (σ_{ap,λ}) had two contributions: absorption by BC and absorption by BrC.

$$\sigma_{ap,\lambda} = \sigma_{BC,\lambda} + \sigma_{BrC,\lambda} \quad (2)$$

The contribution of BrC to σ_{ap,λ} was estimated using the methodology described in Kaskaoutis et al. (2021), named “BrC model”. This procedure has been widely used to determine the value of σ_{BrC,λ} from Aethalometer measurements (Gilardoni et al., 2020; Nicolás et al., 2018; Pani et al., 2021; Ran et al., 2016). Briefly, it was assumed that pure BC is the only absorbing component at λ = 880 nm and that its spectral dependence for the remaining wavelengths is a function of λ⁻¹. The contribution of BrC for each wavelength was subsequently estimated according to equation (2) from the deviations between measured σ_{ap} values for every λ and those obtained as a function of λ⁻¹.

2.3.2. Determination of σ_{WSOC}

Alternatively, the absorption coefficient of BrC can also be determined by spectrophotometric analysis of the water extracts of PM samples without the interference of BC and other water-insoluble particles (Hecobian et al., 2010). It has been reported that the

methanol-soluble fraction of OC (MSOC) shows higher $\sigma_{\text{BrC},\lambda}$ values than the water-soluble OC (WSOC), since methanol (unlike water) can extract chromophores with greater molecular weights and higher absorption characteristics (Zhang et al., 2013). On this basis, water extraction allows to determine the absorption of water soluble BrC (WSBrC), whereas methanol extraction is an alternative approach to measure the total BrC light absorption. Nowadays, the use of the absorption coefficients of BrC and/or WSBrC determined by spectrophotometric analysis is the most widely employed procedure to measure light absorption by BrC (Du et al., 2014; Soleimani et al., 2020; Paraskevopoulou et al., 2023 and so on).

In spite of this, the methodology used in the present work to estimate the absorption by WSBrC (σ_{WSOC}) was the multilinear regression (MLR) analysis. For this, we assumed that BrC mass concentrations were the same as those of OC (Pani et al., 2021). The equation for the model is as follows:

$$y = b_0 + b_1 x_1 + b_2 x_2 + \dots + b_k x_k + \varepsilon \quad (3)$$

where y is the output data to be predicted by the model (in this work, $\sigma_{\text{BrC},\lambda}$), x_i are independent input variables (in the present study, WSOC and WIOC mass concentrations), b_i are the linear regression constants, b_0 is the y-intercept (constant term) and ε is the residual term. In this case, the value of the intercept is zero, since light absorption by BrC is the sum of that by WSOC and WIOC. The regression coefficients of the model correspond to the MAE values (in $\text{m}^2 \cdot \text{g}^{-1}$) of the carbonaceous components. The relative contribution of each chemical component was then estimated from the linear regression coefficients multiplied by their mass concentrations. Nevertheless, it should be noted that the calculation of MAE values according to the procedure described by Pani et al. (2021) is based on the assumption that the whole organic fraction exhibits light absorbing properties. Since a fraction of OC does not absorb light, the use of this approach that considers an upper-limit BrC concentration will underestimate the mass absorption efficiency. Therefore, the real MAE for brown carbon will surely be higher than the values presented here (Yang et al., 2009). Likewise, the application of the MLR analysis to estimate MAE_{WSOC} and MAE_{WIOC} values will provide lower limits for these parameters.

A similar procedure is described in Izhar et al. (2020). The authors reported a good correlation ($R^2 = 0.72$) between σ_{WSOC} estimated by this method and that measured by water extraction at $\lambda = 365$ nm, although the estimated absorption by WSBrC was 1.8 times that obtained in aqueous extracts. The same factor was obtained by Gilardoni et al. (2020) when absorption coefficients for methanol-soluble BrC were compared with aethalometer measurements.

Finally, in order to quantify the sources of WSOC light absorption, PMF factors were coupled with multilinear regression (MLR) analysis. PMF factors were previously identified by López-Caravaca et al. (2023). The contribution from each factor to WSOC levels is shown in Fig. 1S (Supplementary material).

3. Results

3.1. Characterization of aerosol absorption and chemical components

Table 1 shows summary statistics of optical properties, PM_{10} and carbonaceous compounds during the study period. The mean value obtained for σ_{ap} (8.1 Mm^{-1} ; $\lambda = 520$ nm) was in the lower range of those recorded in medium size cities of the Iberian Peninsula: Burjassot (18.6 Mm^{-1} ; $\lambda = 520$ nm; Segura et al., 2016), Granada (24 Mm^{-1} ; $\lambda = 550$ nm; Titos et al., 2012), Evora (8.9 Mm^{-1} ; $\lambda = 670$ nm; Nepomuceno et al., 2014) or Valladolid (4 Mm^{-1} ; $\lambda = 550$ nm; Mogo et al., 2017). The low value obtained in this study could be explained considering that at the beginning of the study period traffic in the vicinity of the sampling site was reduced due to COVID-19 restrictions. For the same reason the concentrations of PM_{10} and carbonaceous components were lower than

Table 1

Statistics of absorption coefficients (Mm^{-1}), AAE (dimensionless), PM_{10} and carbonaceous compounds ($\mu\text{g}\cdot\text{m}^{-3}$) at the urban background site of Elche. Statistics are based on daily mean values.

Parameters	Mean (SD)	P5	Median	P95
σ_{ap} ($\lambda = 370$ nm)	14.0 (10.4)	4.2	10.9	31.9
σ_{ap} ($\lambda = 440$ nm)	12.2 (7.1)	3.2	8.2	23.1
σ_{ap} ($\lambda = 520$ nm)	8.1 (5.5)	2.6	6.5	18.6
σ_{ap} ($\lambda = 590$ nm)	6.7 (4.5)	2.2	5.5	15.4
σ_{ap} ($\lambda = 660$ nm)	5.7 (3.8)	1.8	4.7	13.2
σ_{ap} ($\lambda = 880$ nm)	4.2 (2.7)	1.3	3.4	9.7
σ_{ap} ($\lambda = 950$ nm)	3.9 (2.5)	1.2	3.2	9.0
AAE (370-950 nm)	1.34 (0.13)	1.17	1.32	1.57
PM_{10}	7.6 (6.1)	2.4	6.1	17.2
OC	2.11 (1.05)	1.09	1.86	3.87
WSOC	0.95 (0.40)	0.41	0.85	1.75
WIOC	1.14 (0.58)	0.50	0.96	2.24
EC	0.37 (0.20)	0.15	0.33	0.78
Levogluconan	0.049 (0.066)	0.004	0.018	0.194

expected for an urban background environment, particularly for EC ($0.37 \mu\text{g}\cdot\text{m}^{-3}$). Likewise, WSOC concentrations were relatively low compared with the values reported for most European urban background areas (López-Caravaca et al., 2023). Carbonaceous compounds accounted for approximately one third of the average PM_{10} concentration. The AAE mean value (1.34) indicates that BC was the main absorbing aerosol component, although there was also a contribution from BrC.

Temporal variations of PM_{10} and carbonaceous components during the study period are described in López-Caravaca et al. (2023). Briefly, average monthly PM_{10} concentrations were highest during late autumn and winter. Mean WIOC levels were slightly higher than those of WSOC ($\sim 17\%$). The difference between WIOC and WSOC concentrations was lowest during summer. The mean levoglucosan concentration in the PM_{10} fraction was $49 \text{ ng}\cdot\text{m}^{-3}$, varying between $6 \text{ ng}\cdot\text{m}^{-3}$ in summer and $89 \text{ ng}\cdot\text{m}^{-3}$ in autumn.

Fig. 1 presents the temporal evolution of $\sigma_{\text{ap},370}$ and AAE. The seasonal cycle of $\sigma_{\text{ap},370}$ is explained by the seasonal variations in the concentrations of carbonaceous compounds, which showed concentrations 35% higher in the cold period than during the warm months (López-Caravaca et al., 2023). Maximum daily values of 40 Mm^{-1} were registered during this season. Significant seasonal variations were also observed for the AAE, whose median values ranged from 1.21 in summer to 1.42 in winter. This seasonal pattern can be attributed to a higher contribution from biomass burning emissions during the cold period. This is analysed in detail in the following section.

3.2. Light absorption by BrC

Following the methodology described in section 2.3.1, $\sigma_{\text{BrC},\lambda}$ and $\sigma_{\text{BrC},\lambda}$ were estimated. Fig. 2a shows the spectral dependence of σ_{ap}

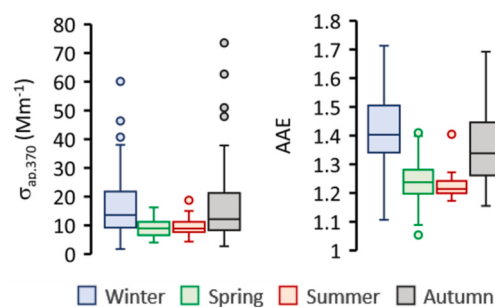


Fig. 1. Seasonal evolution of σ_{ap} (Mm^{-1}) at 370 nm and AAE (dimensionless). The upper and lower edges of the box represent the 75th and 25th percentiles respectively, and the whiskers are the maximum and minimum values. The line inside the box plot represents the median value. Dots are outlier values.

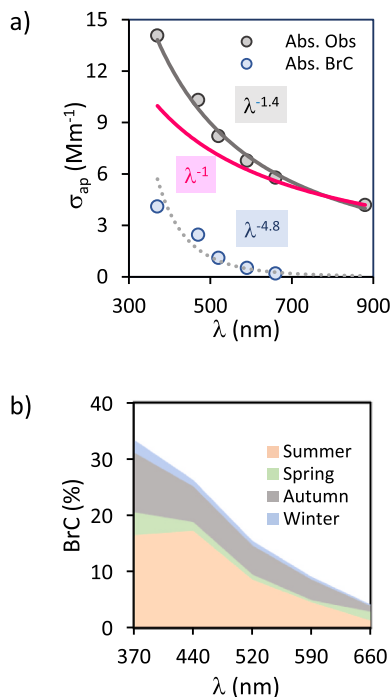


Fig. 2. a) Average wavelength dependent light absorption coefficients for: total absorption (grey dots), absorption by BC (pink line) and BrC (blue dots); b) Spectral variation of seasonal percentage contributions of σ_{BrC} .

obtained in the present study, the spectral dependence as a function of λ^{-1} and the AAE_{BrC} value (4.8 ± 0.1). The AAE_{BrC} values calculated in this work with those reported in previous studies are difficult since different approaches for the determination of the BrC absorption were used, and calculations were performed at different wavelength (Paraskevopoulou et al., 2023). Keeping this in mind, the obtained value was slightly higher than those calculated from Aethalometer measurements at other UBS in Europe such as Athens (3.6 ± 0.9 ; Liakakou et al., 2020), Genoa (4.02 ± 0.19 ; Masabó et al., 2015) or Milan (3.81 ± 0.11 ; Bernardoni et al., 2017). Average values for $\sigma_{BrC,\lambda}$ are shown in Table 1S. Lower estimates of MAE values can be calculated from $\sigma_{BrC,\lambda}$ values using the following equation:

$$MAE_{BrC,\lambda} = \sigma_{BrC,\lambda} / [OC] \quad (4)$$

where [OC] is the mass concentration (in $\mu\text{g}\cdot\text{m}^{-3}$) of organic carbon (Pani et al., 2021; Zhou et al., 2022). The value for $\lambda = 370$ nm was $1.9 \text{ m}^2\cdot\text{g}^{-1}$. This value was higher than those reported in the literature probably due to the abundance of fresh BB-derived organic aerosols. A comprehensive list of MAE_{BrC} values obtained at different locations around the world can be found in Pani et al. (2021).

The contribution of BrC to total absorption for each season is shown in Fig. 2b. The average contribution in the ultraviolet range was 29.2%. A remarkable seasonal trend was observed, with highest values in winter (33.4% at $\lambda = 370$ nm) and lowest in summer (16.5% at $\lambda = 370$ nm). At mid-visible wavelengths ($\lambda = 590$ nm), the contribution of BrC to total absorption was still significant ($\sim 8\%$). Considering the main sources of WSOC shown in Fig. 1S, it can be assumed that during the cold period BB was the predominant source of BrC, since traffic was fairly constant throughout the year and the secondary source was predominant in the warmer months. This was confirmed by the variation of $\sigma_{BrC,370}$ as a function of daily AAE values and levoglucosan concentrations (used as a tracer of BB emissions) (Fig. 3).

As can be seen, AAE and $\sigma_{BrC,370}$ values increased as levoglucosan

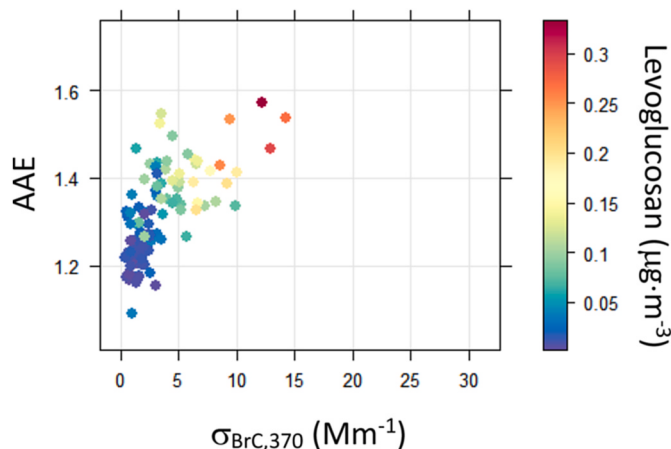


Fig. 3. Variation of AAE according to levoglucosan concentration ($\mu\text{g}\cdot\text{m}^{-3}$) and $\sigma_{BrC,370}$ (Mm⁻¹) levels.

concentrations increased. In fact, AAE values higher than 1.4 and $\sigma_{BrC,370}$ values higher than 5 Mm^{-1} were generally associated with levoglucosan concentrations greater than $0.15 \mu\text{g}\cdot\text{m}^{-3}$, indicating that BB was the dominant source of BrC on those days.

3.3. Relationship of WSOC absorption with different aerosol components

3.3.1. Contributions of σ_{WSOC} and σ_{WIOC} to σ_{BrC}

In order to estimate the absorption by WSOC, the MLR technique was used. Since the homoscedasticity assumption was not met in this case, a generalisation of the model (Weighted least squares, WLS) to solve this problem was used. The results are presented in Table 2.

The standardized coefficients were almost the same for WSOC and WIOC, which indicates a similar contribution from both components. The MAE values ($\lambda = 370$ nm) were $1.72 \text{ m}^2\cdot\text{g}^{-1}$ for WSOC and $1.70 \text{ m}^2\cdot\text{g}^{-1}$ for WIOC, suggesting that both components absorb UV light with the same efficiency and play the same role in determining the MAE_{BrC} value. The MAE_{WSOC} value cannot be compared with those estimated from σ_{WSOC} values measured in the aqueous extracts of aerosol samples. As previously mentioned, the values obtained by this procedure are approximately half those reported from aethalometer measurements. Furthermore, it is important to mention that recent outcomes point out that BrC optical properties show a pH-dependence in aqueous media (Hennigan et al., 2023). The authors found that absorption and MAE values increased linearly with increasing pH. Therefore, the optical properties of the water-soluble BrC depend on the pH of the measurement media, which is likely different from that of ambient aerosols.

The correlation between modelled and measured σ_{BrC} values is shown in Fig. 2S. The model was able to explain 86% of the total variance of BrC light absorption. Fig. 4 presents average monthly values for the absorption by WSOC and WIOC ($\lambda = 370$ nm).

The contribution from WSOC and WIOC to light absorption showed the same seasonality, with maximum values in winter and minimum during the summer period. The same seasonal pattern has been previously reported in other urban areas (Gilardoni et al., 2020; Kim et al., 2016; Paraskevopoulou et al., 2023; Soleimanian et al., 2020). The most likely reason for the higher σ_{WSOC} values during the cold months is the increase in biomass burning emissions, in addition to the higher WSOC

Table 2

Parameters of the multilinear regression analysis of $\sigma_{BrC,370}$.

	Unstandardized coefficients	Std. error	Standardized coefficients	p-value	R ²
WSOC	1.72	0.57	0.43	0.003	0.75
WIOC	1.70	0.53	0.45	0.002	

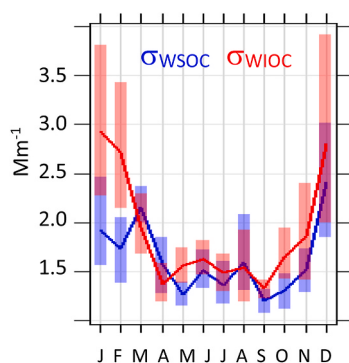


Fig. 4. Monthly evolution of $\sigma_{\text{WSOC},370}$ and $\sigma_{\text{WIOC},370}$ during the study period.

concentrations. On the other hand, fossil fuel combustion and BB are dominant sources of WIOC (Dusek et al., 2017) and the contributions from these sources to PM_{10} levels are highest during the cold period (López-Caravaca et al., 2023), which explains the higher σ_{WIOC} values registered during autumn and winter. From the data shown in Fig. 4, it can also be observed that absorption by WIOC was significantly higher than that by WSOC during part of the winter. On the other hand, the minimum σ_{WSOC} value during summer can be explained considering that SOA (which is the major contributor to WSOC during this season; López-Caravaca et al., 2023) is mainly comprised of low-molecular weight colourless chromophores during the warm period (Huang et al., 2018, Soleimanian et al., 2020).

The annual average contributions (\pm SD) obtained from the model were: $\sigma_{\text{WSOC},370} = 1.6 (\pm 0.7) \text{ Mm}^{-1}$ and $\sigma_{\text{WIOC},370} = 1.9 (\pm 1.1) \text{ Mm}^{-1}$, indicating that light absorption by water-insoluble organic components significantly contributed to σ_{BrC} . This result shows that light absorption by BrC would be largely underestimated if WSOC was used as a surrogate of BrC (Cheng et al., 2016). As already indicated, the $\sigma_{\text{WSOC},370}$ value was higher in winter (1.9 Mm^{-1}) than in summer (1.3 Mm^{-1}), although the loss of chromophores during the warm months was not as high as that observed in other urban areas, where the winter/summer ratio was higher than the value obtained in the present study (Table 3).

3.3.2. Source apportionment of σ_{WSOC}

The contribution of different sources to light absorption by WSOC was estimated from the results previously obtained by applying the PMF model (López-Caravaca et al., 2023). In the mentioned study, five sources of WSOC were identified: Road Traffic (RT), Biomass Burning (BB), Soil Dust (SD), Secondary Organic Aerosols (SOA) and Secondary Nitrate (SN). Fig. 1S shows the temporal evolution of WSOC concentrations for each source and the average annual contribution of the identified sources to WSOC levels. Since the MLR model can be very sensitive to the choice of the species included in the analysis (Hand and Malm, 2007), only SOA, RT and BB were considered for the application of this model. The contribution of the SN and SD factors to WSOC concentrations was lower than 10%; therefore, attempts to include these

Table 3

Values of σ_{WSOC} (Mm^{-1}) reported for other urban areas.

Site	Station	σ_{WSOC}^a Winter/ Summer	Reference
Elche (Spain)	UBS	1.9/1.3	This study
Milan (Italy)	Urban	3/0.5	Gilardoni et al. (2020)
Zurich (Switzerland)	UBS	2.2/1.0	Moschos et al. (2018)
Xi'an (China)	Urban	25.2/5.0	Huang et al. (2018)
Ioannina (Greece)	UBS	13.9/0.4	Paraskevopoulou et al. (2023)
Los Angeles (USA)	Urban	2.0/0.9	Soleimanian et al., 2020

^a Light absorption values from aqueous extracts.

factors in the model resulted in unrealistic mass absorption efficiencies and statistically non-significant regression coefficients for absorption (Ponczek et al., 2022).

For the application of the MLR analysis $\sigma_{\text{WSOC},370}$ was the dependent variable and the three PMF factors (F_i) were the independent variables:

$$\sigma_{\text{WSOC},370} = b_0 + b_1F_1 + b_2F_2 + b_3F_3 + \varepsilon \quad (5)$$

In this case, b_i represents the mass absorption efficiency of each component, while ε is the residual term and b_0 the y-intercept. The intercept accounts for the chemical components that were not included in the model (SN and SD). The relative contribution of each factor was then estimated from the linear regression coefficients multiplied by their mass concentrations. Table 4 shows the results obtained from the model separately for the cold (autumn and winter) and warm (spring and summer) seasons.

During the cold season the value of the constant b_0 was 0.48 ($p < 0.001$), suggesting that a fraction of $\sigma_{\text{WSOC},370}$ was not explained by the sources considered in the present study. This value corresponds to the absorption by WSOC coming from SN and SD. The highest contribution ($>50\%$) was from BB (0.83-standardized coefficient). These results can be considered similar to those found by Soleimanian et al. (2020) at an urban site in Los Angeles (USA) if the traffic source of our study is equated to the fossil fuel combustion source. During summer, SOA was the highest contributor to $\sigma_{\text{WSOC},370}$ and the value of the constant ε was almost zero. This implies a negligible contribution from SN and SD to $\sigma_{\text{WSOC},370}$ during that period. Nevertheless, the MLR model was able to explain only 52% of the total variation of WSOC light absorption during this period.

The average contribution from each source to $\sigma_{\text{WSOC},370}$ during the cold and warm periods is shown in Fig. 5. The correlation between σ_{WSOC} modelled by the MLR-PMF technique and σ_{WSOC} predicted by WLS can be seen in Fig. 3S.

Traffic (~31%) and SOA (~56%) were the major sources contributing to WSOC light absorption in the warm period, while BB was the dominant source (~37%) during the cold season. During this season, the sources not considered in the model significantly contributed to the absorption by WSOC (~27%). This can be explained considering that high atmospheric stability conditions favouring the formation of secondary nitrate are more frequent during winter (Galindo et al., 2020). The important contribution of SN to σ_{WSOC} points to the formation of nitrogen-containing light-absorbing organics under high nitrate concentrations (Zhou et al., 2022).

Fig. 6 presents monthly contributions from each source to σ_{WSOC} . The values of $\sigma_{\text{WSOC}}(\text{BB})$ were highest during late autumn and winter due to higher emissions from biomass burning. The average value registered in December (~1.8 Mm^{-1}) could be attributed to biomass burning activities near the sampling site. The temporal variability of σ_{WSOC} from road traffic was smoother than those of $\sigma_{\text{WSOC}}(\text{BB})$ and $\sigma_{\text{WSOC}}(\text{SOA})$. During summer $\sigma_{\text{WSOC}}(\text{SOA})$ was highest, with an average seasonal value of

Table 4

Results from the multilinear regression analysis between $\sigma_{\text{WSOC},370}$ and PMF factors (independent parameters).

Source	Unstandardized coefficients	Std. error	Standardized coefficients	p-value	R ²
Cold Season					0.70
b₀	0.48	0.12		0.000	
BB	1.46	0.11	0.83	0.000	
SOA	1.79	0.29	0.36	0.000	
RT	1.32	0.25	0.31	0.000	
Warm Season					0.52
b₀	0.06	0.19		0.770	
BB	2.33	1.20	0.19	0.050	
SOA	1.74	0.24	0.84	0.000	
RT	2.42	0.51	0.55	0.000	

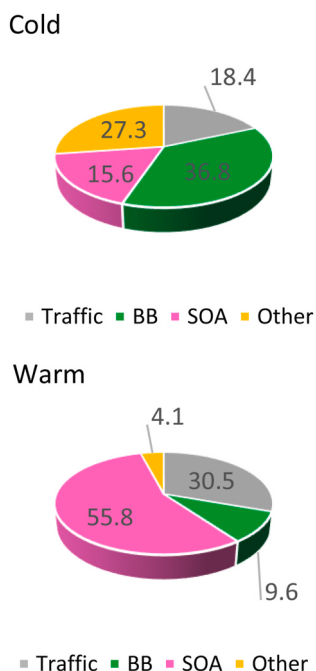


Fig. 5. Relative contribution of sources to total WSOC light absorption during the warm and cold periods.

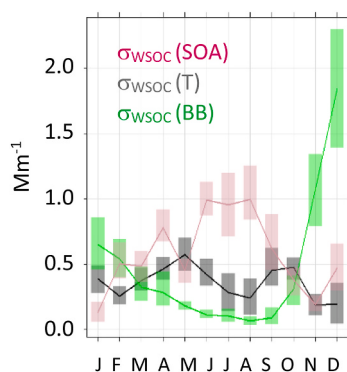


Fig. 6. Monthly evolution of $\sigma_{\text{WSOC},370}$ sources.

$\sim 1.0 \text{ Mm}^{-1}$. This was not unexpected since SOA was the predominant source of WSOC during the warm period. The annual mean contributions ($\pm \text{SD}$) calculated by the model ($\lambda = 370 \text{ nm}$) were: $\sigma_{\text{WSOC}}(\text{BB}) = 0.42 (\pm 0.57) \text{ Mm}^{-1}$, $\sigma_{\text{WSOC}}(\text{SOA}) = 0.46 (\pm 0.36) \text{ Mm}^{-1}$ and $\sigma_{\text{WSOC}}(\text{RT}) = 0.35 (\pm 0.25) \text{ Mm}^{-1}$.

4. Conclusions

In this study, the sources of σ_{WSOC} were characterised from the analysis of carbonaceous compounds in PM_{10} , light absorption measurements and statistical techniques (PMF and MLR). The mean value ($\pm \text{SD}$) of $\sigma_{\text{BrC},370}$ ($4.1 \pm 4.5 \text{ Mm}^{-1}$) represented $\sim 29\%$ of the total aerosol absorption, underlining the significant influence of light absorption by BrC in the region. The contribution of WSOC and WIOC absorption to $\sigma_{\text{BrC},370}$ was very similar, indicating that both components have a similar light absorption efficiency in the UV range. Both contributions were highest during the coldest months, although the winter/summer ratio of WSOC absorption was lower than those found at other urban stations. In the warm season, SOA (55.8%) was the main contributor to σ_{WSOC} . This source, in addition to road traffic (30.5%) and BB (9.6%), explained a high percentage of the variability of σ_{WSOC}

during this period. BB was the most important source during the cold period (36.8%). A significant influence of sources such as mineral dust and secondary nitrate was also detected ($\sim 27\%$) during the colder months.

CRedit authorship contribution statement

A. López-Caravaca: Formal analysis, Investigation, Visualization, Writing – original draft. J. Crespo: Conceptualization, Funding acquisition, Project administration. N. Galindo: Investigation, Supervision, Writing – review & editing. E. Yubero: Supervision, Writing – review & editing. A. Clemente: Data curation, Formal analysis. R. Castañer: Data curation, Investigation. J.F. Nicolás: Funding acquisition, Investigation, Methodology, Writing – original draft, Writing – review & editing.

Declaration of competing interest

The authors declare that they have no known competing financial interests or personal relationships that could have appeared to influence the work reported in this paper.

Data availability

Data will be made available on request.

Acknowledgements

This work was supported by the Spanish Ministry of Science, Innovation and Universities (COSMOS Project, ref. RTI2018-098639-B-I00). A. López-Caravaca thanks the Spanish Ministry of Science and Innovation for a predoctoral grant (PRE2019-089098).

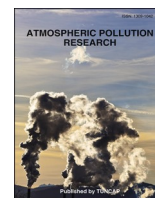
Appendix A. Supplementary data

Supplementary data to this article can be found online at <https://doi.org/10.1016/j.atmosenv.2024.120435>.

References

- Bernardini, V., Pileci, R.E., Caponi, L., Massabò, D., 2017. The Multi-Wavelength Absorption Analyzer (MWAA) model as a tool for source and component apportionment based on aerosol absorption properties: application to samples collected in different environments. *Atmosphere* 8, 218.
- Bond, T.C., Bergstrom, R.W., 2006. Light absorption by carbonaceous particles: an investigative review. *Aerosol Sci. Technol.* 40, 27–67.
- Brito, J., Carbone, S., Monteiro dos Santos, D.A., Dominutti, P., de Oliveira Alves, N., Rizzo, L.V., Artaxo, P., 2018. Disentangling vehicular emission impact on urban air pollution using ethanol as a tracer. *Sci. Rep.* 8, 10679.
- Cesari, D., Merico, E., Dinioi, A., Gambaro, A., Morabito, E., Gregoris, E., Barbaro, E., Feltracco, M., Alebić-Juretić, A., Odorčić, D., Kontosić, D., Mifka, B., Contini, D., 2020. An inter-comparison of size segregated carbonaceous aerosol collected by low-volume impactor in the port-cities of Venice (Italy) and Rijeka (Croatia). *Atmos. Pollut. Res.* 11, 1705–1714.
- Cheng, Y., He, K.B., Du, Z.Y., Engling, G., Liu, J.M., Ma, Y.L., Zheng, M., Weber, R.J., 2016. The characteristics of brown carbon aerosol during winter in Beijing. *Atmos. Environ.* 127, 355–364.
- Du, Z., He, K., Cheng, Y., Duan, F., Ma, Y., Liu, J., Zhang, M., Weber, R., 2014. A yearlong study of water-soluble organic carbon in Beijing II: light absorption properties. *Atmos. Environ.* 89, 235–241.
- Dusek, U., Hitznerberger, R., Kasper-Giebl, A., Kistler, M., Meijer, H., Szidat, S., Wacker, L., Holzinger, R., Röckmann, T., 2017. Sources and formation mechanisms of carbonaceous aerosol at a regional background site in The Netherlands: insights from a year-long radiocarbon study. *Atmos. Chem. Phys.* 17, 3233–3251.
- Ealo, M., Alastuey, A., Pérez, N., Ripoll, A., Querol, X., Pandolfi, M., 2018. Impact of aerosol particle sources on optical properties in urban, regional and remote areas in the north-western Mediterranean. *Atmos. Chem. Phys.* 18, 1149–1169.
- Fan, X., Wei, S., Zhu, M., Song, J., Peng, P.A., 2016. Comprehensive characterization of humic-like substances in smoke $\text{PM}_{2.5}$ emitted from the combustion of biomass materials and fossil fuels. *Atmos. Chem. Phys.* 16, 13321–13340.
- Feng, Y., Ramanathan, V., Kotamarthi, V.R., 2013. Brown carbon: a significant atmospheric absorber of solar radiation? *Atmos. Chem. Phys.* 13, 8607–8621.
- Galindo, N., Yubero, E., Clemente, A., Nicolás, J.F., Varea, M., Javier Crespo, J., 2020. PM events and changes in the chemical composition of urban aerosols: a case study in the western Mediterranean. *Chemosphere* 244 (125520).

- Geng, X., Mo, Y., Li, J., Zhong, G., Tang, J., Jiang, H., Ding, X., Malik, R.N., Zhang, G., 2020. Source apportionment of water-soluble brown carbon in aerosols over the northern South China Sea: influence from land outflow, SOA formation and marine emission. *Atmos. Environ.* 229, 117484.
- Gilardoni, S., Massoli, P., Marinoni, A., Mazzoleni, C., Freedman, A., Lonati, G., De Iulius, S., Gianelle, V., 2020. Spatial and temporal variability of carbonaceous aerosol absorption in the Po Valley. *Aerosol Air Qual. Res.* 20, 2624–2639.
- Hand, J.L., Malm, W.C., 2007. Review of aerosol mass scattering efficiencies from ground-based measurements since 1990. *J. Geophys. Res.* 112, D16203.
- Hecobian, A., Zhang, X., Zheng, M., Frank, N., Edgerton, N.E.S., Weber, R.J., 2010. Water-soluble organic aerosol material and the light-absorption characteristics of aqueous extracts measured over the Southeastern United States. *Atmos. Chem. Phys.* 10, 5965–5977.
- Hennigan, C.J., McKee, M., Pratap, V., Boegner, B., Reno, J., Garcia, L., McLaren, M., Lance, S.M., 2023. pH-Dependence of brown-carbon optical properties in cloud water. *Atmos. Chem. Phys.* 23, 14437–14449.
- Huang, R.J., Yang, L., Cao, J., Chen, Y., Chen, Q., Li, Y., Duan, J., Zhu, C., Dai, W., Wang, K., Lin, C., Ni, H., Corbin, J.C., Wu, Y., Zhang, R., Tie, X., Hoffmann, T., O'Dowd, C., Dusek, U., 2018. Brown carbon aerosol in urban Xi'an, Northwest China: the composition and light absorption properties. *Environ. Sci. Technol.* 52, 6825–6833.
- Izhar, S., Gupta, T., Panday, A.K., 2020. Improved method to apportion optical absorption by black and brown carbon under the influence of haze and fog at Lumbini, Nepal, on the Indo-Gangetic Plains. *Environ. Pollut.* 263, 114640.
- Jin, Y., Yan, C., Sullivan, A.P., Liu, Y., Wang, X., Dong, H., Chen, S., Zeng, L., Collett, J.L., Mei Zheng, M., 2020. Significant contribution of primary sources to water-soluble organic carbon during spring in Beijing, China. *Atmosphere* 11, 395.
- Kaskaoutis, D.G., Grivas, G., Stavroulas, I., Bougiatioti, A., Liakakou, E., Dumka, U.C., Gerasopoulos, E., Mihalopoulos, N., 2021. Apportionment of black and brown carbon spectral absorption sources in the urban environment of Athens, Greece, during Winter. *Sci. Total Environ.* 801, 149739.
- Kim, H., Kim, J.Y., Jin, H.C., Lee, J.Y., Lee, S.P., 2016. Seasonal variations in the light absorbing properties of water-soluble and insoluble organic aerosols in Seoul, Korea. *Atmos. Environ.* 129, 234–242.
- Kirilova, E.N., Marinoni, A., Bonasoni, P., Vuilleumoz, E., Facchini, M.C., Fuzzi, S., Decesari, S., 2016. Light absorption properties of brown carbon in the high Himalayas. *J. Geophys. Res.* Atmosphere 121, 9621–9639.
- Lambe, A.T., Cappa, C.D., Massoli, P., Onasch, T.B., Forestieri, S.D., Martin, A.T., Cummings, M.J., Croasdale, D.R., Brune, W.H., Worsnop, D.R., Davidovits, P., 2013. Relationship between oxidation level and optical properties of secondary organic aerosol. *Environ. Sci. Technol.* 47 (12), 6349–6357.
- Laskin, A., Laskin, J., Nizkorodov, S.A., 2015. Chemistry of atmospheric brown carbon. *Chem. Rev.* 115, 4335–4382.
- Liakakou, E., Kaskaoutis, D.G., Grivas, G., Stavroulas, I., Tsagkaraki, M., Paraskevopoulou, D., Bougiatioti, A., Dumka, U.C., Gerasopoulos, E., Mihalopoulos, N., 2020. Long-term brown carbon spectral characteristics in a Mediterranean city (Athens). *Sci. Total Environ.* 708, 135019.
- Liu, J., Bergin, M., Guo, H., King, L., Kotra, N., Edgerton, E., Weber, R.J., 2013. Size resolved measurements of brown carbon in water and methanol extracts and estimates of their contribution to ambient fine-particle light absorption. *Atmos. Chem. Phys.* 13, 12389–12404.
- López-Caravaca, A., Crespo, J., Galindo, N., Yubero, E., Juárez, N., Nicolás, J.F., 2023. Sources of water-soluble organic carbon in fine particles at a southern European urban background site. *Atmos. Environ.* 306, 119844.
- Massabó, D., Caponi, L., Bernardoni, V., Bove, M.C., Brotto, P., Calzolari, G., et al., 2015. Multi-wavelength optical determination of black and brown carbon in atmospheric aerosols. *Atmos. Environ.* 108, 1–12.
- Mo, Y., Li, J., Cheng, Z., Zhong, G., Zhu, S., Tian, C., Chen, Y., Zhang, G., 2021. Dual carbon isotope-based source apportionment and light absorption properties of water-soluble organic carbon in PM_{2.5} over China. *J. Geophys. Res.: Atmosphere* 126, e2020JD033920.
- Mogo, S., López, J.F., Cachorro, V.E., de Frutos, A., Zocca, R., Barroso, A., Mateos, D., Conceicao, E., 2017. Comparison between the optical properties of aerosols in the fine and coarse fractions over Valladolid, Spain. *Environ. Sci-Proc. Imp.* 19, 123–133.
- Moschos, V., Kumar, N.K., Daellenbach, K.R., Baltensperger, U., Prévôt, A.S.H., El Haddad, I., 2018. Source apportionment of brown carbon absorption by coupling ultraviolet-visible spectroscopy with aerosol mass spectrometry. *Environ. Sci. Technol. Lett.* 5, 302–308.
- Nepomuceno, S., Wagner, F., Silva, A.M., 2014. Multiyear measurements of the aerosol absorption coefficient near the surface in a small-sized urban area in Portugal. *Adv. Meteorol.* 2014, 830349.
- Nicolás, J.F., Castañer, R., Crespo, J., Yubero, E., Galindo, N.C., Pastor, C., 2018. Seasonal variability of aerosol absorption parameters at a remote site with high mineral dust loads. *Atmos. Res.* 210, 100–109.
- Nicolás, J.F., Lucarelli, F., Galindo, N., Yubero, E., Crespo, J., Calzolari, G., Nava, S., 2020. Impact of traffic flows and meteorological events on the hourly elemental composition of fine and coarse particles at an urban site. *Aerosol Air Qual. Res.* 20, 991–1001.
- Pani, S.K., Lin, N.-H., Griffith, S.M., Chantara, S., Lee, C.-T., Thepnuan, D., Tsai, Y.I., 2021. Brown carbon light absorption over an urban environment in northern peninsular Southeast Asia. *Environ. Pollut.* 276, 116735.
- Paraskevopoulou, D., Liakakou, E., Gerasopoulos, E., Theodosi, C., Mihalopoulos, N., 2014. Long-term characterization of organic and elemental carbon in the PM_{2.5} fraction: the case of Athens, Greece. *Atmos. Chem. Phys.* 14, 13313–13325.
- Paraskevopoulou, D., Kaskaoutis, D.G., Grivas, G., Bikkina, S., Tsagkaraki, M., Vrettou, I. M., Tavernaraki, K., Papoutsidaki, K., Stavroulas, I., Liakakou, E., Bougiatioti, A., Oikonomou, K., Gerasopoulos, E., Mihalopoulos, N., 2023. Brown carbon absorption and radiative effects under intense residential wood burning conditions in Southeastern Europe: new insights into the abundance and absorptivity of methanol-soluble organic aerosols. *Sci. Total Environ.* 860, 160434.
- Ponczek, M., Franco, M.A., Carbone, S., Rizzo, L.V., Monteiro dos Santos, D., Morais, F. G., Duarte, A., Barbosa, H., Artaxo, P., 2022. Linking the chemical composition and optical properties of biomass burning aerosols in Amazonia. *Environ. Sci.: Atmos.* 2, 252–269.
- Ran, L., Deng, Z.Z., Wang, P.C., Xia, X.A., 2016. Black carbon and wavelength-dependent aerosol absorption in the North China Plain based on two-year aethalometer measurements. *Atmos. Environ.* 142, 132–144.
- Saarikoski, S., Timonen, H., Saarnio, K., Aurela, M., Järvi, L., Keronen, P., Kerminen, V.-M., Hillamo, R., 2008. Sources of organic carbon in fine particulate matter in northern European urban air. *Atmos. Chem. Phys.* 8, 6281–6295.
- Satish, R., Rastogi, N., Singh, A., Singh, D., 2020. Change in characteristics of water-soluble and water-insoluble brown carbon aerosols during a large-scale biomass burning. *Environ. Sci. Pollut. Res.* 27, 33339–33350.
- Savadkoohi, M., Pandolfi, M., Reche, M.C., Niemi, J.V., Mooibroek, D., Gloria Titos, G., Green, D.C., Tremper, A.H., Hueglin, C., Liakakou, E., Mihalopoulos, M., Stavroulas, I., Artiñano, B., Coz, E., Alados-Arboledas, L., Beddows, D., Riffault, V., De Brito, J.F., Bastian, S., Baudic, A., Costabile, F., Chazeau, B., Gómez-Amo, J.L., Estellés, V., Matos, V., van der Gaag, E., Gille, G., Luoma, K., Manninen, H.E., Norman, M., Silvergren, S., Petit, J.-E., Putaud, J.-P., Rattigan, O.V., Timonen, H., Tuch, T., Merkel, M., Weinhold, K., Vratolis, S., Vasilescu, J., Favez, O., Harrison, R. M., Lag, P., Wiedensohler, A., Hopke, P.H., Petäjä, T., Querol, X., 2023. The variability of mass concentrations and source apportionment analysis of equivalent black carbon across urban Europe. *Environ. Int.* 178, 108081.
- Segura, S., Estellés, V., Esteve, A.R., Marcos, C.R., Utrillas, M.P., Martínez-Lozano, J.A., 2016. Multiyear in-situ measurements of atmospheric aerosol absorption properties at an urban coastal site in western Mediterranean. *Atmos. Environ.* 129, 18–26.
- Soleimani, E., Mousavi, A., Taghvae, S., Shafer, M.M., Sioutas, C., 2020. Impact of secondary and primary particulate matter (PM) sources on the enhanced light absorption by brown carbon (BrC) particles in central Los Angeles. *Sci. Total Environ.* 705, 135902.
- Titos, G., Foyo-Moreno, I., Lyamani, H., Querol, X., Alastuey, A., Alados-Arboledas, L., 2012. Optical properties and chemical composition of aerosol particles at an urban location: an estimation of aerosol mass scattering and absorption efficiencies. *J. Geophys. Res.* 117, D04206.
- Viana, M., Maenhaut, W., ten Brink, H.M., Chi, X., Weijers, E., Querol, X., Alastuey, A., Mikuška, P., Večeřa, Z., 2007. Comparative analysis of organic and elemental carbon concentrations in carbonaceous aerosols in three European cities. *Atmos. Environ.* 41 (28), 5972–5983.
- Yan, J., Wang, X., Gong, P., Wang, C., Cong, Z., 2018. Review of brown carbon aerosols: recent progress and perspectives. *Sci. Total Environ.* 634, 1475–1485.
- Yang, M., Howell, S.G., Zhuang, J., Huebert, B.J., 2009. Attribution of aerosol light absorption to black carbon, brown carbon, and dust in China – interpretations of atmospheric measurements during EAST-AIRE. *Atmos. Chem. Phys.* 9, 2035–2050.
- Zhang, X., Lin, Y.-H., Surratt, J.D., Weber, R.J., 2013. Sources, composition and absorption Ångström exponent of light-absorbing organic components in aerosol extracts from the Los Angeles Basin. *Environ. Sci. Technol.* 47 (8), 3685–3693.
- Zhou, Y., Chen, J., Fan, F., Feng, Y., Wang, S., Fu, Q., Feng, J., 2022. Deconvolving light absorption properties and influencing factors of carbonaceous aerosol in Shanghai. *Sci. Total Environ.* 839, 156280.



WSOC in accumulation mode aerosols: Distribution and relationship with BrC light absorption at an urban background site

A. López-Caravaca, J. Crespo, N. Galindo, E. Yubero, N. Juárez, J.F. Nicolás*

Atmospheric Pollution Laboratory (LCA), Department of Applied Physics, Miguel Hernández University, Avenida de la Universidad S/N, 03202 Elche, Spain

ARTICLE INFO

Keywords:

Urban background
Size distribution
WSOC
 σ_{BrC}
Stagnant conditions

ABSTRACT

This paper presents the outcomes of a one-month long campaign (Jan 11, 2021 to Feb 11, 2021) of size segregated particulate matter (PM) in the accumulation mode (AM). Samples were collected at an urban background station (southeastern Iberian Peninsula) using a micro-orifice uniform deposit impactor (MOUDI). PM mass and water-soluble organic carbon (WSOC) were subsequently measured. The main goals of this research were: (1) to explore differences in WSOC mass size distributions under different meteorological conditions and (2) to determine the most efficient size for light absorption by WSOC. For the second objective, measurements of absorption coefficients ($\sigma_{\text{ap},\lambda}$) were obtained by means of an Aethalometer (AE33). Significant differences in WSOC concentrations and $\sigma_{\text{ap},\lambda}$ values during stagnation episodes compared to non-event days were observed. Increases in WSOC concentrations during these episodes were most likely associated with the photochemical production of secondary compounds (in small-size ranges of the AM) and with water uptake (in large-size ranges of the AM). The average $\sigma_{\text{ap},\lambda}$ value during this type of event was 2.6 higher than for non-event days. No significant increases in WSOC levels were detected under Saharan dust events. The average contribution of BrC to light absorption at 370 nm was ~35%, revealing a significant influence of BrC on the absorption process. High contributions from BrC to light absorption were associated with AAE values above 1.5 and, in general, with high WSOC concentrations. WSOC in the smallest size mode (0.25 μm) was mainly emitted from biomass burning (BB) and showed the highest light absorption efficiency.

1. Introduction

Organic Carbon (OC) is composed of primary and secondary compounds originating from anthropogenic and biogenic sources. The water-soluble fraction of organic carbon (WSOC) accounts for 30–90% of OC (Chalbot et al., 2014). This percentage depends on the season, location, time-of-day and particle size (Agarwal et al., 2010; Park et al., 2011). Concentrations of WSOC are generally used as a proxy for water-soluble BrC, which is the organic carbon component that absorbs radiation efficiently in the near-UV and visible ranges (Laskin et al., 2015). Therefore, WSOC can contribute significantly to light absorption in the UV and visible regions, leading to a higher absorption of solar radiation and contributing to the direct effect of aerosols on climate (Duarte et al., 2004). Additionally, there is an increased interest in the measurement of the water-soluble fraction of the organic aerosol since, once inhaled, it can cause specific adverse effects on human health (Tuet et al., 2016; Velali et al., 2016). Thus, WSOC is closely linked to climate

change and air quality (Ni et al., 2021).

WSOC has both a primary (e.g., biomass burning (BB) or motor vehicle exhausts) and a secondary (e.g., secondary organic aerosol (SOA) formation) origin. At urban sites, a significant fraction of WSOC is formed by oxidation of organic compounds during the warmer months, while during the rest of the year it mainly derives from direct emissions from sources (Snyder et al., 2009; López-Caravaca et al., 2023). WSOC size distributions depend on its emissions sources (Duarte et al., 2008; Timonen et al., 2008). Most studies show that WSOC is mainly found in the accumulation mode (from ~0.1 to ~2 μm) (Rinaldi et al., 2007; Lin et al., 2010; Paulovic and Hopke, 2012; Chalbot et al., 2014; Sandrini et al., 2016; Frka et al., 2018). Accumulation-mode WSOC is associated with BB emissions and SOA formation processes (Yu et al., 2017), while WSOC in the coarse fraction comes from marine aerosol (Timonen et al., 2008) or primary biogenic sources (Yttri et al., 2011).

It should be noted that light absorption properties of BrC/WSOC coming from different sources may be different (Feng et al., 2013; Zhou

Peer review under responsibility of Turkish National Committee for Air Pollution Research and Control.

* Corresponding author. Laboratory of Atmospheric Pollution, Miguel Hernández University, Av. de la Universidad s/n, Edif. Alcudia, 03202, Elche, Spain.

E-mail address: j.nicolas@umh.es (J.F. Nicolás).

<https://doi.org/10.1016/j.apr.2024.102133>

Received 18 January 2024; Received in revised form 27 March 2024; Accepted 28 March 2024

Available online 3 April 2024

1309-1042/© 2024 Turkish National Committee for Air Pollution Research and Control. Production and hosting by Elsevier B.V. This is an open access article under the CC BY-NC-ND license (<http://creativecommons.org/licenses/by-nc-nd/4.0/>).

et al., 2022). This is due to the distinct chemical composition of chromophores (Huang et al., 2018). WSOC from BB shows the highest absorption efficiency (Fan et al., 2016), while WSOC formed from biogenic precursors has a lower light absorption capacity (Lambe et al., 2013). Therefore, the contribution of BrC to light absorption depends on the dominant sources. Meteorological conditions and air-mass history may also affect BrC absorption (Park and Yu, 2019). For these reasons, the contribution of BrC (σ_{BrC}) to total light absorption (σ_{ap}) at short wavelengths in urban locations may be highly variable (~5–46%) (Pani et al., 2021).

The main goal of the present work is to explore differences in WSOC mass size distributions under different meteorological conditions at an urban background site located in the southeast of the Iberian Peninsula. Understanding the size distribution and formation processes of WSOC is essential to tackle the problems of both air pollution and regional climate change (Ni et al., 2021). On the other hand, there are few works on this topic in the western Mediterranean basin. The relationship between σ_{BrC} and size-resolved WSOC was also addressed in order to determine the most efficient size for light absorption by WSOC.

2. Methodology

2.1. Measurement site

Size-segregated particle samples were collected daily between 11 January and 11 February 2021. The sampling site was located at the campus of the Miguel Hernández University of Elche (UMH, 38°16' N; 0°41' W; 93 m. a.s.l), in the southeast of the Iberian Peninsula. The sampling station can be classified as an urban background site (UBS) because it is not directly influenced by traffic or industrial emissions. More details on the characteristics of the sampling site and the predominant meteorological conditions can be found in López-Caravaca et al. (2023).

2.2. Measurements and analysis

2.2.1. PM and WSOC

Aerosol samples were collected at 2.3 m above ground level using a Micro-Orifice Uniform Deposit Impactor (MOUDI MS Model 130 B HFI) operating at 100 l·min⁻¹. Thirty-two consecutive 24-h samples were collected on Polycarbonate Track Etched (PCTE) membrane filters (76 mm in diameter, GVS). Particles were classified in 4 stages. The size cut-off (particle size for which the channel has 50% collection efficiency) of the different stages was: 1.4, 1, 0.44, and 0.25 μm . A total of 128 samples were collected (32 sampling days x 4 stages). The number of samples ensures a good representativeness of the results regarding the impact of different atmospheric dynamics on PM and WSOC concentrations.

Particulate matter (PM) concentrations were determined by gravimetric analysis under stable humidity (50 \pm 5 %) and temperature (20 \pm 1 °C) conditions. The inaccuracy in the determination of the PM mass was ~20%.

WSOC concentrations were measured using a TOC-L CSH analyzer (Shimadzu). The instrument uses a 680 °C combustion catalytic oxidation method. In the present study, WSOC was quantified as the non-purgeable organic carbon (NPOC). For this, an aliquot of the water extract was diluted 1:2 with ultrapure water, acidified with 1 M HCl (PanReac AppliChem) and purged with pure air in order to remove dissolved inorganic carbon and volatile organics. Analyses were run in triplicate and WSOC concentrations were calculated as the average value of the three measurements. Calibration was conducted using a standard solution of potassium hydrogen phthalate (PanReac AppliChem). Concentrations of all samples were above the MDL (0.07 $\mu\text{g}\cdot\text{m}^{-3}$).

PM₁ samples (N = 12) collected during the study period at the same site were analyzed to determine levoglucosan concentrations. These samples are part of a complementary research campaign whose results

have been presented in López-Caravaca et al. (2023). The analytical procedure to determine levoglucosan concentrations is described in the aforementioned work.

2.2.2. Aerosol absorption properties

Measurements of σ_{ap} were performed using an Aethalometer (model AE33, Magee Scientific, USA). The Aethalometer provides the absorption coefficient at seven wavelengths (370, 470, 520, 590, 660, 880 and 950 nm). To obtain aerosol absorption coefficients from aerosol attenuation coefficients, the harmonization factor for M8060 filter tape (H^* factor = 1.76) was used (Savadooghi et al., 2023). The instrument operated at a constant air flow rate of 3.9 l·min⁻¹. The time resolution was 5 min. Hourly and daily averages were subsequently calculated. Absorption measurements and PM collection were carried out simultaneously.

The absorption Angstrom exponent (AAE) was obtained from σ_{ap} :

$$\text{AAE} = \frac{\ln \frac{\sigma_{\text{ap}}(\lambda_1)}{\sigma_{\text{ap}}(\lambda_2)}}{\ln \frac{\lambda_1}{\lambda_2}} \quad (1)$$

where $\lambda_1 = 370$ nm and $\lambda_2 = 950$ nm.

In order to determine the contribution from BrC to σ_{ap} (σ_{BrC}), the methodology described in Kaskaoutis et al. (2021) (named *BrC model*) was used. This approach is based on the assumption that light absorption was no influenced by mineral dust (MD) and therefore σ_{ap} can be expressed as:

$$\sigma_{\text{ap},\lambda} = \sigma_{\text{BC},\lambda} + \sigma_{\text{BrC},\lambda} \quad (2)$$

where $\sigma_{\text{BC},\lambda}$ is the contribution from black carbon (BC) to $\sigma_{\text{ap},\lambda}$. Then, it was assumed that BC is the only absorbing component at $\lambda = 880$ nm and that its spectral dependence for the remaining wavelengths is a function of λ^{-1} . σ_{BrC} for each wavelength was subsequently estimated according to Eq. (2) from the differences between measured σ_{ap} values for each λ and those obtained as a function of λ^{-1} .

2.3. Meteorological data

Meteorological parameters were obtained from a station belonging to the regional air quality monitoring network, located on the outskirts of the city. Table 1 shows a statistic summary of meteorological variables during the monitoring period.

Data presented in Table 1 were calculated from daily values. There was only one rainy day during the measurement period (22 January), with an accumulated precipitation of 6 l·m⁻². The hourly evolution of RH, SR and T is shown in Fig. S1 (Supplementary Material).

The Global Data Assimilation System (GDAS1) model from the NOAA Air Resources Laboratory (<http://www.ready.noaa.gov/READYamet.php>) was used for the determination of the mixing layer height and the origin of air masses. The identification of Saharan dust episodes was based on the results of the predictive model BSCDREAM8b (<https://ess.bsc.es/bsc-dust-daily-forecast>). The analysis of PM time series helped to confirm the occurrence of SDE over the study area.

Table 1

Statistic summary of meteorological parameters during the study period.

Parameter	Mean (SD)	P5	Median	P95
T (°C)	15.0 (3.6)	9.3	15.3	21.0
SR (W·m ⁻²)	100.0 (32.5)	30.1	107	141.5
WS (m·s ⁻¹)	1.8 (1.2)	0.6	1.4	4.4
RH (%)	62.3 (15.7)	42.1	58.5	93.4

SD: Standard Deviation; T: Temperature; SR: Solar Radiation; WS: Wind Speed; RH: Relative Humidity.

3. Results

3.1. WSOC in size segregated aerosols

3.1.1. PM and WSOC concentrations

A statistic summary of PM and WSOC concentrations, as well as the contribution of WSOC to PM levels in each size fraction, is shown in Table 2. The highest mean PM concentration was found in the PM_{1,4} fraction. Conversely, the maximum WSOC concentration (0.23 µg·m⁻³) was obtained in the smallest size fraction (0.25 µm). The percentage contributions of WSOC to PM levels were also highest in the smallest size fractions, with values above 14%.

In some size intervals, a significant difference between mean and median values was found. Specifically, notable differences between average and median concentrations were observed for PM in the stage of 1.4 µm and for WSOC in the stage of 0.25 µm. These results point to the occurrence of PM episodes having a significant impact on PM and WSOC levels in these size ranges. The influence of such events is studied in Section 3.1.2.

As expected, WSOC at the sampling site was mainly distributed in the small sizes (condensation mode). Table 3 shows the particle size for which WSOC concentrations were maxima at different European sites. It has to be considered that samples were collected using impactors having different size ranges. As can be observed, maximum WSOC concentrations were usually found in the size intervals between ~0.2 and ~0.6 µm, regardless of the type of site and the measurement period. Therefore, the maximum WSOC concentration in the study area was found in the lower range of this interval.

3.1.2. Daily variability in WSOC concentrations

Fig. 1 shows time series of PM and WSOC size-segregated concentrations during the study period. At the beginning of the second sampling week, WSOC concentrations significantly increased in all size fractions. For the smallest size ranges WSOC levels were almost three times higher than those recorded during the previous week due to a high pollution episode (HPE) occurring between 18 and 20 January. A detailed characterization of this episode can be found in the supplementary material (Fig. 2S). Near the end of the measurement period, WSOC concentrations increased again, although the increase was not as high as that observed during the second sampling week. In this case, the rise in WSOC levels was due to a Saharan dust event (SDE) occurring between 3 and 5 February (see Fig. 2S). The last day of this episode had a significant impact on the coarser size ranges. Fig. 1 also shows the contribution of WSOC to PM levels in size each fraction. For all size ranges, the increases in WSOC concentrations observed during both events coincided with a decrease in the percentage contribution of WSOC to PM levels, in particular during the SDE. This implies that the relative increase in the concentrations of other PM constituents was higher than that observed for WSOC.

Fig. 2 shows the influence of HPE and SDE on WSOC and PM concentrations. On non-event days (NE), PM concentrations were lower than 2.5 µg·m⁻³ for all size ranges. The highest PM levels were reached during the SDE. The PM_{1,4} fraction was the most affected size range, with an average three-day concentration above 20 µg·m⁻³. The transport of MD during SDE has a greater influence on coarse particles, as

Table 2

Statistic summary of PM and WSOC concentrations (in µg·m⁻³), and percentage contribution of WSOC to PM concentrations in each size fraction.

	0.25 µm			0.44 µm			1.0 µm			1.4 µm		
	PM	WSOC	%	PM	WSOC	%	PM	WSOC	%	PM	WSOC	%
Mean	2.3	0.23	14.1	1.1	0.14	16.3	2.4	0.16	10.3	5.5	0.19	7.2
SD	2.5	0.18	6.4	1.0	0.06	7.7	3.4	0.06	6.6	10.6	0.10	5.9
P5	0.4	0.07	6.1	0.5	0.08	6.4	0.6	0.08	3.2	0.9	0.09	1.7
Median	1.5	0.17	14.0	0.8	0.13	15.7	1.6	0.15	8.9	2.6	0.17	6.3
P95	8.3	0.55	24.2	2.7	0.13	30.8	3.8	0.29	22.4	11.5	0.41	16.1

Table 3

Particle size ranges for which WSOC concentrations are highest (WSOC_{max}) at different sites in Europe.

Site	Station ^a	Season	WSOC _{max}	Study
Budapest (Hungary)	Urban	Spring	0.37 µm	Salma et al. (2013)
Lecce (Italy)	UB	Feb to Oct	0.24–0.75 µm	Contini et al. (2014)
Finokalia (Grecce)	MB	Summer	0.225–0.585 µm	Bougatioti et al. (2013)
Ljubljana (Slovenia)	UB	Winter	0.60 µm	Frka et al. (2018)
Helsinki (Finland)	UB	Winter	0.32–0.56 µm	Timonen et al. (2008)
Bologna (Italy)	Urban	Fall-Winter	0.42–1.20 µm	Matta et al. (2003)
Mace Head (Ireland)	MB	Spring-Autumn	0.225 µm	Cavalle et al. (2004)
Oporto (Portugal)	Urban	Summer	<0.49 µm	Duarte et al. (2008)
Elche (Spain)	UB	Winter	0.25 µm	This study

^a UB: Urban Background; MB: Marine Background.

reported in previous studies performed in southern European countries (Titos et al., 2017; Cesari et al., 2020; Nicolás et al., 2020). During the HPE, PM_{0,25} concentrations increased approximately 8 times with respect to the average value registered on NE days. The PM_{1,4} fraction also experienced a significant increase. The increase in fine PM concentrations during HPE has been well documented and is due to air stagnation. Atmospheric conditions typical of these events (low wind speeds and mixing layer heights, high relative humidity and clear skies) contribute to the accumulation of aerosols emitted from anthropogenic sources and favor secondary aerosol formation (Jiang et al., 2015; Diémoz et al., 2019; Galindo et al., 2020).

Increases in WSOC concentrations for all size ranges were considerably lower during the SDE than during the HPE. In fact, average levels during NE days and SDE were very similar for all size ranges. This result is in line with those previously reported for the same study area, where increases in fine OC concentrations during SDE were lower than those observed for other chemical constituents (Galindo et al., 2020). Likewise, Park and Yu (2019) did not find increases in WSOC levels in the AM during Asian dust events. The highest WSOC concentrations during HPE were registered in the 0.25 µm size range. The average concentration for this size fraction was three times higher than that calculated on NE days. Similar increases in the concentrations of particles in the small AM (condensation mode) under stagnant conditions have been previously found in Bologna (Italy) (Sandrini et al., 2016) and Gwangju (Korea) (Park and Yu, 2019). These increases are most likely associated with the diurnal photochemical production of WSOC. WSOC concentrations for larger size ranges (droplet mode) were also significantly affected by this type of event. In this case, increases in WSOC levels were probably due to water uptake by accumulation-mode particles under high ambient RH conditions (Salma et al., 2013; Sandrini et al., 2016).

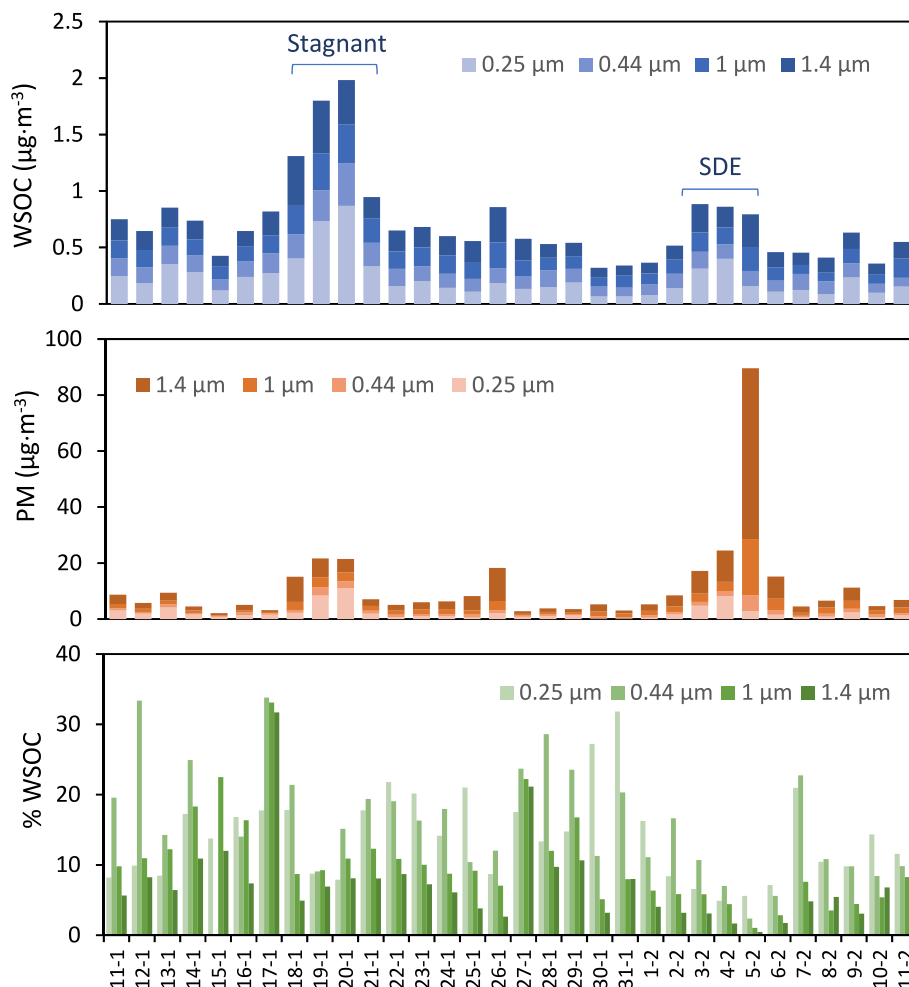


Fig. 1. Daily variability of WSOC and PM concentrations. Contribution of WSOC to PM levels for each size fraction is also shown.

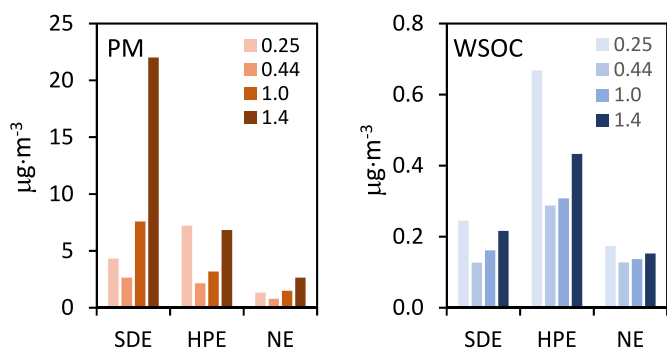


Fig. 2. Size distribution of PM and WSOC during non-event days (NE) and pollution events (HPE and SDE).

3.2. Relationship between WSOC and σ_{BrC}

3.2.1. Hourly evolution of σ_{ap}

σ_{ap} values obtained in this study (Table 4) were lower than those registered in other cities of similar size in Spain (Titos et al., 2012; Esteve et al., 2012; Segura et al., 2016). This could be due to lower PM emissions from traffic during the measurement period, when COVID-19 restrictive measures were still in force. The AAE value can provide information on the aerosol composition. When BC is the dominant absorbing aerosol component, the AAE value is close to 1, while MD and BrC aerosols have AAE values significantly higher than 1. The AAE value

Table 4

Statistic summary of σ_{ap} (Mm^{-1}) at different wavelengths and AAE values (dimensionless).

σ_{ap} (Mm^{-1})	370 nm	470 nm	520 nm	590 nm	660 nm	880 nm	950 nm	AAE
Mean	18.3	13.0	10.2	8.3	7.0	5.0	4.7	1.42
SD	13.5	9.2	7.1	5.8	4.9	3.5	3.2	0.14
P5	2.5	1.9	1.5	1.3	1.1	0.8	0.7	1.22
Median	16.1	12.2	9.7	8.1	7.0	5.0	4.7	1.40
P95	46.7	31.4	24.7	20.3	16.9	12.1	11.2	1.62

obtained in the present study (1.42) indicates that BC was the main light absorbing component during the measurement period, although other PM constituents (BrC and MD) also contributed to radiation absorption.

Fig. 3 shows the average hourly variability of $\sigma_{ap,370}$ values during NE days and pollution events. On NE days the variation was that expected for urban environments during winter, with maxima during the morning (08:00–09:00 h) and evening rush hours (19:00–20:00 h) (Segura et al., 2016; Forello et al., 2019). These peaks were associated with the increase in local traffic emissions (Segura et al., 2014, 2016). $\sigma_{ap,370}$ values decreased rapidly from 12:00 h to 17:00 h due to the increase in the boundary layer height and the reduction in traffic emissions (Piñeiro-Iglesias et al., 2021). During the SDE, the same daily pattern was observed, although $\sigma_{ap,370}$ values were higher due to the contribution of MD to light absorption, as previously observed at the same site (López-Caravaca et al., 2021).

Peak $\sigma_{ap,370}$ values during HPE were three time higher than on NE

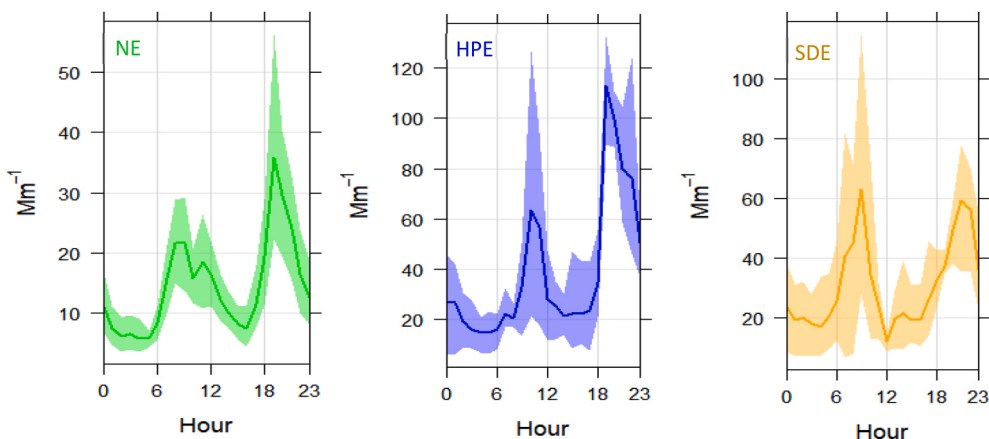


Fig. 3. Mean hourly variation in $\sigma_{ap,370}$ values during NE days, high pollution episode and Saharan dust event.

days. This was due to the observed increase in WSOC concentrations, in addition to the known increase in BC levels during these episodes (Segura et al., 2013; Park and Yu, 2019; Galindo et al., 2020). The average relative increase in $\sigma_{ap,370}$ values with respect to NE days was 2.6. It can also be observed that the maximum value reached at the end of the day was significantly higher than the daytime maximum. This could be explained considering that during high atmospheric stability periods WSOC concentrations increase more significantly at night (Sandrini et al., 2016).

3.2.2. Light absorption by BrC

The contribution of BrC to light absorption for each wavelength was estimated from the differences between measured σ_{ap} values and those calculated for BC (see Section 2.2.2). Fig. 4 (left) shows the results of the application of this procedure. The percentage contribution of BrC to light absorption is denoted by the blue area. For the shortest wavelength, this contribution was around 35%.

AAE_{BrC} values represent the wavelength dependence of light absorption by BrC and can be highly dependent on sources and atmospheric processes (Mo et al., 2021). BrC from BB and fresh SOA show higher AAE values than BrC from vehicle emissions and aged SOA. The $AAE_{(370-660\text{ nm})}$ value obtained for BrC (determined by fitting each set of 5- λ data by a λ^{-AAE} function) was 5.2 ± 0.6 . This value was slightly higher than those found at other European urban sites such as Athens (3.6 ± 0.9 ; Liakakou et al., 2020), Genoa (4.02 ± 0.19) or Milan (3.81 ± 0.11 ; Bernardoni et al., 2017), suggesting a higher contribution of BB and/or fresh SOA to BrC levels at the sampling site.

The right panel of Fig. 4 shows the daily evolution of light absorption by BrC (σ_{BrC}) at $\lambda = 370\text{ nm}$ and the percentage contribution to total absorption ($\sigma_{ap,370}$). Days under the influence of Saharan dust were not included in this analysis to avoid the influence of MD on the absorption

process. Increases in $\sigma_{BrC,370}$ values during the HPE are clearly observed. The increase in the concentrations of WSOC, which is an important constituent of BrC, explains peak $\sigma_{BrC,370}$ values during this event.

The percentage contribution of $\sigma_{BrC,370}$ to total absorption was slightly higher in the first third of the sampling period. A possible reason is that biomass burning emissions were more important at the beginning of the monitoring period, in addition to the significant increase in WSOC levels during the HPE. During this period, the average contribution of BrC to light absorption at 370 nm was $\sim 42\%$ (higher than the average for the whole study period) and AAE values were highest (1.5–1.7). The relationship between $\sigma_{BrC,370}$, AAE and WSOC concentrations is presented in Fig. 5. Those days under the influence of Saharan dust were excluded from the analysis.

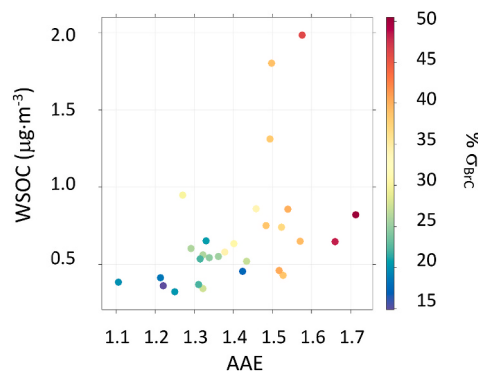


Fig. 5. Variation of the contribution of BrC to light absorption at 370 nm as a function of WSOC concentrations ($\mu\text{g}\cdot\text{m}^{-3}$) and AAE values.

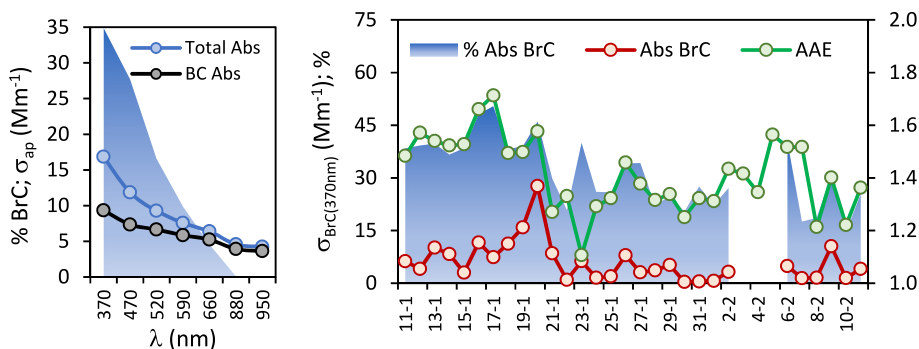


Fig. 4. a) Spectral dependence of: σ_{ap} , σ_{BC} and the percentage contribution of BrC to light absorption (blue area); b) Evolution of AAE, $\sigma_{BrC,370}$ and the percentage contribution of $\sigma_{BrC,370}$ to $\sigma_{ap,370}$ during the measurement period.

The increment in the contribution of BrC to light absorption at 370 nm was associated with high AAE values and WSOC concentrations (calculated as the sum of all stages of the MOUDI impactor). In general, AAE and % σ_{BrC} values higher than average values for the whole study period were simultaneously observed. Likewise, most WSOC concentrations were also higher than the average value ($\sim 0.7 \mu\text{g}\cdot\text{m}^{-3}$). However, on some of these days, WSOC concentrations were not especially high. This could be due to a larger contribution from water-insoluble organic carbon to the σ_{BrC} value. In fact, previous studies have shown a significant contribution of insoluble OC to BrC absorption in the near UV range (Kaskaoutis et al., 2022; Zhou et al., 2022; López-Caravaca et al., 2024).

The hourly variation in background conditions of σ_{BrC} and σ_{BC} at 370 nm is presented in Fig. 6. Both contributions showed a very similar daily pattern. Nevertheless, the morning peak for $\sigma_{\text{BrC},370}$ was observed around 3–4 h later than the $\sigma_{\text{BC},370}$ peak. This delay can explain the width of the morning peak for $\sigma_{\text{ap},370}$ shown in Fig. 3.

Since BC and primary BrC are emitted by the same sources, mainly BB and fossil fuel combustion (Zhu et al., 2021), a significant contribution of secondary BrC to the morning $\sigma_{\text{BrC},370}$ peak is suggested. In fact, a substantial contribution of secondary aerosol to WSOC/BrC concentrations in the study area has been found ($\sim 16\%$ in the cold season, López-Caravaca et al., 2024). The increase in solar radiation after sunrise promote photochemical reactions that can result in the formation of secondary BrC. Between 12:00 h and 17:00 h, light-absorbing chromophores are bleached through oxidative processes, leading to a decrease in secondary BrC concentrations (Wang et al., 2019). The formation of secondary BrC via aqueous phase reactions was not considered, since the RH was below 60% (see Fig. S1) at the time of the $\sigma_{\text{BrC},370}$ morning peak. Studies on the gas-particle partitioning of water-soluble organic compounds revealed a shift to the particle phase for RH greater than or equal to 70% (Henningan et al., 2008).

3.2.3. Size dependence of WSOC with BrC light absorption

In order to determine the most efficient size for light absorption by WSOC, a Spearman's correlation analysis between $\sigma_{\text{BrC},370}$ and size-segregated WSOC concentrations was performed (blue dots in Fig. 7).

Although correlations were statistically significant for all size ranges, the correlation coefficient was highest for WSOC concentrations in the impaction stage of $0.25 \mu\text{m}$ ($\rho \sim 0.9$). This result indicates that the capacity of WSOC to absorb radiation depends to some extent on its size distribution, and that small WSOC particles are the most efficient in

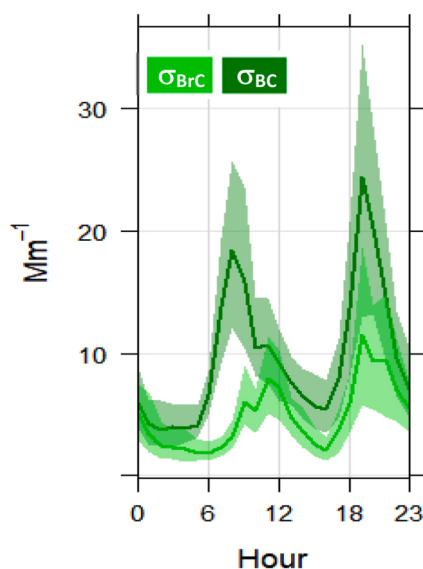


Fig. 6. Hourly variation of σ_{BC} and σ_{BrC} at 370 nm in background conditions.

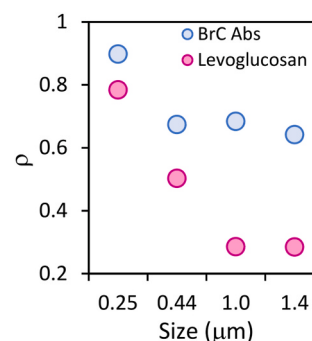


Fig. 7. Spearman's correlation coefficients (ρ) between size resolved WSOC and $\sigma_{\text{BrC},370}$ ($N = 29$, blue dots) and Levoglucosan ($N = 12$, pink dots).

terms of light absorption. This result can be explained considering that WSOC emitted by different sources may not have the same absorption efficiency. In fact, previous works have shown that emission sources play an important role in the light absorption capacity of BrC (Mo et al., 2021), since the light absorption of WSOC may be affected by the chromophore source. In this regard, BB has been identified as an important source of WSOC with high light absorption capacity (Fan et al., 2016). During the study period, BB emissions were one of the most important sources of WSOC in the study area (López-Caravaca, et al., 2023), suggesting that WSOC emitted from this source was mainly distributed in the smaller sizes ranges. This hypothesis was confirmed by the correlation between levoglucosan and size-resolved WSOC concentrations (Fig. 7, pink dots). A statistically significant correlation (p -value < 0.01) was only found between levoglucosan and WSOC concentrations in the stage of $0.25 \mu\text{m}$ ($\rho = 0.78$). For the remaining size intervals correlation coefficients were much lower. These results indicate that WSOC in the $0.25 \mu\text{m}$ size range was mainly emitted by BB and showed the highest light absorption capacity.

4. Conclusions

WSOC size-segregated concentrations in accumulation mode particles were determined during winter at an urban background site in southeastern Spain. The highest WSOC concentrations were observed in the smallest size range ($0.25 \mu\text{m}$). The WSOC size distribution was modified under stagnant conditions. WSOC levels in the condensation mode showed significant increases during these events, probably due to the diurnal photochemical production of WSOC, while increases in WSOC concentrations in the droplet mode were associated with water uptake. No remarkable increases in WSOC concentrations were detected under Saharan dust events.

The average contribution of BrC to light absorption at 370 nm during the study period was $\sim 35\%$. Percentages higher than the average value were associated with high AAE values (> 1.5) and, in general, with high WSOC concentrations. Nevertheless, on some days with BrC contributions higher than the average, WSOC levels were lower, indicating that water insoluble organic compounds may play a significant role in light absorption at short wavelengths.

WSOC in the $0.25 \mu\text{m}$ size range was mainly emitted by BB and showed the highest light absorption capacity.

CRediT authorship contribution statement

A. López-Caravaca: Formal analysis, Investigation, Visualization, Writing – original draft, Writing – review & editing. **J. Crespo:** Conceptualization, Funding acquisition, Project administration. **N. Galindo:** Supervision, Writing – review & editing. **E. Yubero:** Supervision, Writing – review & editing. **N. Juárez:** Formal analysis, Investigation. **J.F. Nicolás:** Funding acquisition, Investigation, Project administration, Supervision, Writing – original draft, Writing – review &

editing.

Declaration of competing interest

The authors declare that they have no known competing financial interests or personal relationships that could have appeared to influence the work reported in this paper.

Acknowledgements

This work was supported by the Spanish Ministry of Science, Innovation and Universities (COSMOS Project, ref. RTI 2018-098639-B-I00). A. López-Caravaca thanks the Spanish Ministry of Science and Innovation for a predoctoral grant (PRE 2019-089098).

Appendix A. Supplementary data

Supplementary data to this article can be found online at <https://doi.org/10.1016/j.apr.2024.102133>.

References

- Agarwal, S., Aggaewal, S.G., Okuzawa, K., Kawamura, K., 2010. Size distributions of dicarboxylic acids, ketoacids, α -dicarbonyls, sugars, WSOC, OC, EC and inorganic ions in atmospheric particles over Northern Japan: implication for long-range transport of Siberian biomass burning and East Asian polluted aerosols. *Atmos. Chem. Phys.* 10, 5839–5858.
- Bernardoni, V., Pileci, R.E., Caponi, L., Massabò, D., 2017. The Multi-Wavelength Absorption Analyzer (MWA) model as a tool for source and component apportionment based on aerosol absorption properties: application to samples collected in different environments. *Atmosphere* 8, 218.
- Bougiatioti, A., Zarnpas, P., Koulouri, E., Antoniou, M., Theodosi, C., Kouvarakis, G., Saarikoski, S., Mäkelä, T., Hillamo, R., Mihalopoulos, N., 2013. Organic, elemental and water-soluble organic carbon in size segregated aerosols, in the marine boundary layer of the Eastern Mediterranean. *Atmos. Environ.* 64, 251–262.
- Cavalli, F., Facchini, M.C., Decesari, S., Mircea, M., Emblico, L., Fuzzi, S., Ceburnis, D., Yoo, Y.-J., O'Dowd, C.D., Putaud, J.-P., Dell'Acqua, A., 2004. Advances in characterization of size-resolved organic matter in marine aerosol over the North Atlantic. *J. Geophys. Res.* 109, D24215.
- Cesari, D., Merico, E., Dinoi, A., Gambaro, A., Morabito, E., Gregoris, E., Barbaro, E., Feltracco, M., Alebić-Juretić, A., Odorić, D., Kontosić, D., Miška, B., Contini, D., 2020. An inter-comparison of size segregated carbonaceous aerosol collected by low-volume impactor in the port-cities of Venice (Italy) and Rijeka (Croatia). *Atmos. Pollut. Res.* 11 (10), 1705–1714.
- Chalbot, M.-C.G., Brown, J., Chitranshi, P., Gamboa da Costa, G., Pollock, E.D., Kavouras, I.G., 2014. Functional characterization of the water-soluble organic carbon of size-fractionated aerosol in the southern Mississippi Valley. *Atmos. Chem. Phys.* 14, 6075–6088.
- Contini, D., Cesari, D., Genga, A., Siciliano, M., Ielpo, P., Guascito, M.R., Conte, M., 2014. Source apportionment of size-segregated atmospheric particles based on the major water-soluble components in Lecce (Italy). *Sci. Total Environ.* 472, 248–261.
- Diémöz, H., Barnaba, F., Magri, T., Pession, G., Dionisi, D., Pittavino, S., Tombolato, I.K.F., Campanelli, M., Della Cecca, L.S., Hervò, M., Di Liberto, L., Ferrero, L., Gobbi, G.P., 2019. Transport of Po valley aerosol pollution to the northwestern alps – Part 1: phenomenology. *Atmos. Chem. Phys.* 19, 3065–3095.
- Duarte, R., Pio, C.A., Duarte, A.C., 2004. Synchronous scan and excitation-emission matrix fluorescence spectroscopy of water-soluble organic compounds in atmospheric aerosols. *J. Atmos. Chem.* 48, 157–171.
- Duarte, R., Miegro, C.L., Penetra, A., Pio, C.A., Duarte, A.C., 2008. Carbonaceous materials in size-segregated atmospheric aerosols from urban and coastal-rural areas at the Western European Coast. *Atmos. Res.* 90, 253–263.
- Esteve, A.R., Estellés, V., Utrillas, M.P., Martínez-Lozano, J.A., 2012. In-situ integrating nephelometer measurements of the scattering properties of atmospheric aerosols at an urban coastal site in western Mediterranean. *Atmos. Environ.* 47, 43–50.
- Fan, X.J., Song, J.Z., Peng, P.A., 2016. Temporal variations of the abundance and optical properties of water soluble humic-like substances (HULIS) in PM_{2.5} at Guangzhou, China. *Atmos. Res.* 172–173, 8–15.
- Feng, Y., Ramanathan, V., Kotamarthi, V.R., 2013. Brown Carbon: a Significant atmospheric absorber of solar radiation. *Atmos. Chem. Phys.* 13, 8607–8621.
- Forello, A.C., Bernardoni, V., Calzolari, G., Lucarelli, F., Massabò, D., Nava, S., Pileci, R.E., Prati, P., Valentini, S., Valli, G., Vecchi, R., 2019. Exploiting multi-wavelength aerosol absorption coefficients in a multi-time resolution source apportionment study to retrieve source-dependent absorption parameters. *Atmos. Chem. Phys.* 19, 11235–11252.
- Frka, S., Grgić, I., Turšić, J., Gini, M.I., Eleftheriadis, K., 2018. Seasonal variability of carbon in humic-like matter of ambient size-segregated water-soluble organic aerosols from urban background environment. *Atmos. Environ.* 173, 239–247.
- Galindo, N., Yubero, E., Clemente, A., Nicolás, J.F., Varea, M., Crespo, J., 2020. PM events and changes in the chemical composition of urban aerosols: a case study in the western Mediterranean. *Chemosphere* 244, 125520.
- Henningan, C.J., Bergin, M.H., Dibb, J.E., Weber, R.J., 2008. Enhanced secondary organic aerosol formation due to water uptake by fine particles. *Geophys. Res. Lett.* 35, L18801.
- Huang, R.J., Yang, L., Cao, J., Chen, Y., Chen, Q., Li, Y., Duan, J., Zhu, C., Dai, W., Wang, K., Lin, C., Ni, H., Corbin, J.C., Wu, Y., Zhang, R., Tie, X., Hoffmann, T., O'Dowd, C., Dusek, U., 2018. Brown carbon aerosol in urban Xi'an, Northwest China: the composition and light absorption properties. *Environ. Sci. Technol.* 52, 6825–6833.
- Jiang, J., Zhou, W., Cheng, Z., Wang, S., He, K., Hao, J., 2015. Particulate matter distributions in China during a winter period with frequent pollution episodes (January 2013). *Aerosol Air Qual. Res.* 15, 494–503.
- Kaskaoutis, D.G., Grivas, G., Stavroulas, I., Bougiatioti, A., Liakakou, E., Dumka, U.C., Gerasopoulos, E., Mihalopoulos, N., 2021. Apportionment of black and brown carbon spectral absorption sources in the urban environment of Athens, Greece, during Winter. *Sci. Total Environ.* 801, 149739.
- Kaskaoutis, D.G., Grivas, G., Oikonomou, K., Tavernaraki, P., Papoutsidaki, K., Tsagkaraki, M., Stavroulas, I., Zarnpas, P., Paraskevopoulou, D., Bougiatioti, A., Liakakou, E., Gavrouzou, M., Dumka, U.C., Hatzianastassiou, N., Sciare, J., Gerasopoulos, E., Mihalopoulos, N., 2022. Impacts of severe residential wood burning on atmospheric processing, water-soluble organic aerosol and light absorption, in an inland city of Southeastern Europe. *Atmos. Environ.* 280, 119139.
- Lambe, A.T., Cappa, C.D., Massoli, P., Onasch, T.B., Forestieri, S.D., Martin, A.T., Cummings, M.J., Croasdale, D.R., Brune, W.H., Worsnopand, D.R., Davidovits, P., 2013. Relationship between oxidation level and optical properties of secondary organic aerosol. *Environ. Sci. Technol.* 47 (12), 6349–6357.
- Laskin, A., Laskin, J., Nizkorodov, S.A., 2015. Chemistry of atmospheric brown carbon. *Chem. Rev.* 115, 4335–4382.
- Liakakou, E., Kaskaoutis, D.G., Grivas, G., Stavroulas, I., Tsagkaraki, M., Paraskevopoulou, D., Bougiatioti, A., Dumka, U.C., Gerasopoulos, E., Mihalopoulos, N., 2020. Long-term brown carbon spectral characteristics in a Mediterranean city (Athens). *Sci. Total Environ.* 708, 135019.
- Lin, P., Huang, X.-F., He, L.-Y., Yu, J.Z., 2010. Abundance and size distribution of HULIS in ambient aerosols at a rural site in South China. *J. Aerosol Sci.* 41 (1), 74–87.
- López-Caravaca, A., Castañer, R., Clemente, A., Yubero, E., Galindo, N., Crespo, J., Nicolás, J.F., 2021. The impact of intense winter Saharan dust events on PM and optical properties at urban sites in the southeast of the Iberian Peninsula. *Atmosphere* 12, 1469.
- López-Caravaca, A., Crespo, J., Galindo, N., Yubero, E., Juárez, N., Nicolás, J.F., 2023. Sources of water-soluble organic carbon in fine particles at a southern European urban background site. *Atmos. Environ.* 306, 119844.
- López-Caravaca, A., Crespo, J., Galindo, N., Yubero, E., Clemente, A., Castañer, R., Nicolás, J.F., 2024. Characterization of water-soluble organic carbon absorption at an urban background site in the south-eastern Iberian Peninsula. *Atmos. Environ.* 324, 120435.
- Matta, E., Facchini, M.C., Decesari, S., Mircea, M., Cavalli, F., Fuzzi, S., Putaud, J.-P., Dell'Acqua, A., 2003. Mass closure on the chemical species in size-segregated atmospheric aerosol collected in an urban area of the Po Valley, Italy. *Atmos. Chem. Phys.* 3, 623–637.
- Mo, Y., Li, J., Cheng, Z., Zhong, G., Zhu, S., Tian, C., Chen, Y., Zhang, G., 2021. Dual carbon isotope-based source apportionment and light absorption properties of water-soluble organic carbon in PM_{2.5} over China. *J. Geophys. Res.* 126, e2020JD033920.
- Ni, X., Pan, Y., Shao, P., Tian, S., Zong, Z., Gu, M., Liu, B., Liu, J., Cao, J., Sun, Q., Wang, Y., Jiang, C., 2021. Size distribution and formation processes of aerosol water-soluble organic carbon during winter and summer in urban Beijing. *Atmos. Environ.* 244, 117983.
- Nicolás, J.F., Lucarelli, F., Galindo, N., Yubero, E., Crespo, J., Calzolari, G., Nava, S., 2020. Impact of traffic flows and meteorological events on the hourly elemental composition of fine and coarse particles at an urban site. *Aerosol Air Qual. Res.* 20, 991–1001.
- Pani, S.K., Lin, N.-H., Griffith, S.M., Chantara, S., Lee, C.-T., Thepnuan, D., Tsai, Y.I., 2021. Brown carbon light absorption over an urban environment in northern peninsular Southeast Asia. *Environ. Pollut.* 276, 116735.
- Park, S.S., Ko, J.M., Cho, S.Y., 2011. Investigation of possible sources of water-soluble organic carbon particles observed with an online monitoring system. *Atmos. Environ.* 45, 3257–3266.
- Park, S., Yu, G.-H., 2019. Absorption properties and size distribution of aerosol particles during the fall season at an urban site of Gwangju, Korea. *Environ. Eng. Res.* 24 (1), 159–172.
- Paulovic, J., Hopke, P.K., 2012. Chemical nature and molecular weight distribution of the water-soluble fine and ultrafine PM fractions collected in a rural environment. *Atmos. Environ.* 59, 264–271.
- Piñeiro-Iglesias, M., Andrade-Garda, J., Suárez-Garaboa, S., Muniategui-Lorenzo, S., López-Mahía, P., Prada-Rodríguez, D., 2021. Study of temporal variations of equivalent black carbon in a coastal city in northwest Spain using an atmospheric aerosol data management software. *Appl. Sci.* 11, 516.
- Rinaldi, M., Emblico, L., Decesari, S., Fuzzi, S., Facchini, M.C., Librando, V., 2007. Chemical characterization and source apportionment of size-segregated aerosol collected at an urban site in sicily. *Water, Air, Soil Pollut.* 185, 311–321.
- Sandrini, S., van Pinxteren, D., Giulianelli, L., Herrmann, H., Poulain, L., Facchini, M.C., Gilardoni, S., Rinaldi, M., Paglione, M., Turpin, B.J., Pollini, F., Bucci, S., Zanca, N., Decesari, S., 2016. Size-resolved aerosol composition at an urban and a rural site in the Po Valley in summertime: implications for secondary aerosol formation. *Atmos. Chem. Phys.* 16, 10879–10897.

- Salma, I., Mészáros, T., Maenhaut, W., 2013. Mass size distribution of carbon in atmospheric humic-like substances and water-soluble organic carbon for an urban environment. *J. Aerosol Sci.* 56, 53–60.
- Savadkoochi, M., Pandolfi, M., Reche, C., Niemi, J.V., Mooibroek, D., Titos, G., Green, D. C., Tremper, A.H., Hueglin, C., Liakakou, E., Mihalopoulos, N., Stavroulas, I., Artiñano, B., Coz, E., Alados-Arboledas, L., Beddows, D., Riffault, V., De Brito, J.F., Bastian, S., Baudic, A., Colombi, C., Costabile, F., Chazeau, B., Marchand, N., Gómez-Amo, J.L., Estellés, V., Matos, V., van der Gaag, E., Gille, G., Luoma, K., Manninen, H.E., Norman, M., Silvergren, S., Petit, J.E., Putaud, J.P., Rattigan, O.V., Timonen, H., Tuch, T., Merkel, M., Weinhold, K., Vratolis, S., Vasilescu, J., Favez, O., Harrison, R.M., Laj, P., Wiedensohler, A., Hopke, P.K., Petäjä, T., Alastuey, A., Querol, X., 2023. The variability of mass concentrations and source apportionment analysis of equivalent black carbon across urban Europe. *Environ. Int.* 178, 108081.
- Segura, S., Estellés, V., Esteve, A.R., Utrillas, M.P., Martínez-Lozano, J.A., 2013. Analysis of severe pollution episode in valencia (Spain) and its effect on ground level particulate matter. *J. Aerosol Sci.* 56, 41–52.
- Segura, S., Estellés, V., Titos, G., Lyamani, H., Utrillas, M.P., Zotter, P., Prévôt, A.S.H., Mocnik, G., Alados-Arboledas, L., Martínez-Lozano, J.A., 2014. Determination and analysis of in situ spectral aerosol optical properties by a multi-instrumental approach. *Atmos. Meas. Tech.* 7, 2373–2387.
- Segura, S., Estellés, V., Esteve, A.R., Marcos, C.R., Utrillas, M.P., Martínez-Lozano, J.A., 2016. Multiyear in-situ measurements of atmospheric aerosol absorption properties at an urban coastal site in western Mediterranean. *Atmos. Environ.* 129, 18–26.
- Snyder, D.C., Rutte, A.P., Collins, R., Worley, C., Schauer, J.J., 2009. Insights into the origin of water-soluble organic carbon in atmospheric fine particulate matter. *Aerosol Sci. Technol.* 43 (11), 1099–1107.
- Timonen, H., Saarikoski, S., Tolonen-Kivimäki, O., Aurela, M., Saarnio, K., Petäjä, T., Aalto, P.P., Kulmala, M., Pakkanen, T., Hillamo, R., 2008. Size distributions, sources and source areas of water-soluble organic carbon in urban background air. *Atmos. Chem. Phys.* 8, 5635–5647.
- Titos, G., Foyo-Moreno, I., Lyamani, H., Querol, X., Alastuey, A., Alados-Arboledas, L., 2012. Optical properties and chemical composition of aerosol particles at an urban location: an estimation of aerosol mass scattering and absorption efficiencies. *J. Geophys. Res.* 117, D04206.
- Titos, G., Ealo, M., Pandolfi, M., Pérez, N., Sola, Y., Sicard, M., Comerón, A., Querol, X., Alastuey, A., 2017. Spatiotemporal evolution of a severe winter dust event in the western Mediterranean: aerosol optical and physical properties. *J. Geophys. Res.* 122, 4052–4069.
- Tuet, W.Y., Fok, S., Verma, V., Tagle Rodriguez, M.S., Grosberg, A., Champion, J.A., Ng, N.L., 2016. Dose-dependent intracellular reactive oxygen and nitrogen species (ROS/RNS) production from particulate matter exposure: comparison to oxidative potential and chemical composition. *Atmos. Environ.* 144, 335–344.
- Velali, E., Papachristou, E., Pantazaki, A., Choli-Papadopoulou, T., Planou, S., Koura, A., Manoli, E., Besis, A., Voutsas, D., 2016. Redox activity and in vitro bioactivity of the water-soluble fraction of urban particulate matter in relation to particle size and chemical composition. *Environ. Pollut.* 208, 774–786.
- Wang, Q., Han, Y., Ye, J., Liu, S., Pongpiachan, S., Zhang, N., Han, Y., Tian, J., Wu, C., Long, X., Zhang, Q., Zhang, W., Zhao, Z., Cao, J., 2019. High contribution of secondary brown carbon to aerosol light absorption in the southeastern margin of Tibetan Plateau. *Geophys. Res. Lett.* 46, 4962–4970.
- Yttri, K.E., Simpson, D., Stenström, K., Puxbaum, H., Svendby, T., 2011. Source apportionment of the carbonaceous aerosol in Norway – quantitative estimates based on ¹⁴C, thermal-optical and organic tracer analysis. *Atmos. Chem. Phys.* 11, 9375–9394.
- Yu, G., Zhang, Y., Cho, S.Y., Park, S., 2017. Influence of haze pollution on water-soluble chemical species in PM_{2.5} and size-resolved particles at an urban site during fall. *J. Environ. Sci.* 57, 370–382.
- Zhu, C.-S., Qu, Y., Huang, H., Chen, J., Dai, W.-T., Huang, R.-J., Cao, J.-J., 2021. Black carbon and secondary brown carbon, the dominant light absorption and direct radiative forcing contributors of the atmospheric aerosols over the Tibetan Plateau. *Geophys. Res. Lett.* 48, e2021GL092524.
- Zhou, Y., Chen, J., Fan, F., Feng, Y., Wang, S., Fu, Q., Feng, J., 2022. Deconvolving light absorption properties and influencing factors of carbonaceous aerosol in Shanghai. *Sci. Total Environ.* 839, 156280.